Abel Andree Barreto Alcántara

Sensing and automatic scoring of sugar-beet fields by using UAV-imagery systems for disease quantification

ifZ

Sensing and automatic scoring of sugar-beet fields by using UAV-imagery systems for disease quantification

Dissertation

to attain the doctoral degree (Dr. sc. agr.)

of the Faculty of Agricultural Sciences

Georg-August-Universität Göttingen, Germany

by

Abel Andree Barreto Alcántara

born in Ancash, Peru

Göttingen, November 2023

Kurzfassung

Die Cercospora-Blattfleckenkrankheit (*Cercospora leaf spot*, CLS) ist die bedeutendste Blattkrankheit im Zuckerrübenanbau. Sie wird durch den pilzlichen Erreger *Cercospora beticola* Sacc. verursacht und kann zu erheblichen Ertragseinbußen führen. Die Kontrolle von CLS ist aufgrund einer schnellen Sporenproduktion und einer hohen genetischen Variabilität äußerst herausfordernd. Derzeit besteht die Bekämpfungsstrategie hauptsächlich aus den Leitlinien des integrierten Pflanzenschutzes. Diese umfassen ackerbauliche Maßnahmen, Sortenresistenzen und Strategien zum Fungizideinsatz. Die Bewertung der Krankheitsintensität spielt eine entscheidende Rolle für das Resistenzscreening in der Pflanzenzüchtung und für die Empfehlung von Pflanzenschutzmaßnahmen in der landwirtschaftlichen Praxis. Der Einsatz von Drohnen (UAVs), ausgestattet mit optischer Sensortechnologie wie beispielweise multispektralen oder hyperspektralen Kameras bietet eine neuartige Alternative für das Krankheitsmonitoring von CLS gegenüber den herkömmlich durchgeführten manuellen Bonituren. Maschinelle- und Deep-Learning Verfahren können eingesetzt werden, um multispektrale UAV-Bilder zu analysieren und relevante Informationen zur Krankheitsbewertung zu extrahieren. Durch diesen methodischen Ansatz kann eine Automatisierung der Erfassung von Parametern wie der Befallshäufigkeit (*disease incidence*, DI) und der Befallsstärke (*disease severity*, DS) erreicht werden, welche eine Grundlage für die Entscheidungsfindung bilden.

Die vorliegende Arbeit konzentriert sich auf den Einsatz von UAVs, ausgestattet mit bildgebender RGB- und multispektraler Sensortechnologie, und die Nutzung von maschinellem Lernen zur Überwachung und Bewertung von CLS im Zuckerrübenanbau. Zwei Anwendungsgebiete wurden untersucht: eine digitale Bewertung von Toleranzen und Resistenzen in Sortenversuchen; sowie die Beurteilung von Parametern zur Entscheidungsfindung für integrierte Bekämpfungsmaßnahmen von CLS. Die Ergebnisse dieser Arbeit empfehlen den Einsatz von multispektralen UAV-Systemen zur Bewertung der CLS-Resistenz, insbesondere durch eine bildbasierte und pixelweise Quantifizierung gesunder Blattbereiche und Differenzierung von symptomatischen Bereichen und Boden. Der enge Zusammenhang zwischen gesundem Blattapparat und Ertragsergebnissen betont die Bedeutung der vorgeschlagenen pixelweisen Methoden für

Züchtungsverfahren. Darüber hinaus ist die Identifizierung und Standardisierung von bildbasierten Bewertungseinheiten für Kontrollmaßnahmen und die Anwendung von Pflanzenschutzmittel von entscheidender Bedeutung. Die digitale Erkennung von Befallsparametern ist für ein zeitlich präzises und teilflächenspezifisches Krankheitsmanagement unerlässlich. In der vorliegenden Arbeit wurden Modelle des maschinellen Lerners angepasst und entwickelt, um mit hoher Genauigkeit die Parameter DI und DS zu erfassen. Für die Optimierung der Entscheidungsfindung wurden Verfahren zur Berücksichtigung der Bewertungseinheiten Pflanze, Kreis und Blatt integriert. Einschränkungen bei der räumlichen Auflösung des Sensors und der Nadir UAV-Perspektive sowie Probleme bei der Unterscheidung von krankem Gewebe und Boden unter bestimmten Lichtverhältnissen können jedoch die Verlässlichkeit bei der Erkennung erster Krankheitssymptome beeinträchtigen. Kurative und teilflächenspezifische Fungizidapplikationen und die Erstellung von Applikationskarten für mehrere, simultan auftretende Krankheiten sind weitere potenzielle Anwendungsgebiete.

Insgesamt zeigt die Arbeit das Potenzial von multispektralen UAV-basierten Methoden zur Anwendung in der Resistenzzüchtung und dem präzisen Pflanzenschutzmitteleinsatz und bietet weitere wertvolle Ansätze zur Verbesserung der integrierten Kontrolle von CLS. Das im Rahmen der Dissertationsschrift gewonnene Wissen kann auf weitere relevante Zuckerrübenkrankheiten wie den Echter Mehltau, Rübenrost oder die viröse Vergilbungen übertragen werden.

Abstract

Cercospora leaf spot (CLS) in sugar beet is a damaging leaf disease caused by the fungal pathogen *Cercospora beticola* Sacc. This disease leads to substantial yield diminishment, and its management poses a challenge owing to rapid sporulation and high genetic variability. Integrated pest management strategies, including cultural practices, cultivar resistance, and fungicide management, are used to mitigate the disease. Disease intensity evaluation plays a crucial role in plant breeding for resistance screening and in agricultural practice for guiding control measures. The use of optical sensor technology and unmanned aerial vehicles (UAVs) with multispectral or hyperspectral cameras provides a novel alternative to human-based disease assessment. These sensors capture reflected light in multiple wavelength bands, allowing high spatial resolution imaging with spectral information. Machine and deep learning techniques are utilized to analyze multispectral UAV images and extract relevant disease assessment information. The combination of multispectral UAV data and machine learning approaches holds great promise for assessing parameters such as disease incidence (DI) and disease severity (DS) as a basis for decision-making.

This thesis focuses on using RGB and multispectral imaging sensor technologies, UAVs, and machine learning to monitor and assess CLS in sugar beet. Two main application scenarios were investigated: evaluating tolerance and resistance in variety trials, and assessing parameters for decision-making in integrated CLS control in agricultural practice. The results of this dissertation recommended utilizing multispectral UAV systems for evaluating CLS resistance, particularly through an image-based and pixel-wise quantification of healthy foliage and soil regions. The close association between healthy foliage and yield outcomes emphasizes the importance of the proposed pixel-wise methods in breeding procedures. Furthermore, the identification and standardization of image-based scoring units are crucial for crop protection. Accurate detection of diseased specimens is essential for efficient site-specific disease management. In the present work, machine learning models were adapted and developed to detect DI and DS parameters with high accuracy. Procedures considering plant, circle, and leaf scoring units were incorporated to optimize decision-making. However, limitations in spatial resolution and nadir UAV-perspective, as well as challenges in discriminating diseased tissue from bare

soil under certain light conditions, may impact the sensitivity for detecting first symptoms of disease. Curative site-specific fungicide application and generation of multidisease application maps are potential future developments.

Overall, the dissertation demonstrates the potential of multispectral UAV-based methodologies for advancing disease resistance breeding and precise disease control, offering valuable applications in practical agriculture for integrated control of CLS. The knowledge gained from studying *Cercospora beticola* Sacc. and sugar beet can be transferred to other relevant sugar beet diseases such as Powdery mildew, Rust, and virus yellows using the established UAV-based assessment pipeline.

Publications and manuscripts

Manuscript I:

Abel Barreto, Philipp Lottes, Facundo Ramón Ispizua Yamati, Stephen Baumgarten, Nina Anastasia Wolf, Cyrill Stachniss, Anne-Katrin Mahlein, Stefan Paulus; 2021. Automatic UAV-based counting of seedlings in sugar-beet field and extension to maize and strawberry. Computers and Electronics in Agriculture 191. DOI: 10.1016/j.compag.2021.106493

Manuscript II:

Facundo Ramón Ispizua Yamati, **Abel Barreto**, Maurice Günder, Christian Bauckhage, Anne-Katrin Mahlein; 2022.

Sensing the occurrence and dynamics of Cercospora leaf spot disease using UAV-supported image data and deep learning. Sugar Industry. DOI: 10.36961/si28345

Manuscript III:

Abel Barreto, Facundo Ramón Ispizua Yamati, Mark Varrelmann, Stefan Paulus and Anne-Katrin Mahlein; 2022.

Disease Incidence and Severity of Cercospora Leaf Spot in Sugar Beet Assessed by Multispectral Unmanned Aerial Images and Machine Learning. Plant Disease, 107, 188-200. DOI: 10.1094/PDIS-12-21-2734-RE

Manuscript IV:

Abel Barreto, Lasse Reifenrath, Fabian Sinz and Anne-Katrin Mahlein; 2023.

Using UAV imagery for leaf segmentation in diseased plants via mask-based data augmentation and extension of library for leaf-based phenotyping parameters. Accepted in *KI* – Künstliche Intelligenz. 2023.

Manuscript V:

Abel Barreto and Anne-Katrin Mahlein; 2023.

Site-specific fungicide application based on automated scoring.

Abbreviations

General abbreviations

ANN	Artificial neural network
AUC	Area under the curve
AUDPC	Area under disease progress curve
AP	Average precision
BVL	German Federal Office of Consumer Protection and Food Safety
CLS	Cercospora leaf spot
CS	Confidence score
DI	Disease incidence
DS	Disease severity
DSM	Digital surface model
DMIs	Demethylation Inhibitors
DSM$_f$	Abbreviation for DSM features
FN	False negative classification
FP	False positive classification
FCN	Fully convolutional network
GSD	Ground sample distance
IPM	Integrated pest management
KNN	K-nearest neighbors
ML	Machine learning
IoU	Intersection over union
PLS-DA	Partial least squares discriminant analysis
PR	Precision-recall
QoIs	Quinone outside Inhibitors
RE	Abbreviation for resolution features
RF	Random forest
RI	Registration identifier
ROI	Region of interest
SB	Abbreviation for single bands features

SH	Abbreviation for shadow feature or $NSVDI$
SVML	Support vector machine linear
SVMR	Support vector machine radial
UAV	Unmanned aerial vehicle
VI	Vegetation index and abbreviation for VI features
WSY	White sugar yield
WSY_{loss}	Loss of white sugar yield

Mathematical Expressions

Angle of incidence between the canopy surface and light source within instance	θ_s
Area based disease severity within leaf instance	DS_l
Average cluster area within leaf instance	$A_{\bar{c}}$
Average cover of CLS cluster by unit of foliage cover	$C_{\bar{c}/F}$
Average slope or angle between surface and normal to horizontal within a leaf instance	ζ_l
Average surface area of CLS cluster by unit of foliage area	$A_{\bar{c}/F}$
Cover based disease severity at I level	ds_I
Cover based disease severity within leaf instance	ds_l
Cover of diseased foliage within instance	FC_d
Cover of foliage within instance	FC
Cover of healthy foliage within instance	FC_h
Difference between RED and BLUE band index	D_{678500}
Image slope or angle between surface and normal to Horizontal within a leaf instance	ζ_L
Image surface area within leaf instance	A_L
Individual instance	I
Individual leaf instance	L
Green vegetation index	GVI
Modified chlorophyll absorption in reflectance and optimized soil adjusted vegetation index	$MCARIOSAVI$

Table of Contents

CHAPTER 1:   Introduction

1.1. Sugar beet production and pests and diseases

Sugar, the common name of sucrose, is a basic component of food, pharmaceuticals and beverages (Meghana and Shastri, 2020). Worldwide, approximately 20% of the sugar production is originated from sugar beet (*Beta vulgaris* ssp. *vulgaris*) reaching about 37Mt. of total raw sugar produced (WVZ and VdZ, 2021). In 2020/2021, sugar beet was cultivated on approximately 1.49 million hectares within the EU including the UK, whereas 350,000 hectares were produced in Germany (WVZ and VdZ, 2021). The expectation for productivity in sugar beet cultivation is high; especially because of the low cost of cane sugar (Stevanato *et al.*, 2019). Since 1930, sugar yield has been increased from 3.2 to 10.3 t/ha in average (Draycott, 2006; WVZ and VdZ, 2021). Breeding has been the driving force for this yield improvement by introducing tolerant and resistant varieties to biotic and abiotic stresses (Loel *et al.*, 2014). The introduction of hybrids in sugar beet was the first breeding stone for increasing root yield in the early 20th century. The finding of monogerminity in the mid-1960 allowed efficiency in cultivation; moreover, improved sugar mass accumulation was fomented with the development of mechanism of genetic control arising a sugar production never seen before (Hoffmann *et al.*, 2021). High-yield varieties, optimized plant nutrition, soil and weed management secured sugar beet productivity and quality (Draycott, 2006). However, there is a tradeoff between yield and plant susceptibility to fungal pathogens, viral diseases and pest attack since those breeding traits and yield are negatively correlated to each other (Oerke and Dehne, 2004). In the early 19th century, farmers learned to avoid repeated narrow rotations after observing a steady decline in yield due to the proliferation of the Beet cyst nematode (*Heterodera schachtii*)(Draycott, 2006). Fast forward two centuries, pests continue to expand into new areas in Central Europe, likely propelled by climate change, giving rise to emerging diseases such as the syndrome basses richesses disease (SBR), capable of reducing yields by up to 26% (Pfitzer *et al.*, 2022). SBR is caused by the phloem-restricted γ-3 proteobacterium Candidatus Arsenophonus phytopathogenicus which is transmitted by *P. leporinus* and becomes a focus of research in recent years. Viral diseases account for up to 6% sugar yield losses (Oerke and Dehne, 2004). The green peach aphid (*Myzus persicae*) is the principal vector for transmission of different and economically important

virus yellows species (Hossain *et al.*, 2021; Kozłowska-Makulska *et al.*, 2009). At least two years of cropping interval are suggested to avoid the damage of soil borne diseases such Beet cyst nematode, Rhizoctonia root rots (*Rhizoctonia solani*), and damping off (*Aphanomyces cochlioides*, *Pythium* ssp. (Koch *et al.*, 2018). In addition to viral and root diseases, beet yield losses are attributed to the impairment of the photosynthetic leaf area. Among these, fungal leaf diseases emerge as the primary cause of direct leaf tissue damage, posing a significant risk to productivity. Some diseases such as Powdery mildew (*Erysiphe betae*), Rust (*Uromyces betae*), Ramularia leaf Spot (*Ramularia beticola*) present for the moment minor risk in productivity due to their late appearance in the growing season and slow development (Wolf and Verreet, 2002). Moreover the leaf disease caused by the fungus *Cercospora beticola* has posed a serious threat to high production standards in recent decades, leading to intensive research on plant breeding for resistance and on disease control (Jones and Windels, 1991; Wolf and Verreet, 2002, 1997).

1.2. Cercospora leaf spot, yield effect, infection biology and integrated management

Cercospora leaf spot (CLS) is the leaf disease caused by the ascomycete fungus *Cercospora beticola* Sacc. CLS represents a significant obstacle for sugar beet farmers, as it has detrimental effects on productivity and presents challenges in efficiently mitigating pathogen spread (Windels *et al.*, 1998). In the absence of disease management strategies, fields containing infected sugar beets exhibit compromised processing quality and can incur up to 50% in yield losses (Shane and Teng, 1992; Vogel *et al.*, 2018; Wolf *et al.*, 1998). The availability of primary *C. beticola* inoculum, an asexual and polycyclic manner of propagation, as well as the capacity to produce substomatal pseudostromata as survival structure (Rangel *et al.*, 2020; Weiland and Koch, 2004), are relevant epidemiological parameters to establish knowledge based measures of CLS control. Previous research identified various factors responsible for the spread of conidia, including wind, water splash, rain, irrigation, but also insects and contaminated machinery (Khan *et al.*, 2009; Lawrence and Meredith, 1970; Rangel *et al.*, 2020). Currently, there is a lack of definitive evidence regarding the wind-mediated dispersal of primary inoculation, and the origins of the primary inoculum source remain a subject of ongoing investigation

(Imbusch *et al.*, 2021). The infection initiates when conidia make contact with abaxial surface of sugar beet leaves (Rangel *et al.*, 2020). Conidia germination requires relative humidity close to 100%, and temperatures higher than 17°C (optimal by 25°C) (Khan *et al.*, 2009; Skaracis *et al.*, 2010). After germination and hyphae elongation, appressoria is produced to penetrate stomata and spread intercellularly without visual symptoms (Rathaiah, 1977; Steinkamp *et al.*, 1979). The initiation of the necrotic phase occurs through the synthesis of phytotoxins and degradative enzymes, leading to the demise of infected cells (Steinkamp *et al.*, 1979). Infected leaves with *C. beticola* present the following symptoms: they develop spots that appear in shades ranging from tan to gray. These spots are frequently surrounded by borders that range in color from tan-brown to reddish-purple, and they can measure between 3 to 5 millimeters in diameter (Rangel *et al.*, 2020; Weiland and Koch, 2004). Spots can merge to form bigger areas of dead tissue, leading to the withering and death of the leaves that are severely affected.

Due to its high reproductive ability and fast sporulation, the pathogen can complete a lifecycle in only 9-12 days under field conditions (Varrelmann and Märländer, 2018). This polycyclic property, coupled with high genetic variability, produces epidemic which can only be controlled with repeated fungicide applications, leading to increased production costs and the risk of developing pathogen-resistant strains (Birla *et al.*, 2012). In the 1980s, reports of immoderate use of fungicides due to continuous strong epidemics in the USA led to the first cases of pathogen resistance being reported (Windels *et al.*, 1998). Fungicide applications took place every 10 to 14 days in some regions; this results those fungicides especially for benzimidazole group, were no longer recommended for growers. A similar case was reported in the south of Germany a decade later (Wolf *et al.*, 1995). In the USA, an early integrated pest management (IPM) model was based on three pillars: cultural practices, cultivar resistance, and fungicide management (Windels *et al.*, 1998). Cultural practices recommended a minimum rotation of sugar beets every third year with non-host crops. Varieties with low susceptibility and high yield performance even under no infection pressure suggested ensuring high sugar beet productivity. Fungicide management based on protectant and curative fungicides supported by forecast models such as Daily Infection Values (DIVs) for the first application were recommended (Windels *et al.*, 1998). The same pillars are used for an integrated management of CLS in Germany,

Italy, France and Spain (Cioni *et al.*, 2014; Gummert and Ladewig, 2012; Jarroudi*et al.*, 2021; Martín Gil *et al.*, 2018). In Germany, the IPM model differs slightly to the American. The principal difference is on the fungicide management, which require additionally to the warning signal a disease assessment on field. A forecasting model called CERCBET 3 triggers a warning signal (Gummert and Ladewig, 2012). Then, this signal alerts growers to perform visual assessments in the field, followed by a decision on application if threshold values of CLS incidence are achieved.

The losses caused by a pathogen such as *C. beticola* are strongly associated with the intensity of disease (Nutter *et al.*, 1991). The evaluation of disease intensity through phytopathometry supports two important applications for integrated disease management, namely screening for resistance in plant breeding and providing indicators for control measures (Kranz, 1988).

1.3. Phytopathometry, disease intensity and sources of error for disease assessment

Phytopathometry is a branch discipline of plant pathology, focusing on measuring the amount of plant disease or disease assessment. The intensity of the disease is estimated using parameters such as disease incidence (DI) and disease severity (DS). DI refers to the proportion of diseased specimens, while DS measures the degree of the diseased region within specimens (Bock *et al.*, 2021; Kranz, 1988; Madden *et al.*, 2007a).

The definition of the specimen or scoring unit can significantly influence disease estimation over time. The most common scoring units for diseases are individual plants, leaves, and roots (Madden *et al.*, 2007a). In the case of CLS, a descriptive epidemic development is mostly expressed as DI at plant level (DI_{plant}), and DI and DS at leaf level (DI_{leaf} and DS_{leaf}) (Wolf and Verreet, 2002).

The choice of whether to use DI or DS depends on the objectives of the epidemiological or breeding study. DI is a parameter with high sensitivity for pathogen spread, particularly during the initial stages of disease development (Madden *et al.*, 2007a). As a result of this characteristic, levels of DI parameter have been applied in thresholds as indicators to trigger warning signals for fungicide management (Wolf, 2002). DS, on the other hand, is

commonly used to evaluate productivity and yield loss and its principal application is for assessing new varieties for resistance and fungicide tests (Madden *et al.*, 2007a).

Nature of data is relevant for quantifying disease intensity, especially in the case of determining DS. Ordinal and ratio scales are the most common data types for quantifying DS. Ordinal scales are commonly used to give levels of severity during disease development. Examples for quantifying severity in CLS in an ordinal scale are the KWS scale and the Agronomica diagram (Anonymous, 1970; Vereijssen *et al.*, 2003). The KWS scale is a severity diagram that ranges from 1 to 9. A rating of 1 indicates the complete absence of symptoms, while a rating of 3 indicates the presence of leaf spots on older leaves. A rating of 5 signifies the merging of leaf spots, resulting in the formation of necrotic areas. A rating of 7 is assigned when the disease advances from the oldest leaves to the inner leaves, leading to their death. Finally, a rating of 9 is given when the foliage experiences complete death (Anonymous, 1970). A ratio scale is data assessed in a continues but truncated range. For CLS, the ratio scale represents the ratio of diseased tissue from complete leaf area (Wolf *et al.*, 1998). The principal advantage of a ratio scale consists in delivering more detailed epidemiolocal information in comparison to ordinal scales supporting significant differences in the statistic (Madden *et al.*, 2007a; Vereijssen *et al.*, 2003). However, a ratio scale is less reliable and accurate than ordinal requiring a high level of expertise for the assessment.

Decisions are taken based on parameters assessed on the field, farmers decide for disease control by determining DI, breeders identify a potential resistance line based on DS. Therefore, trained, well-structured and aided raters are required, the so-called experts. Experts can produce or estimate acute measurements close to "standard gold" values (Madden *et al.*, 2007a). Experts' assessment fulfills two characteristics, these are reliability and accuracy (Bock *et al.*, 2010). An assessment is reliable when repeated estimations or measurements of the same specimen are close to each other. Reliability can be divided on inter-rater reliability (reliability of different raters) or intra-rater reliability (reliability of the rater) (Madden *et al.*, 2007a; Nutter *et al.*, 1991). Regarding to accuracy, an accurate assessment has a high degree of closeness to the "gold standard" (Bock *et al.*, 2020; Kranz, 1988; Madden *et al.*, 2007a). The lack of accuracy in disease assessment can result in error of type II, false negative (FN) or missed detection of

diseased specimen; however, the level of accuracy required varies to each disease quantification case (Bock *et al.*, 2020). Up today, no error of type I was reported, false positive (FP) or diseased classification of healthy specimen, in disease assessment.

Beside experts, there are some object-dependent sources of error. Robustness of assessment can drop due to illumination. Varying illumination conditions are more serious in direct sunlight in comparison to cloudy conditions; color blindness caused by direct sunlight in the quantification of powdery mildew in sugar beet is an example for drop of scoring performance (Bock *et al.*, 2020). Complexity of the scoring unit can also affect accuracy, whereas three-dimensional samples are more difficult to assess in comparison with two-dimensional specimens such as leaves. Size and shape of lesions can promote a tendency to overestimation, in the case of CLS, the number and size of spots during the first disease development stages, can be challenging for beginners. Finally, leaf wetness is also source of error leading to deviating estimations (Kranz, 1988). All mentioned points can influence the performance of assessments because affecting in the physiological stimuli and psychological response of raters (Kranz, 1988).

Reliable and accurate quantification of disease intensity are the principal support of two from three pillars for an integrated CLS management: visual assessment for screening disease resistance, and visual assessment for determining indicators for fungicide application. The following sections will provide detailed information on breeding principals for enhancing CLS resistance in plants as well as plant protection measures.

1.4. Resistance breeding

The development of CLS-resistant sugar beet plants through the breeding process has been reported as a crucial factor in preventing yield losses in recent years, where inclusive low yield penalty is mentioned in the absence of the disease (Vogel *et al.*, 2018). In Germany, cultivating less susceptible varieties can help reduce fungicide usage and extend the authorization period for the application of a fungicide product (Bundessortenamt, 2022). Resistant and tolerant varieties have two further advantages. They reduce the intensity of fungicide application, increasing eco-efficiency (Wiessner *et al.*, 2010), and they reduce the risk of stronger epidemics in the following years by contributing less plant debris (Wolf and Verreet, 2002). Gene sources of CLS resistance

have been identified in the wild sea beet, *Beta vulgaris ssp. maritima* (Rossi, 1995). At least four quantitative trait loci have been identified to be responsible for CLS resistance to present time (Rangel *et al.*, 2020). The *maritima* line is the primary genetic resource used in breeding programs to develop CLS-resistant varieties (Stevanato *et al.*, 2019). (Weltmeier *et al.*, 2011) documented a molecular mechanism for sugar beet defense response against CLS, which is based on high expression of pathogenesis-related (PR) and WRKY genes. This defense response can be triggered 1 day after inoculation and inhibit *C. beticola* biomass development in monogenic resistance varieties, while susceptible varieties require 15 days to initiate this gene expression. PR and WRKY gene expression might overcome pathogen-induced suppression of phenylalanine ammonia lyase (PAL) gene which is the initial defense response of interaction between sugar beet and *C. beticola* (Schmidt *et al.*, 2008). PAL gene expression is involved in plant-related pathways for secondary metabolites such as lignin, flavonoids, and phytoalexins (Rangel *et al.*, 2020).

The breeding process for producing new resistant varieties is divided in four stages; mass selection, family selection, recurrent selection, and hybrid production (Biancardi *et al.*, 2010). During mass selection an improved population with resistance characteristics is generated after intercrossing by open pollination. In the family selection stage, undesired F1 hybrids are discarded by half-sib or full-sib selection. Seeds of this last stage can be already used as pollinators for hybrid production. The aim of the recurrent selection is to increase the frequency of superior alleles and allelic combinations of desired traits including disease resistance in lines which are used as pollinators. The last stage of breeding process uses potential disease resistant family lines and pollinator and a selected phenotypic male sterile hybrid with complementary desired traits to generate offspring with combined abilities in yield and resistance (Biancardi *et al.*, 2010; Setiawan *et al.*, 2000). Overall, multiyear field trials must be designed in multiple locations. Disease assessment, specially DS, is the principal quantification parameter for phenotyping disease resistance under field conditions (Setiawan *et al.*, 2000). When resistant hybrids are identified, breeders produce a large amount of seeds to initiate the registration procedure (Biancardi *et al.*, 2010). In Germany, the national variety offices corroborate this superiority and approve a new variety for commercialization by after testing resistance

of candidates in multi-year and multi-site variety trials (Gummert *et al.*, 2015; Ossenkop *et al.*, 2005, 2002). Here again intensive phenotyping activities are required for screening susceptibility, quality and yield performance (Bundessortenamt, 2022).

1.5. Plant protection and limitations of expert assessment

In situations where cultural practices and cultivar resistance fail to effectively control the spread of CLS, plant protection emerges as the final recourse to ensure the preservation of sugar production in terms of both quantity and quality (Hoffmann, 2010). As mentioned in Section 1.2, nowadays the intensive use of pesticides promoted natural selection of fungal pathogens including *C. beticola*. Considering a sustainable use of fungicide applications as integrated management to control CLS, epidemic thresholds were proposed as spraying indicators by using DI and DS at plant and leaf level (Wolf *et al.*, 1995). During the nineties by implementing an early IPM model in Germany, the first epidemic threshold considered the plant-to-plant spread of CLS and was defined as half of infested plants from a complete sugar beet population (50% DI_{plant}; Wolf and Verreet, 1997). A diseased plant was counted when at least a CLS spot is identified in complete canopy. For the plant protection measure of this IPM, further thresholds of epidemics were identified such as 25-35% DI_{leaf} or 0.2-0.4 DS_{leaf} (Wolf *et al.*, 1998). However, the monitoring of two different scoring units (leaf and plant) and two different disease intensity parameters (DI and DS) unable the practical application of the threshold-based fungicide management in early German IPM (Wolf *et al.*, 1998). As a solution, correlations were evaluated to standardize scoring unit and parameter, moreover, middle leaves were identified as the most informative samples in the sugar beet canopy to describe CLS epidemic. The chosen standardized parameter was DI_{leaf} considering middle leaves as scoring unit for the sampling. Standardized the unit, equivalent thresholds were determined to describe epidemics; five infested from 100 middle leaves sampled should equivalent the half of infested plant in the population (50% $DI_{plant} \approx 5\%$ DI_{leaf}), in addition, 25-35% DI_{leaf} from the complete canopy should equivalent 35-45% DI_{leaf} from middle leaves (Wolf *et al.*, 1998).

Epidemic threshold and economic damage threshold are two different concepts in plant protection. As mentioned before, the first concept describes development of epidemics, while the second is defined as the tolerance limit for economic damage (Wolf and Verreet,

2002). For CLS, economic damage threshold was determined by 5% DS $_{leaf}$ from complete canopy at harvesting (Wolf *et al.*, 1998). With a magnitude for economic damage threshold, the decision system is further oriented based on the developing stage of the sugar beet crop during the vegetation period and calendar. Fungicide spraying should take place if 5% DI$_{leaf}$ was overcome in the period July to mid-August. From mid to end August sprays should take place if 45% DI$_{leaf}$ was overcome (Wolf and Verreet, 2002). With this last condition the second application should also take place in the case of unsuccessful first application. After some years of practical use of epidemics thresholds as indicators in the IPM, two negative aspects were observed (Lang, 2005). Firstly, applications performed at the beginning of August based on the overcome from 5% DI$_{leaf}$ threshold were not necessary because by harvesting economic damage threshold was not achieved. Dry and cold locations were frequently the exceptions. Secondly, strong epidemic development was observed also in September with significant yield losses for late harvested fields, requiring an extension of disease monitoring and control period. As improvement, new guidelines for a IPM model against leaf diseases were published in Germany including the management of CLS (Gummert and Ladewig, 2012). The new model is adjusted with an additional epidemic threshold (15% DI$_{leaf}$) for the first application. The first application is DI$_{leaf}$ and calendar dependent, where the indicator is 5% DI$_{leaf}$ until 31.07, 15% DI$_{leaf}$ until 15.08, and since 16.08 the indicator is 45% DI$_{leaf}$. A second application takes place when this last epidemic threshold is achieved (Lang, 2005).

In summary, disease assessment plays a crucial role in IPM by contributing to both plant breeding and plant protection efforts. The selection of appropriate disease parameters, scoring units, and thresholds greatly influences the effectiveness of identifying resistant lines against CLS and implementing successful disease control strategies. Consequently, the importance of reliable and accurate disease assessment cannot be overstated. While expert assessment is highly accurate, there are certain drawbacks associated with human-based disease quantification. Expert assessments tend to be time-consuming, costly, and have limited throughput capacity for large-scale (Bock *et al.*, 2020). In the breeding process, screening for resistance requires exhaustive and time-consuming phenotyping activities to identify suitable plant materials (Mahlein, 2015). In plant

protection, disease intensity within a field can exhibit heterogeneity, as observed in cases involving *R. solani* and *H. schachtii* (Hillnhütter *et al.*, 2011), leading to the potential for varying indicators for fungicide application within the same field (Mahlein *et al.*, 2018). However, for experts the determination of disease intensity parameters is only feasible by sampling methods that represents with a single magnitude disease intensity of the complete field. To optimize CLS management, it is imperative to enhance the efficiency, reliability, and site-specificity of disease assessment information. This can be achieved by improving assessment methods, utilizing advanced technologies, and incorporating spatial variability analyses to ensure more precise and targeted disease management strategies.

1.6. Optical sensor technology and UAV-systems

A novel alternative for the human-based disease assessment is the use of optical sensors such multispectral or hyperspectral cameras (Bohnenkamp *et al.*, 2021; Hillnhütter *et al.*, 2012; Leucker *et al.*, 2016; Mahlein, 2015; Mahlein *et al.*, 2018; Reynolds *et al.*, 2011). The principle of optical sensors is based on the measure of the amount of light, commonly the reflected light, reaching the imaging sensor and store as information (Thomas *et al.*, 2018). The recorded information or two-dimensional image present high spatial and spectral resolution, containing up to several bands of spectral information within the wavelength range of sensor. Many optical sensors are able to address the visible part of the electromagnetic spectrum (400-700 nm, VIS), but also, they are able to measure the near-infrared wavelength (700-1000 nm, NIR) calling them as VISNIR sensors (Maes and Steppe, 2019; Mahlein *et al.*, 2018). The main distinction between multispectral and hyperspectral sensors lies in their spectral resolution. Multispectral sensors typically capture broad wavelength bands within the BLUE, GREEN, and RED spectral regions, as well as bands within the NIR range (Mahlein, 2015). Moreover, current multispectral sensors present relatively high spatial resolution, low integration time, wide field of view, and parallel camera arrangement allowing multispectral cameras to record multispectral information on the field with high throughput (Aasen *et al.*, 2018; Wierzbicki, 2018).

When proper image-processing techniques are applied, unmanned aerial vehicles (UAVs) carrying multispectral imaging sensors becomes a tool for field mapping, and constitute a monitoring system with potential to solve previous mentioned drawbacks of disease

assessments by experts: regarding bias, limitations of workload and low throughput (Bock *et al.*, 2020). Easy mapping operation, flexibility, and a continuous technological improvement of the last years from both components, UAV and image sensor, makes the past limitations of flight time and image resolution no longer an aspect for restricting the support in disease monitoring tasks (Deng *et al.*, 2018). Optical sensors were used in the past to monitor CLS development. The first study reported, used multispectral, ground based non-imaging data to assess disease severity of CLS under field conditions based single reflectance of wavelength bands and vegetation indices (Steddom, 2005). Since the commencement of this preliminary investigation, significant advancements have occurred in sensor technology. Furthermore, remarkable progress has been witnessed in the field of machine learning (ML) and deep learning, which have harnessed the potential of high-resolution multispectral data for disease assessment applications (Mahlein *et al.*, 2018).

1.7. Data analysis: machine learning, deep learning and image post-processing

In the analysis of multispectral UAV images, ML and deep learning are the principal support to extract relevant information for disease assessment. ML and deep learning are subsets of artificial intelligence that allows systems to learn automatically from data by identifying patterns (Bishop and Nasrabadi, 2006). Statistical models and singular algorithms are trained and learn how to make predictions and take decisions based on delivered data not just with such as data like spectral information, but also 3D arrays like RGB images. Supervised learning are machine learning techniques that learn from labelled data (Bishop and Nasrabadi, 2006). Some typical supervised learning techniques are K-nearest neighbors (KNN), partial least squares discriminant analysis (PLS-DA), random forest (RF), support vector machines (SVM). In previous studies, the utilization of spectral imaging data, specifically employing RF and PLS-DA techniques, demonstrated in the past high reliability in determining DI and enabling early detection of *R. solani* infection in sugar beet plants (Barreto *et al.*, 2020).

The principal difference between deep learning and machine learning is the use of artificial neural networks (ANNs) arranged in multiple layers in a deep learning approach (Schmidhuber, 2015). ANNs are designed to emulate the structure of human brain. ANNs past through multiple layers collected data, optimize prediction or decisions, learning

complex features from data. Convolutional Neural Networks (CNNs) and Fully Convolutional Networks (FCNs) are types of ANNs, which are specialized in learning patterns from images. To segment objects from an image, computer vision techniques are available including semantic segmentation and instance segmentation, those computer vision techniques contain as main structure CNNs and or FCNs models. Semantic segmentation involves ordering a label to each pixel belonging to a kind of object (Chen *et al.*, 2018; Long *et al.*, 2015). Furthermore, instance segmentation delivers more details and segment within a kind of object a pixel-wise label for each individual (instance) (He *et al.*, 2017; Neven *et al.*, 2019). The analysis of RGB and multispectral images by ML and deep learning approaches have been reported to detect infected tissue and quantify DS of CLS in more recent works on sugar beet (Görlich *et al.*, 2021; Jay *et al.*, 2020; Mahlein *et al.*, 2013; Ziya *et al.*, 2018), however, most of them requiring a post-processing step.

Post-processing techniques are relevant in computer vision because they can help to improve the accuracy and robustness of algorithms, making them more suitable for real-world applications. An example of post-processing technique for agriculture application was proposed by (Lottes *et al.*, 2018b). Here an FCNs output, a probabilistic and multiclass array for detecting stems of sugar beet and weeds, was adapted to local maximal in order to deliver stem location to make comparable with the plant counting assessments on the field. Post processing techniques were applied for disease quantification as described in (Jay *et al.*, 2020). In this work, post-processing algorithms were employed to extract a list of disease severity parameters including spot density, area of healthy tissue, and an ordinal scaled CLS DS parameter. With this post-processing a time-series analysis via Area Under Disease Progress Curve (AUDPC) (Madden *et al.*, 2007b) of DS parameters was performed allowing resistance screening in two years variety trials (Jay *et al.*, 2020).

The aforementioned studies collectively underscore the substantial potential of harnessing multispectral UAV information for disease assessment purposes. This encompasses the utilization of UAV data to determine essential disease intensity parameters, namely DI and DS. These parameters play a pivotal role in facilitating the successful integrated management of CLS.

CHAPTER 2: Research objectives

The objectives of this thesis focus on the challenge of using optical sensor technologies and unmanned aerial vehicles (UAVs) in a methodological approach with machine learning for assessing and monitoring Cercospora leaf spot (CLS) in sugar beet. The investigated applications scenarios were (A) evaluating tolerance and resistance in variety trials to substitute the manual phenotyping process and (B) the assessment of the parameters disease incidence (DI) and disease severity (DS) for decision-making in integrated control of CLS. To provide practicable solutions and process pipelines for these application scenarios, the objectives of this thesis were:

I.   Identify plants as scoring unit within UAV images from experimental fields. A deep learning approach for semantic segmentation was adapted to this aim, and the best timing for plant unit quantification was determined. Subsequently, to understand CLS epidemiologic, an image-processing pipeline for calculating DS_{plant} in an ordinal scale emulating KWS scale will be proposed and tested.

II. The automatic determination of DS with a continuous ratio scale. For this task a machine learning multiclass classifier was trained to quantify diseased and healthy tissue in a pixel-wise manner. Due to incompatibility to merge a plant-level scoring, arbitrary scoring units must be temporally proposed. The pipeline was applied in variety trials to rank resistance against CLS.

III. Develop and evaluate image-based leaf segmentation for seeking segmented scoring unit, using an instance segmentation technique called Mask-RCNN. Subsequently, the previously trained multiclass classifier was integrated to the leaf instance segmentation to deliver, DS_{leaf}, as output.

IV. Utilizing the most promising approach for site-specific disease control. Therefore UAV-based assessments of DI were conducted to generate application maps using threshold values for fungicide applications. Additionally, the control efficiency in terms of fungicide consumption was investigated.

At the end of this thesis, current challenges, and perspectives for further research in automatic disease quantification and site-specific CLS control by using multispectral UAV-systems are critically discussed.

CHAPTER 3: Detection of sugar beet plants - Manuscript I

Automatic UAV-based counting of seedlings in sugar-beet field and extension to maize and strawberry

Abel Barreto[1]*, Philipp Lottes[2], Facundo Ramón Ispizua Yamati[1], Stephen Baumgarten[3], Nina Anastasia Wolf[3], Cyrill Stachniss[4], Anne-Katrin Mahlein[1], Stefan Paulus[1]

[1] Institute of Sugar Beet Research (IfZ), Holtenser Landstraße 77, 37079 Göttingen, Germany

[2] Pheno-Inspect GmbH, Straßburger Straße 109, 46047 Oberhausen, Germany

[3] ARGE NORD e.V., Helene-Künne-Allee 5, 38122 Braunschweig, Germany

[4] University of Bonn, Photogrammetry & Robotics Lab, Nussallee 15, Bonn 53115, Germany

*Corresponding author: barreto@ifz-goettingen.de

Author contributions

Original papers

Automatic UAV-based counting of seedlings in sugar-beet field and extension to maize and strawberry

Abel Barreto [a,*], Philipp Lottes [b], Facundo Ramón Ispizua Yamati [a], Stephen Baumgarten [c], Nina Anastasia Wolf [c], Cyrill Stachniss [d], Anne-Katrin Mahlein [a], Stefan Paulus [a]

[a] Institute of Sugar Beet Research (IfZ), Holtenser Landstraße 77, 37079 Göttingen, Germany
[b] Pheno Inspect GmbH, Straßburger Straße 109, 46047 Oberhausen, Germany
[c] ARGE NORD e.V., Helene-Künne-Allee 5, 38122 Braunschweig, Germany
[d] University of Bonn, Photogrammetry & Robotics Lab, Nussallee 15, Bonn 53115, Germany

ARTICLE INFO

ABSTRACT

Counting crop seedlings is a time-demanding activity involved in diverse agricultural practices like plant cultivating, experimental trials, plant breeding procedures, and weed control. Unmanned Aerial Vehicles (UAVs) carrying RGB cameras are novel tools for automatic field mapping, and the analysis of UAV images by deep learning methods can provide relevant agronomic information. UAV-based camera systems and a deep learning image analysis pipeline are implemented for a fully automated plant counting in sugar beet, maize, and strawberry fields in the present study. Five locations were monitored at different growth stages, and the crop number per plot was automatically predicted by using a fully convolutional network (FCN) pipeline. Our FCN-based approach is a single model for jointly determining both the exact stem location of crop and weed plants and a pixel-wise plant classification considering crop, weed, and soil. To determinate the approach performance, predicted crop counting was compared to visually assessed ground truth data. Results show that UAV-based counting of sugar-beet plants delivers forecast errors lower than 4.6%, and the main factors for performance are related to the intra-row distance and the growth stage. The pipeline's extension to other crops is possible; the errors of the predictions are lower than 4% under practical field conditions for maize and strawberry fields. This work highlight the feasibility of automatic crop counting, which can reduce manual effort to the farmers.

1. Introduction

The counting of sugar-beet seedlings is a time-demanding activity necessary in diverse aspects of beet production such as plant cultivating, experimental trials, plant breeding, plant phenotyping, and weed control. At the beginning of the cultivation season and few days after sowing (das), plant population and location becomes a relevant parameter to describe plant distribution's homogeneity on the field.

Previous studies highlighted the relevance of plant density in final beet yield and quality, as well as for the white sugar yield (WSY; Märländer, 1990). Sub-optimal plant distribution can be caused not only by biotic factors like insects or fungi but also by abiotic factors like drought, crust formation, hail, wind, or frost damage (Smit, 1993). In Germany, farmers determine plant population by an intensive manual

counting of sugar-beet seedlings at a growing stage (BBCH) 10–12 in a previously defined and representative patches of 10 m², the average value of all counts are extrapolated to the entire field. In Europe, the counted number of emerged plants defines the decision of resowing, where fields with a population lower than 45 thousand plants per hectare are decided to be replanted. Moreover, plant populations between 82 and 110 thousand plants per hectare are considered as optimal (Märländer, 1990), where seeds are frequently sown with a row distance of 45 and 50 cm and an intra-row distance from 18 to 25 cm. In experimental fields, a narrow sowing method is used where seeds are sown with a intra-row distance from 4 to 16 cm (Durrant et al., 1985; Pospišil et al., 2000; Söğüt and Arioglu, 2004) to achieve two or three times the population number employed in the practice, later young plants are commonly thinned out to manually achieve the optimal

* Corresponding author.
E-mail addresses: barreto@ifz-goettingen.de (A. Barreto), philipp.lottes@phenoimpect.de (P. Lottes), ispizua@ifz-goettingen.de (F.R. Ispizua Yamati), stephen.baumgarten@arge-nord.de (S. Baumgarten), ninaanastasia.wolf@arge-nord.de (N.A. Wolf), cyrill.stachniss@igg.uni-bonn.de (C. Stachniss), mahlein@ifz-goettingen.de (A.-K. Mahlein), paulus@ifz-goettingen.de (S. Paulus).

population.

Automatic counting of sugar-beet plants presents a potential for experimental fields. In the European Union (EU), the demand for improvements in the sugar-beet cultivation to secure the crop yield and fulfill the principles of integrated pest management (IPM) leads to constant evaluations of new sugar-beet varieties, fungicides, insecticides and herbicides. Unlike counting made by sugar-beet growers, counting in field experiments varies according to experimental aims and requires a precise number of emerged plants per plot. Manual counting of field trials could amount from 120 to 250 person-hours per counted hectare, and counted area can represent 20 to 50% of the entire experimental field. Plant breeding trials also require the detailed monitoring of plant emergence, germination capacity of seeds under the field conditions is a time-demanding key parameter to quantify seed quality. Emergence rate, together with vigorous seedlings, determine if a new sugar-beet variety is accepted or rejected by the market (Milošević et al., 2010). Finally, competition for light and nutrients between uncontrolled weed and sugar beet can cause root yield losses from up to 95% (Petersen, 2004); therefore, modern post-emergence weed control activities like weeding through tractor-mounted hoes or herbicide application in weed-infested areas demands techniques for precise weed detection, location and distribution on the field to ensure crop yield and avoid the environmental impact of intensive herbicide application (Cioni and Maines, 2010; Kunz et al., 2015).

Unmanned Aerial Vehicles carrying RGB cameras appear as a novel automatic approach to sequential images for field mapping. Advantages for plant phenotyping are related to ease of operation, high spatial resolution, and acquisition of data on demand (Deng et al., 2018). RGB and RGB-NIR images were used in the past to detect sugar beet and weeds. The image processing pipeline includes the use of an end-to-end trainable fully convolutional network acquired from field robot platforms (Lottes et al., 2018; Wu et al., 2020; McCool et al., 2017). This algorithm can deliver information to track crops and weeds, including the number of plants, their location, and distribution on the field. The FCN is also able to detect stem position of sugar beets and weeds from RGB images with a ground sampling distance (GSD) of 2 mm (Lottes et al., 2018). To emulate the complexity of field conditions, an improvement of this algorithm was also developed for field robot platforms and RGB-NIR images with 1 mm GSD to detect sugar-beet and weed stems under varying weed pressure, various weed types, and for different locations and growth stages of 2-, 4-leaf and 6-to-8-leaf (Lottes et al., 2019). Nevertheless, and although mentioned advantages of the image processing approach, there is still a lack of knowledge in following aspects: (1) the possibility to extend the approach to UAV-RGB systems and its robustness in different locations and in time-series, especially because UAV-systems in comparison with field robots deliver, due to distance camera-object, higher spatial resolution and output images quality depends of the sunlight conditions; (2) behavior of forecast performance for crop counting between different growth stages; and (3) the effect of different intra-row distances in the forecast performance of crop counting, considering the most demanding counting activities for experimental fields but also for practice.

Besides, the performance of UAV-recorded RGB images and a FCN pipeline to determine the plant number in other crops is also unknown but valuable for practitioners to predict the yield. RGB images and deep-learning approaches were already reported to be useful for counting diverse plant species like rice plants and acacia trees (Lu et al., 2021; Tong et al., 2021). The use of a previously trained model to other crop species has to consider differences in shape and color which could decrease the robustness of the methodology. Despite this disadvantage, two points might be beneficial in the extension of the method to other crops: (1) the reliability of the plant identification step (plant-soil segmentation), and (2) the ability of previously trained FCN based approach to differentiate diverse weeds of various botanical families (crop-weed discrimination). Whereas the sugar-beet experimental fields include natural weed development, it is proposed to evaluate a practical

approach close to the productive application on strawberry and maize fields. In this study, the described FCN pipeline, which is modeled for sugar beet will be adapted and applied to strawberries, and maize for crop counting.

The general objectives of this study are: (1) evaluate the performance of forecasting the number of sugar-beet plants on the field by using a FCN-based approach and RGB images of mapped fields with two different intra-row distances, (2) determinate the best performance of the approach comparing different growing stages and in time-series and (3) evaluate the possibility of extending the methodology established for sugar-beets to strawberry and maize.

2. Materials and methods

2.1. Experimental fields

Location 1 - sugar-beet variety trial This field presented a simplified sugar-beet variety trial design, and was located in Göttingen, Lower Saxony, Germany. The design showed 24 plots arranged in six rows, each plot with a size of 2.7×8.0 m. The trial field presented two sugar-beet varieties with different leaf orientation, a planophile and an erectophile. Seeds were sowed on the 9th of April in 2019; the initial intra-row distance was 6.8 cm, and the distance between row was 45 cm. Two days before the UAV-measurement, plant population was reduced to $1/3$ in order to increase intra-row to 21 cm. The soil type was Chromic Luvisol.

Location 2 - proof of concept A second trial was located in Börßum, Lower Saxony, Germany (Fig. 1a). The design was structured into 84 plots with a size of 1.35×7 m. The trial field presented 21 sugar-beet varieties. Seeds were sown on the 10th of April in 2019, with an original intra-row distance of 6.8 cm and 45 cm between rows. Previous to UAV-measurement, plant population was reduced as location 1 to 21 cm. The soil type was Chromic Luvisol.

Monitoring and preliminary evaluation of data from locations 1 and 2 were performed as a background for a "proof of concept" and support the design for a time-series monitoring to determinate crop population under "harsh weed conditions.".

Location 3 - time-series monitoring in harsh weed conditions for sugar beet The field trial for weed control was located in Höckelheim, Lower Saxony, Germany. The design was originally structured into 40 plots with a size of 1.35×7 m. The sowing date was the 15th of August 2019, and the initial intra-row distance was 6.8 cm and 45 cm between rows. Previous to UAV-measurement, plant population was reduced to $1/2$. No herbicides were applied to this field. The soil type was Chromic Luvisol.

Location 4 and 5 - maize and strawberry These fields were located in Klein-Altendorf, North Rhine-Westphalia, Germany. The maize dataset (location 4) had originally no plot structure (Fig. 1b). Therefore, 20 images were extracted from a single row, each representing a plot with a size of 0.56×28.9 m. The dataset contains almost no weeds and reflects maize plants in its post-emergence growth stage. However, some of the maize plants were already overlapped. The strawberry dataset (location 5) presents also no plot structure. Thus, we define 40 squared regions of 9×9 m. The dataset also contains small weeds that are located between and within the rows of strawberry plants. The soil type for both trials was Haplic Luvisol.

2.2. UAV monitoring systems

Three UAV-monitoring systems were used for the present study. Technical specifications are described in Table 1.

2.3. UAV-monitoring campaign and flight planning

The monitoring campaign started when plants achieved the growing stages between BBCH 12 and 16 for sugar beets, and BBCH 13–17 and
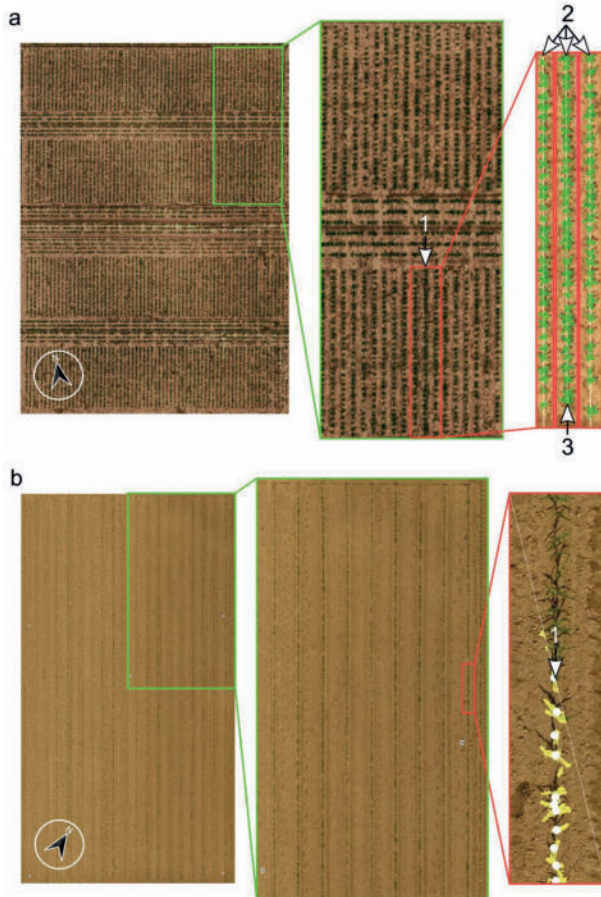
Fig. 1. Experimental fields: (a) UAV-acquisition and analysis of a sugar-beet field at 28th May 2019 in Börßum (location 2), 1) plot segmentation, 2) row detection, 3) stem detection and crop counting. (b) UAV-acquisition and analysis of maize field in Klein-Altendorf (location 4), 1) stem detection and plant counting.

BBCH 13–16 in the case of the maize and strawberry fields, respectively. Flights were performed in all locations in on one occasion with the exception of location 3 (time-series monitoring), which was monitored on three occasions (Table 2). For this location, ground control points (GCPs) were installed in the field corner points. In all locations, flights were performed within three hours of local solar noon. Flight mission was established using the software UgCS (SPH Engineering, Riga, Latvia), and the flight time was between 12 and 22 min. RGB images were captured in the photo mode (single shot) by distance with a shutter speed between 1/1400 s and 1/1000 s, and a sidelap/frontlap of 80%. The resolution in GSD was fitted to field size between 1.5 and 3 mm (Table 2). Image stitching to an orthomosaic was performed using Agi-Soft MetaShape (Agisoft LLC, St. Petersburg, Russia).

Sky conditions of each UAV-measurement was categorized in four classes: (1) clear, (2) low cloudy, (3) middle cloudy, and (4) cloudy; according to cloud covers from 0 to 33, 34 to 65, 66 to 95, and 96 to 100% of effective cloud amounts (Schreiner et al., 1993).

Table 1
Technical specifications of our UAV-based monitoring systems.

| setup	UAV	camera	manufacturer	sensor size	resolution	focal length
1	Inspire 2	Zenmuse X5S	DJI	4/3-inch	5280 × 3956 px	45 mm
2	Phantom 4 RTK	gimbal-attached	DJI	1-inch	5472 × 3648 px	8.8 mm
3	Phantom 4 PRO	gimbal-attached	DJI	1-inch	5472 × 3648 px	8.8 mm

2.4. Collecting ground truth

Ground truth object (GT) was defined as the number of crops counted per plot. Crops were labeled and counted manually in images for each plot from the segmented orthomosaic image. In total, 24, 84, 120, 20, and 40 plots were counted for locations 1–5, respectively. In the case of location 3, the counts were done separately for each flight date (Table 2).

2.5. Estimation of crop density and distance

Crop density (CD) in crops per m^2 was calculated per plot by using the ground truth counts. Because the size of the plots in each location was the same but different between locations, the average GT (counted crops) and the average CD was calculated per location. Intra-row distance (D) was calculated by using GT and the number of rows and row length of each plot.

2.6. Fully convolutional network-based plant classification

In this publication, the principal axis of the young shoot of sugar-beet seedling will be consider as stem. Keeping this clarification in mind, this section describes our FCN-based approach for joint plant classification and stem detection, which is based on a previous publication which was implemented in Python (Keras) (Lottes et al., 2018). This system provides two outputs simultaneously. First, a plant mask represents a pixel-wise classification considering the classes crop, weed, and background (mostly soil). Second, the stems' positions for the detected crop and weed objects are represented by a stem mask. The approach's key architectural design feature is that the network shares the encoded features for classifying the stem regions and the pixel-wise classification using one encoder network and two task-specific decoder networks.

The processing pipeline executes the following key steps and is illustrated in Fig. 2. First, each image was preprocessed. Next, the pre-processed images were fed into the one-encoder-two-decoder structured fully convolutional network. Outputs first include a per-pixel probability distribution $P(\omega^{plant}|Z)$ for describing the plant classification over the desired class labels $\omega^{plant} \in \{crop, weed, soil\}$ for each observed pixel (Z); second, a per-pixel probability distribution $P(\omega^{stem}|Z)$ with $\omega^{stem} \in \{crop, weed, soil\}$ representing regions within the image, which correspond to crop and weed stems. The label for each pixel is determined as the one with the highest probability by: (see Figs. 3 and 4)

$$\hat{\omega} = \underset{\omega}{\mathrm{argmax}} P(\omega^{stem}|Z). \tag{1}$$

Finally, pixel-accurate stem positions were extracted, i.e., the stem mask, through a post-processing step, which will be described in Section 2.7.

Table 2
Trial fields, location, crop, growing stage and flight specifications.

No.	location	GPS-coordinates	crop	BBCH	flight date	sky	setup	height	GSD
1	(1) Göttingen	51°33N9°53E	sugar beet	14–16	22.05.2019	cloudy	1	40 m	3.0 mm
2	(2) Börßum	52°40N10°35E	sugar beet	16–18	28.05.2019	middle cloudy	1	40 m	3.0 mm
3	(3) Höckelheim	51°42N9°57E	sugar beet	12	03.09.2019	cloudy	2	6 m	1.5 mm
4				12–14	11.09.2019	clear	2	6 m	1.5 mm
5				14–16	20.09.2019	low cloudy	2	6 m	1.5 mm
6	(4) Klein-Altendorf	50°36N6°59E	maize	13–17	25.05.2018	low cloudy	3	10 m	3.0 mm
7	(5) Klein-Altendorf	50°36N6°59E	strawberry	13–16	28.06.2018	low cloudy	1	40 m	3.0 mm
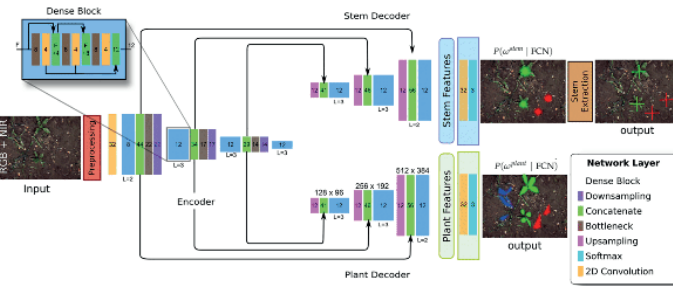
Fig. 2. FCN architecture. Encode of input images using the encoder and following by the pass the feature volumes to the task-specific decoders, the stem and the plant decoder. Obtained outputs were: the plant mask considering the classes crop, weed, soil for the pixel-wise classification of the plants, and the stem mask considering the classes crop, weed, soil for the segmentation crop-weed stem regions. Finally, the extraction of the stem positions from the stem mask in the stem extraction. Inside the layers, it is shown the number of output features maps. L represents the number of stacked consecutive 2D convolutional layers.
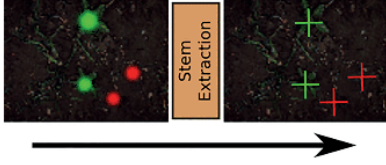
4

30

Fig. 3. **Extraction of pixel-wise stem locations** by computing a weighted center of mass of the stem regions predicted by the FCN. For the weighting, it was considered the predicted probabilities for each pixel belonging to a stem region.

2.6.1. Image preprocessing

The preprocessing step was applied to image patches obtained from orthomosaics. These images presented a width and height dimension of 512 pixels, and 1 *mm* of GSD after downsampling. To deliver high performance of the classifiers the different input data was preprocessed. In preprocessing steps, transformations were applied to the data to reduce its complexity and standardize it to some degree, increasing the chance that the machine-learning algorithm can provide better performance than without preprocessing it. Technically speaking, preprocessing can improve a classification system's generalization capabilities by aligning the training and test data distribution. The preprocessing was performed independently for each image and separately on all channels, i.e., red, green, blue. First, noise from each channel was removed by performing a blurring operation using a $[5 \times 5]$ Gaussian kernel given by the standard normal distribution, i.e., $\mu = 0$ and $\sigma^2 = 1$. Second, each image channel was standardized by its mean and standard deviation, respectively. Third, contrast stretch of the intensities to the range $\lfloor -0.5, 0.5 \rfloor$ was performed, which implies a zero-centering of the data.

2.6.2. One-encoder two-decoder network architecture

Fig. 2 depicts the proposed architecture of our joint plant and stem detection approach. This approach's main processing steps are the preprocessing (red), the encoder, the plant decoder, the stem decoder, and the stem extraction (brown).

Two separate feature volumes were generated from the encoded and compressed visual code, one specialized for pixel-wise plant classification, and another for stem detection. Thus, two task-specific decoders were obtained, which perform an upsampling using a stridden transpose convolution (Dumoulin and Visin, 2016) with $[2 \times 2]$ kernel and a stride of 2. Both decoders also use dense blocks as their main building blocks and follow the same architectural design to produce the plant features and stem features. Moreover, both task-specific decoders use feature maps produced by the encoder through skip connections. The corresponding feature maps was concatenated by sharing the same spatial resolution from the encoder before using dense blocks for feature computation. Skip connections from the encoder to the decoders facilitate the recovery of spatial information (Badrinarayanan et al., 2015).
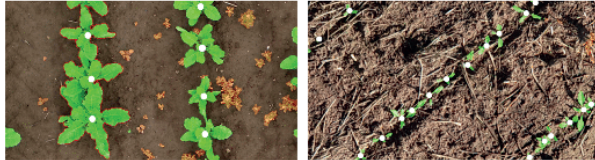
Finally, the feature maps produced by the stem decoder and the plant decoder was transformed into the pixel-wise probability distribution over their respective class labels by a 1×1 convolution followed by a softmax layer to obtain $P(\omega^{plant}|Z)$ and $P(\omega^{stem}|Z)$. Note that It was tried to predict the area of the stem instead of regressing the stem location. This is key to use the same architecture for learning plant classification and stem locations.

2.6.3. FCN training

For learning, an NVIDIA 2080 TI card with 11 GB of VRAM was part of the equipment for our experiment. A dataset of 500 RGB images were used in a ratio of 75%, 5% and 20%, from these 375 images were considered for training and 25 images for validation as mentioned in Lottes et al. (2018,). Additional 100 images were used as testing dataset. For better results, all datasets were diversified according image conditions by considering weed pressure, illumination, and growing stage. A multi-task loss $\mathcal{L}$ was used combining the loss for the plant segmentation $\mathcal{L}_{plant}$ and the loss for the stem region segmentation $\mathcal{L}_{stem}$ as follows:

$$\mathcal{L} = (1 - \alpha)\mathcal{L}_{stem} - \alpha\mathcal{L}_{plant}, \tag{2}$$

where $\alpha = 0.5$. The loss $\mathcal{L}_{plant}$ is the weighted cross-entropy, where errors regarding the crop plants and weeds were penalized by a factor of 10. The loss $\mathcal{L}_{stem}$ is based on an approximation of the intersection over union (IoU) metric, as it is more stable with imbalanced class labels (Rahman and Wang, 2016), which is the case in our problem with underrepresented stems as compared to the amount of soil. The multi-task loss also enables the sharing of information for learning the encoder, which can use the loss information from both decoders in the backward pass of the backpropagation. The stem locations were encoded as blobs with a diameter of 10 mm in object space for training.

2.7. Stem Extraction

Given the probability distribution $P(\omega^{stem}|Z)$ encoding regions within the image, which correspond to crop stems and weed stems, a well-defined stem detection by a specific pixel location for the crop and weeds was desired. To this end, it was firstly calculated the stem mask according to Eq. 1 by selecting the class with the highest label probability for each pixel. Next, the connected components $\mathcal{C}_j^\omega$ was determined for the crop and weed class and computed the weighted mean $\bar{\mathbf{x}}_j^\omega$ of the pixel locations by:

$$\bar{\mathbf{x}}_i^m = \frac{\sum_{\mathbf{x} \in \mathcal{C}_i^\omega} P(\omega = \omega | \mathbf{x}) \cdot \mathbf{x}}{\sum_{\mathbf{x} \in \mathcal{C}_i^\omega} P(\omega = \omega | \mathbf{x})}, \tag{3}$$

with $\omega = $ crop,weed. The weighted means $\bar{\mathbf{x}}_i^m$ for class c are then the stem detections that are reported by our approach.

Fig. 4. Illustration of **difficult conditions for counting plants** using vision-based classification approaches. Left: Mutually overlapping sugar beets. Right: Due to narrow seeding, the sugar beets overlap early after the emergence phase. In addition, individual and contiguous plants are separated by straw in the image space.

2.7.1. FCNs applicability for crop counting using adapted transfer learning

Trained data based on a from previous for sugar beets was used and can therefore realize a stable primary classifier. The classifiers' adaptation to strawberries and maize was made with additional training data from earlier projects in a supervised transfer learning manner, i.e., through a re-training of the model with further training data that includes strawberries and maize samples. The dataset used for training individual classifier for strawberry and maize, consisted of 130 RGB images per crop, considering from this total 120 images for training and 10 images for testing with a resolution of 512 × 512 pixels (Section 2.6.1). No validation set was used in this transfer learning stage because it was tried to minimize modifications in hyperparameter settings. For processing the test dataset, patch images presented a resolution of 2048 × 2048 pixels, and the processing-time per image was around 0.4 s with the hardware mentioned on Section 2.6.3.

2.8. Evaluation Metrics

After checking the absence of outliers, normality of variables, linearity, and homoscedasticity of each location, the Pearson Product-Moment Correlation Coefficient (PPMC) was calculated to determine the degree of linear correlation and whether significant differences exist between prediction (P) and GT in terms of counted crops.

Forecast error of pipeline approach was determined by calculating the mean bias error (MBE), mean absolute error (MAE), and mean absolute percentage error (MAPE) (Shcherbakov et al., 2013; Kato, 2016). For a better agricultural interpretation, MAE was calculated per unit of evaluated area (MAEA) and the area for unitary predicted error is given as A_e.

The systematic error to under- or over-forecast of the pipeline approach was evaluated by using the MBE parameter, this was defined by Eq. 4:

$$MBE = \frac{1}{N} \sum_{i=1}^{N} (P_i - GT_i)$$
(4)

where:

- N = total number of forecast events
- i = forecast event for plant counting in a plot
- GT_i = ground truth plant count
- P_i = prediction count

The magnitude of the forecast error was determined by the MAE of the predicted event given by:

$$MAE = \frac{1}{N} \sum_{i=1}^{N} |P_i - GT_i|$$
(5)

Based on the ground truth plant count, a percentage error of all forecast events was quantified using the MAPE of predicted numbers of crop plants by the following Eq. 6:

$$MAPE = \frac{1}{N} \sum_{i=1}^{N} 100 \times \left| \frac{GT_i - P_i}{GT_i} \right|$$
(6)

By considering MAE as a scaled magnitude of forecast error of events and as a forecast event is applied in a specific area of the field, the MAEA expresses the number of crop units, which are under- or over-counted per unit area (Eq. 7):

$$MAEA = \frac{MAE}{a}$$
(7)

where:

- MAE = mean absolute error expressed in counted crop units

- a = area of forecast event

The area for unitary forecast error (Ae) is derived from MAEA. It is interpreted as the area to under- or over-count a crop by the employed pipeline approach (Eq. 8):

$$A_e = \frac{1}{MAEA}$$
(8)

3. Results

For all locations the average of counted and predicted crops presented a strong and significant correlation (Table 3).

3.1. Proof of concept assessments

The average of counted and predicted plant numbers were 232.3 and 228.1, and 95.9 and 95.8 plants for location 1 and 2, respectively (Table 3). The number of counted plants allows determining the CD values for locations 1 and 2, 10.75 and 10.15 plants/m². The average intra-row distance calculated was 21 and 22 cm, respectively, for locations 1 and 2.

The use of FCN pipeline delivers a negative MBE value in both locations or tends to under-count sugar-beet plants (Table 3). In location 1, MAE's magnitude is four sugar-beet plants in a plot area of 21.6 m^2 and with plants at BBCH 14–16. According to the definition of MAEA and Ae, in location 1 and at BBCH 14–16; for every 4.8 m², one sugar-beet plant is wrongly considered in the count. In location 2, the pipeline presents the lowest MAE and the highest correlation (PPMC = 0.95), the magnitude for the count error is less than a plant for every plot area of 9.5 m² at BBCH 16–18. The Ae value shows that one sugar-beet plant is wrongly counted every 26.0 m² under field arrangement conditions of location 2 and at BBCH 16–18. The lowest MAPE value is shown between both locations with the growing stage of BBCH 16–18 in sugar beet.

3.2. Low intra-row distance in time series

The time-series assessment of location 3 delivers the counted number of crop plants per plot between 181.6 and 184.4, with the highest plant number at 17 das. The predicted average number of crops presents a range from 180.8 to 181.4 plants per plot, with the highest amount of counted plants at 34 das (Table 3). The average value of crop density in the trial decreased from 19.6 to 19.2 plants/m² through the three measurements.

Over the monitoring period, predictions present negative MBE values or a tendency to under-count crop plants similarly to locations 1 and 2 (Table 3). The magnitude of the error count range between 7 and 8 sugar beets per plot. The Ae value range between 1.3 and 1.5 m². Either the smallest error or the highest degree of correlation was found at BBCH 14–16 with a MAPE value of 3.96% and a PPMC of 0.83.

Sugar-beet plants presented an average soil cover of 1.14 ± 0.31%, 1.95 ± 0.67%, and 2.90 − 0.88% at 17, 25 and 34 das (Fig. 5). Furthermore, weeds covered the soil with average values of 1.05%, 1.19%, and 1.80% at the previously mentioned dates, and the respective standard deviations were 0.03%, 0.26%, and 0.46%.

3.3. Generalized application of trained FCN to maize and strawberry

The average of counted and predicted crop numbers for the maize and strawberry field was 153.6 and 157.4, 29.1 and 30.2 plants, respectively (Table 3). The CD value for the maize field was 9.49 plants/m², and in the case of the strawberry field, crop density was 0.36 plants/m².

The forecast events for counting maize and strawberry plants present positive MBE values or a tendency to over-count crops in the plot

Table 3
experimental results for crop counting, calculation of plant distribution parameters, and error metrics based on predicted crop numbers for sugar beet, maize and strawberry fields.

location	crop	trial configuration					prediction & calculations			metrics					
		PN	das	BBCH	GSD	GT	P	PD^a	D^a	MBE	MAE	MAEA	Ae	MAPE	PPMC
1	sugar beet	24	43	14–16	3.0	232.3	228.1	10.75	0.21	4.21	4.46	0.21	4.84	1.92	0.86 *
2	sugar beet	84	48	16–18	3.0	95.9	95.8	10.15	0.22	0.08	0.42	0.04	26.04	0.43	0.95 *
3	sugar beet	40	17	12	1.5	185.4	180.8	19.62	0.11	−4.65	8.40	0.77	1.29	4.57	0.82 *
	sugar beet		25	14–16	1.5	182.0	181.3	19.26	0.12	−0.70	7.10	0.65	1.53	3.96	0.83 *
	sugar beet		34	16–18	1.5	181.6	181.4	19.22	0.12	−0.18	8.03	0.74	1.35	4.44	0.78 *
4	maize	20	-	14–16	3.0	153.6	157.4	9.49	0.19	3.80	3.90	0.24	4.15	2.55	0.92 *
5	strawberry	40	-	16	3.0	29.1	30.2	0.36	0.31	1.05	1.15	0.13	7.83	3.96	0.67 *

where: PN = plot number, das = days after sowing, BBCH = growing stage, GSD = ground sample distance in mm, GT = average value of ground truth expressed in number of plants, P = average value of predictions expressed in number of plants, PD = plant density in plants per m^2, D = distance of crops in the row in m considering a row distance of 45 cm for sugar beets, and 56 and 100 cm for maize and strawberry respectively, MBE = mean bias error, MAE = mean absolute error in $plant/plot$, MAEA = mean absolute error of predicted area in plants per m^2. Ae= area for unitary forecast error in m^2 per plant, MAPE = mean absolute percentage error in percentage, PPMC = Pearson product-moment correlation coefficient. (*) significance level of α = 0.05. (a) Parameter based on ground truth data.
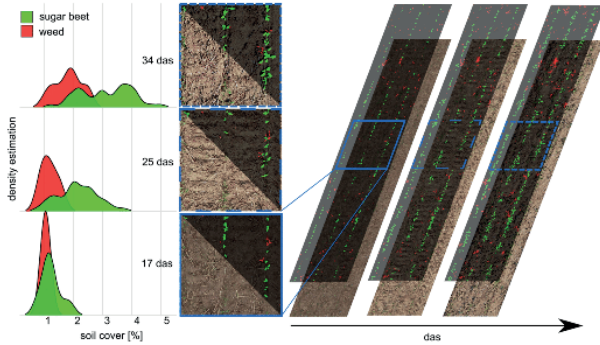
Fig. 5. **Development of vegetation cover**: time series labeling of sugar beet (green) and weed (red) covered area at 17, 25 and 34 das. (*) Density estimation of 40 plots of trial field located in Höckelheim (location 3). Evaluated field area 9.5 m^2.

(Table 3). In the maize field, MAE's magnitude is almost four plants per plot. In the strawberry field, the MAE value is more than one plant in a plot. The Ae value is 4.1 and 7.8 respectively for the maize and strawberry.

4. Discussion

4.1. Effect of the monitoring system and the system resolution for plant counting

A relevant task is the development of approaches which can be generalized across measuring systems, different fields and/or different crops. By using three different sensor and UAV setups, this contribution confirms that the previously tested and used pipeline (Lottes et al., 2018), can be generalized to evaluate RGB UAV-based images. Nevertheless, the principal difference was observed during the establishment of a flight plan, setup 1 in comparison with setup 2 and 3 (Table 1), presented a bigger sensor size (4/3-inch against 1-inch) and a longer focal length (45 against 8.8 mm), that allows a greater field of view in high resolution as mentioned in Pepe et al. (2018), and therefore this system was able to map bigger field area with the same flight time. No advantages in terms of reduced flight lines and use of fewer GCPs were observed for the setup 2 with real-time kinematic (RTK) system (Rabah

et al., 2018), probably related to the small size of the mapped area and the less challenging and planar characteristics of the observed object, in this case, the trial field with small vegetation during first growing stages.

The principal changing factor, the ground sample distance, is not a limiting factor for the dataset with lower resolution (GSD of 0.3 cm). Sa et al. (2018) mentioned that a resolution of 0.85–1.18 cm (GSD) can compromise performance of weed detection by using a Deep Convolutional encoder-encoder architecture for crop/weed segmentation. This study found that in early season a classification between crops and weeds is difficult because of morphological similarities. Using image resolutions of 0.02, 0.2, and 0.5 cm (GSD) and a similar image processing approach, Lottes et al. (2017) mentioned that field arrangement is the best supporter for detection of crop and weeds, highlighting the importance for row detection and the spatial relationships among multiple individual plants which remain constant at the mentioned image resolutions.

4.2. Sky conditions

In the past, it was affirmed that the use of spectral images in high resolution for the analysis of vegetation could negatively affect the classification of areas under shadows. This phenomenon could lead to a false interpretation of physiological and metabolic activities (Zarco-

7

33

Tejada et al., 2013). In our time-series case using RGB-images, the lowest forecast error is acquired under clear sky conditions, which tells us that the used FCN pipeline approach could be used in shaded scenarios without losing performance. Another possibility is to expect a lower MAPE value under more favorable sky conditions; this means that under the same date and place of experimental field, but different sky condition like cloudy/ no-shaded scenario, the forecast error can be lower than 3.96% (Table 3). The employed time series analysis has to be contrasted with similar categories of crop growth stage conditions (BBCH 12, 12–14 and 14–16) and weed pressure and in various sky conditions to determine the effect of shadow in the counting performance.

4.3. Intra-row distance as a critical factor for a FCN pipeline

In this study, the experimental field with 11–12 cm intra-row distance presented a high emergence of wheat from previous seasons, correctly classified as weeds. We furthermore avoid using herbicide in this experiment to increase the chances of emerging intra-row weeds. The detection of sugar-beet stems and hence counting of crop plants can be performed with an average precision of 78.8% by using UAV-RGB images in grass plants' presence according to past results (Lottes et al., 2018), supporting observed outputs of the time-series analysis. In the past, a similar study based on mask R-CNN approach using robot-based RGB images for detection of common beans and maize presented similar precision values for crop segmentation (60–80%) and highlighted the importance of the weed cover for misdetection (Champ et al., 2020), this study found that small weed cover presents a high probability to be pixel-wise classified and counted as a crop by calculating the barycenter. A YOLOv3 CNN architecture also mentioned a high mean average precision of 86% for counting stems in cotton seedling, although the effect of weed pressure was not evaluated, there are some disadvantages by overlapping and detecting small seedling (Oh et al., 2020).

The intra-row distance of 21–22 cm presented, over all categories of growing stages, less counting error than the intra-row distance of 11–12 cm. In the past, CNN and FCN pipelines for crop/weed detection used images containing crops arranged in a typical distribution, 15–25 cm of intra-row distance, and 30–60 cm distance between rows (Sa et al., 2018; Lottes et al., 2018). For the employed pipeline, images for training presented crops distributed in the same fashion. By observing the output images, an explanation of the higher rate of under-counting crops by low

intra-row distance is that neighbor sugar-beet stems are difficult to count. Sometimes two plants are counted as one, mostly if the midrib and tip leaf is aligned and substantially close to the neighbor crop stem (Fig. 6a).

4.4. Importance of growing stage for successful counting

In this paper, one of our main purpose is to specify optimal conditions for plant counting. In the vegetation period, crop growth is dynamic, and UAV-flights to capture images have to be performed on time to obtain the best results. To provide crop numbers, the determination of stem position in different growth stages is a crucial point, the performance to detect stems of plants with two-leaf to later growth stages can achieve 95.5% of precision and 98.0% of recall according to a past experience, but the best growth stage was not specified (Lottes et al., 2019). This study specifies that the optimal growth stage is dependent on intra-row distance. For the case of practice fields or intra-row distance of 20–21 cm and 45 cm between rows, the flight has to be performed in preference between 16–18 BBCH stage compared with the BBCH 14–16. In experimental fields with an intra-row distance of 11–12 cm, UAV-flight provides the best results with the BBCH stage of 14–16.

4.5. RGB-UAV for monitoring sugar beet/weed competition

In a past experiment, Lottes et al. (2018) determined plant-soil cover by labeling pixel-wise images into crop and weed; for their objective, they used RGB-NIR images containing sugar beets in different growth stages obtained from field robot platform and a similar FCN pipeline. After optimization and analysis of performance, the pixel-wise approach achieved 91% of F1-score. Our study is based on the above-mentioned excellent performance to determine the soil cover of weeds and sugar beets. In this way, we have used a similar approach that focuses on UAVs' importance for agronomic application. This includes using the advantage of UAVs for flexible image acquisition in the agronomic goal of weed control (Peña et al., 2013) and the possibility to support the decision for weeding during the entire critical period of competition, which usually takes place between BBCH 14 and 32 during approximately 21–28 days under normal growing conditions (Petersen, 2004). A point to clarify in future studies is which threshold of sugar beet/weed coverage is the most effective to reduce yield losses by using a specific weed control method.
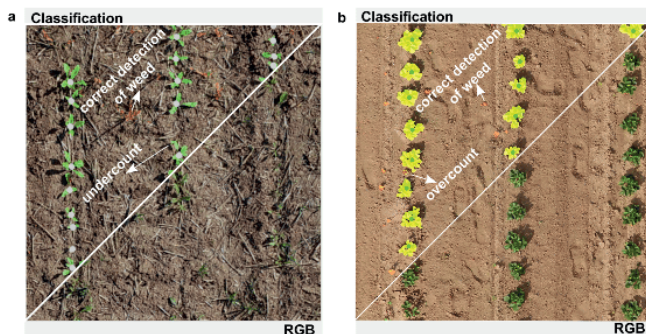

Fig. 6. Counting performance after classification in the upper left triangle: (a) counted sugar-beet plants (white dots) and one under-count of sugar-beet stem at 34 days after sowing in Höckelheim - location 3 (b) performance of a sugar-beet image processing pipeline extended to a strawberry field, counted strawberry (green dots) over-count case of false classification of weed (red dot) - location 5. The lower right triangle shows the original RGB patch image.

4.6. Pipeline extension to additional crops

By analyzing the pipeline outputs, maize and strawberries' over-counting is related to crop counting of stems belonging to weeds located in the intra-row space (Fig. 6b). A similar phenomenon of overestimation was observed in the past, but not by over-counting but by over-segmenting (Bosilj et al., 2019). The mentioned work also transferred learning from a SegNet CNN model by retraining from sugar beets to onions data. This tendency of overestimation must slightly impact the Precision from the transferred crop and is an aspect to study in future investigations. Despite this, calculated results show low counting errors, and as mentioned on Section 4.1 crops distribution, and regular intra-row distance should be the principal reasons for control-ling the counting after retraining a model on a small scale.

In this extension, the counting error for other dicot as strawberry is higher than the error from a monocot as maize. The same effect was observed in a past study using transfer of knowledge of a CNN approach from sugar beets to carrots and onions (Bosilj et al., 2019). In this experience, the monocot crop presented 2% less performance drop than a dicot crop by a pixel-wise classification of the input image. Quan et al. (2019) mentioned, that pixel-wise segmentation of maize seedlings can achieve a segmentation of up to 98% using RGB-images and a faster R-CNN approach, and sunny conditions can negatively influence the performance of seedling detection. Furthermore, a precision of up to 95% was reported using RetinaNet and CenterNet CNN architectures for counting maize seedling (Karami et al., 2020). Nevertheless, the per-formance of this approach could not be contrasted due to the lack of a labeled testing dataset. This paper confirms the feasibility of using a pipeline developed and modeled for sugar beets and applying it with less labeling effort on maize and strawberry fields. Counting error is lower than 4% and less or as high as the experimental field with low intra-row distance.

5. Conclusion

Monitoring and counting crops on the field are of high interest for farmers, experimental fields, and the seed-producing industry. The presented UAV-RGB image processing pipeline can deliver the number of sugar beets on the field with an error lower than 4.6%. The intra-row distance and the growing stage of sugar beets are relevant parameters for accurate plant counting. This evaluated variables present the most effective constellation with a crop distance of 21–22 cm and at BBCH 16–18. In experimental-field plant density, with an intra-row distance of 11–12 cm, the smallest forecast error for crop number is shown at BBCH 12–14. The extension of the previously trained FCN pipeline to other crops is possible with a small training dataset, the errors of predictions are lower than 4% by evaluating practical fields of maize and straw-berry, which highlights the potential use of the image processing approach to wide numbers of crops. Overall, considering the parameters as mentioned earlier, automatic monitoring of crop fields using UAV-images followed by proper processing of these can output reliable in-formation that increases efficiency in the crop production by reducing the manual counting effort of the farmers.

Author contributions

conceptualization, A.B, P.L., C.S., S.B., A.K.M and S.P.; methodology, P.L., A.B., F.I., C.S. and S.P.; validation, A.B, P.L., N.A.W and S.B.; formal analysis, P.L., A.B., F.I and S.P.; investigation, A.B, P.L., N.A.W and S.B.; resources, P.L., C.S, S.B. and A.K.M; writing-original draft preparation, A.B. and P.L.; writing-review and editing, all authors; visualization, A.B., P.L. and S.P.; supervision, C.S., A.K.M. and S.P; funding acquisition, P.L., C.S. and A.K.M.

Declaration of Competing Interest

The authors declare that they have no known competing financial interests or personal relationships that could have appeared to influence the work reported in this paper.

References

Badrinarayanan, V., Kendall, A., and Cipolla, R. (2015). Segnet: a deep convolutional encoder-decoder architecture for image segmentation. Computing Research Repository (CoRR), abs/1511.00561.

Bosilj, P., Aptoula, E., Duckett, T., Cielniak, G., 2019. Transfer learning between crop types for semantic segmentation of crops versus weeds in precision agriculture. Journal of Field Robotics 37 (1), 7–19.

Champ, J., Mora-Fallas, A., Goëau, H., Mata-Montero, E., Bonnet, P., Joly, A., 2020. Instance segmentation for the fine detection of crop and weed plants by precision agricultural robots. Applications in Plant Sciences 8 (7).

Cioni, F., Maines, G., 2010. Weed control in sugarbeet. Sugar Tech 12 (3), 243–255.

Deng, L., Mao, Z., Li, X., Hu, Z., Duan, F., Yan, Y., 2018. UAV-based multispectral remote sensing for precision agriculture: A comparison between different cameras. ISPRS Journal of Photogrammetry and Remote Sensing 146, 124–136.

Dumoulin, V. and Visin, F. (2016). A guide to convolution arithmetic for deep learning. ArXiv, abs/1603.07285.

Durrant, M., Brown, S., Bould, A., 1983. The assessment of the quality of sugar-beet seed. The Journal of Agricultural Science 104 (1), 71–84.

Karami, A., Crawford, M., Delp, E.J., 2020. Automatic plant counting and location based on a few-shot learning technique. IEEE Journal of Selected Topics in Applied Earth Observations and Remote Sensing 13, 5872–5886.

Kato, T., 2016. Prediction of photovoltaic power generation output and network operation. In: Integration of Distributed Energy Resources in Power Systems. Elsevier, pp. 77–108.

Kunz, C., Schröllkamp, C., Koch, H.-J., Eßer, C., Lammers, P.S., 2015. Potentials of post-emergent mechanical weed control in sugar beet to reduce herbicide inputs. Landtechnik 70 (3), 67–81.

Lottes, P., Behley, J., Chebrolu, N., Milioto, A., Stachniss, C., 2018. Joint stem detection and crop-weed classification for plant-specific treatment in precision farming. In: IEEE International Conference on Intelligent Robots and Systems, pp. 8233–8238.

Lottes, P., Behley, J., Chebrolu, N., Milioto, A., Stachniss, C., 2019. Robust joint stem detection and crop-weed classification using image sequences for plant-specific treatment in precision farming. Journal of Field Robotics 37 (1), 20–34.

Lottes, P., Behley, J., Milioto, A., Stachniss, C., 2018. Fully convolutional networks with sequential information for robust crop and weed detection in precision farming. IEEE Robotics and Automation Letters 3 (4), 2870–2877.

Lottes, P., Khanna, R., Pfeifer, J., Siegwart, R., Stachniss, C., 2017. UAV based crop and weed classification for smart farming. In: 2017 IEEE International Conference on Robotics and Automation (ICRA), pp. 3024–3031.

Lu, H., Liu, L., Li, Y.N., Zhao, X.M., Wang, X.Q., Cao, Z.G., 2021. TasselNetV3: Explainable plant counting with guided upsampling and background suppression. IEEE Trans. Geosci. Remote Sens. 1–15.

Märländer, B., 1990. Einfluss der bestandesdichte auf ertrags- und qualitätskriterien sowie über mögliche ursachen der konkurrenz in zuckerrübenbestanden. Agronomy & Crop. Science 130.

McCool, C., Perez, T., Upcroft, B., 2017. Mixtures of lightweight deep convolutional neural networks: Applied to agricultural robotics. IEEE Robotics and Automation Letters 2 (3), 1344–1351.

Milošević, M., Vujaković, M., Karagić, D., 2010. Vigour tests as indicators of seed viability. Genetika 42 (1).

Oh, S., Chang, A., Ashapure, A., Jung, J., Dube, N., Maeda, M., Gonzalez, D., Landivar, J., 2020. Plant counting of cotton from UAS imagery using deep learning-based object detection framework. Remote Sensing 12 (18), 2981.

Peña, J.M., Torres-Sánchez, J., de Castro, A.I., Kelly, M., López-Granados, F., 2013. Weed mapping in early-season maize fields using object-based analysis of unmanned aerial vehicle (UAV) images. PLoS ONE 8 (10), e77151.

Pepe, M., Fregonese. L., Scaioni, M., 2018. Planning airborne photogrammetry and remote-sensing missions with modern platforms and sensors. European Journal of Remote Sensing 51 (1), 412–436.

Petersen, J., 2004. A review on weed control in sugarbeet. In: Weed Biology and Management. Springer, Netherlands, pp. 467–483.

Puspišil, M., Puspišil, A., Rastija, M., 2000. Effect of plant density and nitrogen rates upon the leaf area of seed sugar beet on seed yield and quality. Eur. J. Agron. 12 (1), 69–78.

Quan, L., Feng, H., Lv, Y., Wang, Q., Zhang, C., Liu, J., Yuan, Z., 2019. Maize seedling detection under different growth stages and complex field environments based on an improved faster R-CNN. Biosyst. Eng. 184, 1–23.

Rabah, M., Basiouny, E.-G., Ghanem, E., Elhadary, A., 2018. Using RTK and VRS in direct geo-referencing of the UAV imagery. NRIAG Journal of Astronomy and Geophysics 7 (2), 220–226.

Rahman, M., Wang, Y., 2016. Optimizing intersection-over-union in deep neural networks for image segmentation. 10072, 234–244.

Sa, I., Popović, M., Khanna, R., Chen, Z., Lottes, P., Liebisch, F., Nieto, J., Stachniss, C., Walter, A., Siegwart, R., 2018. WeedMap: a large-scale semantic weed mapping framework using aerial multispectral imaging and deep neural network for precision farming. Remote Sensing 10 (9), 1423.

Schreiner, A.J., Unger, D.A., Menzel, W.P., Elrod, G.P., Strabala, K.I., Pellet, J.L., 1993. A comparison of ground and satellite observations of cloud cover. Bull. Am. Meteorol. Soc. 74 (10), 1851–1862.

Shcherbakov, M., Brebels, A., Shcherbakova, N., Tyukov, A., Janovsky, T., Kamaev, V., 2013. A survey of forecast error measures. World Applied Sciences Journal 24, 171–176.

Smit, A., 1993. The influence of sowing date and plant density on the decision to resow sugar beet. Field Crops Research 34 (2), 159–173.

Söğüt, T., Arioglu, H., 2004. Plant density and sowing date effects on sugarbeet yield and quality. Journal of Agronomy 3 (3), 215–218.

Tong, P., Han, P., Li, S., Li, N., Bu, S., Li, Q., Li, K., 2021. Counting trees with point-wise supervised segmentation network. Eng. Appl. Artif. Intell. 100 (February).

Wu, X., Aravecchia, S., Lottes, P., Stachniss, C., Pradalier, C., 2020. Robotic weed control using automated weed and crop classification. J Field Robotics.

Zarco-Tejada, P., Guillén-Climent, M., Hernández-Clemente, R., Catalina, Á., González, M.-R., Martín, P., 2013. Estimating leaf carotenoid content in vineyards using high resolution hyperspectral imagery acquired from an unmanned aerial vehicle (UAV). Agric. For. Meteorol. 171–172, 281–294.

CHAPTER 4: Plant-based disease quantification - Manuscript II

Sensing the occurrence and dynamics of Cercospora leaf spot disease using UAV-supported image data and deep learning

Facundo Ramón Ispizua Yamati, Abel Barreto, Maurice Günder, Christian Bauckhage, Anne-Katrin Mahlein; 2022.

Author contributions

Agriculture/Landwirtschaft

Facundo R. Ispizua Yamati; Abel Barreto; Maurice Günder; Christian Bauckhage; Anne-Katrin Mahlein

Sensing the occurrence and dynamics of Cercospora leaf spot disease using UAV-supported image data and deep learning

Erfassung des Auftretens und der Dynamik von Cercospora-Blattflecken-krankheit mittels UAV-gestützter Bilddaten und Deep Learning

The most damaging foliar disease in sugar beet is Cercospora leaf spot (CLS), caused by *Cercospora beticola* Sacc. The pathogen is expanding its territory due to climate conditions, generating the need for early and accurate detection to avoid yield losses. In Germany, monitoring and control strategies are based on visual field assessments, with the parameter disease incidence (DI). This parameter triggers warning systems when a threshold is achieved, and decision-making takes place for fungicide application. However, visual scoring is a time-consuming activity that requires well-trained personnel and is the principal bottleneck for CLS control. Digital technologies can support this process. Thus, the present work is based on two trial fields conducted and monitored in 2020 using an unmanned aerial vehicle (UAV) equipped with a multispectral camera. Image data were collected in time series during the vegetation period. Trials were sown with different sugar beet varieties; for field management, there was employed diverse fungicide strategies, and artificial inoculation took place in a spot manner. Parallel to the flight mission and additional assessment of DI, disease severity (DS) via KWS scale was collected by experts as so-called ground truth (GT). Combined with image-processing, it was possible to catalogize plants in field trials, identify them over time, and use them for training and testing models. A convolutional neural network (CNN) supported by cataloged data was trained to perform classification of the disease presence in time-series, and performance was evaluated. As the last image processing step, maps were generated showing site-specific distribution of the diseased plants in the field. Generated maps can serve as a basis for application maps in practical cultivation or the evaluation of variety performance in variety trials. The presented methodological approach provides high precision and sensitivity in CLS detection and offers the potential to automate processes of CLS monitoring for different application areas.

Key words: *Cercospora beticola*, convolutional neural network, disease incidence, disease severity

Die Cercospora-Blattfleckenkrankheit (CLS, engl. Cercospora leaf spot) ist die bedeutendste Blattkrankheit bei Zuckerrüben. Der pilzliche Erreger *Cercospora beticola* Sacc. breitet sich aufgrund klimatischer Bedingungen immer weiter aus, eine frühzeitige und genaue Erkennung ist wichtig, um Ertragseinbußen zu vermeiden. In Deutschland beruhen die Überwachungs- und Bekämpfungsstrategien auf visueller Bewertung der Felder mit dem Parameter Befallshäufigkeit (disease incidence = DI). Dieser Parameter löst bei Erreichen eines Schwellenwerts Warnsysteme aus, woraufhin Entscheidungsschritte für den Einsatz von Fungiziden getroffen werden. Die visuelle Bonitur ist jedoch eine zeitaufwändige Tätigkeit, die gut geschultes Personal erfordert und einen großen Engpass bei der CLS-Bekämpfung darstellt. Digitale Technologien können diesen Prozess unterstützen. Die vorliegende Arbeit basiert daher auf zwei Versuchsfeldern, die im Jahr 2020 mit Hilfe eines unbemannten Luftfahrzeugs (UAV), das mit einer Multispektralkamera ausgestattet ist, angelegt und überwacht wurden. Die Bilddaten wurden während der Vegetationsperiode als Zeitreihe erfasst. In den Versuchen wurden verschiedene Zuckerrübensorten ausgesät, verschiedene Fungizidstrategien eingesetzt und es erfolgte eine künstliche Inokulation. Parallel zur Flugmission und zusätzlichen visuellen Beurteilung der Befallshäufigkeit wurde die Befallsstärke (disease severtity = DS) mittels KWS-Skala von Experten als sogenannte Ground Truth (GT) erhoben. In Kombination mit der Bildverarbeitung war es möglich, Pflanzen in den Feldversuchen individuell zu katalogisieren, über die Zeit zu identifizieren und für das Training und Testen von Modellen zu verwenden. Mit Hilfe der katalogisierten Daten wurde ein Convolutional Neural Network (CNN) Modell trainiert, das die Befallssituation in den Bildzeitreihen klassifiziert. Die Performance des Modells wurde zudem ausgewertet. Als letzter Schritt der Bildverarbeitung wurden Karten erstellt, die die Verteilung der kranken Pflanzen im Feld zeigen. Die erstellten Karten können als Grundlage für Applikationskarten im praktischen Anbau oder zur Bewertung der Sortenleistung in Sortenversuchen dienen. Die vorgestellte Methodik bietet eine hohe Präzision und Empfindlichkeit bei der Erkennung von CLS und hat das Potenzial, Prozesse der CLS-Überwachung für verschiedene Anwendungsbereiche zu automatisieren.

Schlagwörter: *Cercospora beticola*, Convolutional Neural Network, Befallshäufigkeit, Befallsstärke

1 Introduction

The most serious sugar beet leaf disease in the world is Cercospora leaf spot (CLS) Weiland and Koch (2004). CLS affects both the technical quality and the mass of harvested beet (Wolf and Verreet 2009). When infected fields are not adequately treated with fungicides, yield losses can be more than 42% (Smith and Martin 1978). Similarly, final beet mass is reduced when at least 3% of the leaf area is affected (Wolf and Verreet 2009). This disadvantage highlights the importance of early and accurate detection of pathogen emergence for integrated control strategies to avoid yield losses (Wolf and Verreet 2009). In this context, control thresholds have been employed for years for sugar beet growers in Germany. The thresholds are set on the calendar base and disease incidence (DI, Gummert et al. 2018). Such warning systems are based on intensive field monitoring, which is a time-consuming activity that requires well-trained personnel for assessments. In recent years, there have been great advances in field monitoring with the support of remote sensing, especially in the use of systems based on cameras mounted in Unmanned Aerial Vehicles (UAVs). The successes and achievements in plant disease detection with image sensors were described by Mahlein (2016), reporting several types of research being able to detect leaf symptoms caused by CLS. Jay et al. (2020) and Görlich et al. (2021) realized CLS detection under field conditions with imagery systems, and in the same line, Görlich et al. (2021) has shown the power of adding a CNN approach to the analysis. However, the threshold values based on DI are determined for a certain number of individuals (leaves or plants). This leads to the need to be able to individualize and detect plants in the field in order to deliver accurate and standardized DI. There have already been advances in plant detection of sugar beet and counting in the field, as demonstrated by Barreto et al. (2021), but this work has not focused on tracking plants over time for an application after canopy closure. The use of threshold values in integrated pest management (IPM) has as one of its objectives the reduction of pesticide use. This reduction can be supported by aerial mapping and precision guided fungicide application (Booth et al. 2021, Dammer et al. 2015). In this work, a list of image-processing approaches is ensembled that combine machine learning and deep learning approaches to deliver parameters for disease quantification of individual plants in the field during the vegetation period.

2 Material and methods

2.1 Experimental fields

In 2020, within the context of the projects: "COBRI: Sensing of plant diseases by hyperspectral imaging and UAVs" and "PhenoRob: Robotics and Phenotyping for Sustainable Crop Production", two experimental trials were carried out near Göttingen, Germany. The main objective of the first trial, further called "training trial", was to develop a model to estimate the resistance level of cultivars by using a multispectral UAV system and comparison with plot scoring. The information collected was used to train and test different kinds of models. On one side, this will serve as a pipeline for a pixel-wise and multi-class task to classify healthy, diseased, and bare soil-based multispectral data (this will not be the focus of this work). On the other side, a CNN model based on RGB images from the plant level will be elaborated and presented in this paper. The training trial presented a two-factorial randomized complete block design. One factor was the resistance level (susceptible or resistant), the second factor was the fungicide strategy considering three levels: (i) not inoculated and treated with fungicide as a control, (ii) not inoculated without fungicide, and (iii) inoculated without fungicide.

The main objective of the second experiment, also called "testing trial" was to develop models for accurate and early forecasting by monitoring the disease with information from optical and environmental sensors, considering the pathogen's spread and its interaction with the environment. For this purpose, the experimental trial and individual plots were considerably more extensive and had only one susceptible variety; inoculation was applied only in the center of the three plots as a spot manner directly by seeding; for this work and as a use case, the data obtained from this experiment were used to test the created model with the dataset generated by the training trial.

2.2 UAV-data acquisition and image stitching

UAV flights were conducted to take images every week until harvest from May to October onwards. A quadrocopter DJI Matrice 210 (Shenzhen DJI Sciences and Technologies Ltd., China) was used to collect aerial data. The camera mounted was a Micasense Altum multispectral camera (MicaSense, Inc., USA) with six bands: BLUE (475 ± 32 nm), GREEN (560 ± 27 nm), RED (668 ± 14 nm), REDEDGE (717 ± 12 nm), NIR (842 ± 57 nm), and long-wave thermal infrared (LWIR, 8000-14000 nm) with a Downwelling Light Sensor (DLS2). In this work, the information provided by the thermal band has not been considered. The automatic flight missions were designed with the software UGCS (Version 4.4).

In both trials, flight altitude was established to acquire multispectral images with a ground sampling distance (GSD) between 0.3–0.5 cm, allowing single leaf spot detection. However, the testing trial was monitored at a slightly higher altitude, losing some resolution to complete the mission with a single flight.

The multispectral images taken with UAV system were preprocessed with Agisoft Metashape Professional (Version 1.6.5) to generate orthomosaic images of the entire field. The GIS program QGIS (Version 3.18) was used to delimit the analysis areas, manage the scoring data, and generate the visualizations. At the end of the season and after preprocessing, the following data were obtained: 27 multispectral orthomosaics from training trial, and 10 multispectral orthomosaics from testing trial.

2.3 Ground truth

In parallel with all UAV flights, experts determined the disease severity of each plot as ground truth based on the KWS scale. Its ranges from 1 to 9, in which 1 represents the absence of
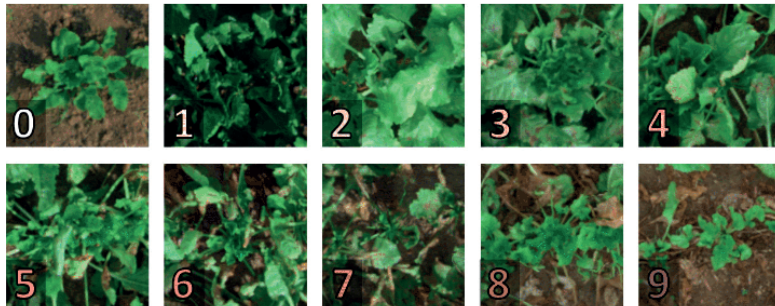
Fig. 1: Representative image categorization to address disease severity based on the KWS scale from 0–9

symptoms of Cercospora leaf spots; 3 when leaf spots are present on old leaves, 5 when leaf spots merge to form necrotic areas, 7 is assigned when the oldest leaves died, and the disease progresses to the internal leaves, and 9 applies to the total death of the foliage (Khan et al. 2007).

However, because plants observed from their adaxial side are analyzed, there are two classes of plants that could be mixed and confused, these being when the plant is too young or when the plant has lost all its foliar material, generating a new healthy leaf growth in the center. For this reason, as is shown in Figure 1, class 0 was added by the authors of this work, which represents healthy plants before canopy closure.

In the test trial, heterogeneity with a range of different plant development stages was expected in each plot. It was scored in 9 georeferenced points of each plot, between 10 and 20 plants, respectively, being a total of 171 measurement points.

2.4 Modeling

The cataloging of plants will be explained in the next section. This step supplies RGB composite images in time series of individual plants. Each plant was labeled with a class according to GT. The plants close to the plot's edges were removed to avoid confusing images and edge effects. The images generated of each plant were 224 × 224 pixels in size, representing 0.2 m². This process of selecting images for use as model training can be seen in Figure 2. Moreover, to further extend the data and to improve the generalizability of the model, data augmentation was applied during training. Images were rotated, mirrored, and slightly zoomed. In total, after filtering, 29,200 images were generated for training. The LeNet CNN model was chosen to deal with this classification task. LeNet was created by Lecun et al. (1989), and has been extensively
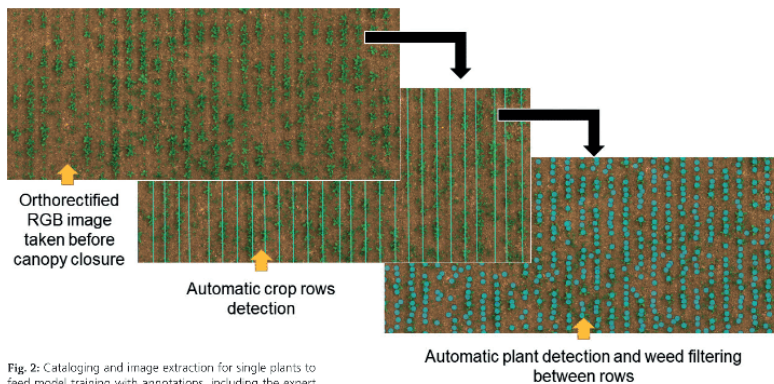

Fig. 2: Cataloging and image extraction for single plants to feed model training with annotations, including the expert scoring, plant labeling and labeled segmentation

Orthorectified RGB image taken before canopy closure

Automatic crop rows detection

Automatic plant detection and weed filtering between rows

40

used for pattern recognition, e.g., in text detection. This net is in fact a simple CNN with a small architecture, widely used to respond to image classification problems. The LeNet architecture used in this work was proposed by Rosebrock (2017) as follow two sets of convolutional, activation, and pooling layers, followed by a fully-connected layer, activation, another fully-connected, and finally a softmax classifier. For this process, the dataset was split in 80:20% (training:validation), the learning rate was fixed to 0.001, the batch size was 8, and classes were balanced by weighting due to imbalance of images during early stages of disease development. The focus of this last technique is to ensure that all classes are present during each training step, and to prevent overfitting. Early stopping was applied if the accuracy did not increase during the last five epochs. The used computer for training and later prediction was an Intel(R) Core (TM) i7-8700 CPU at 3.20GHz 3.19 GHz with a Quadro RTX 5000 GPU and 128 GB of RAM.

2.5 Process flow

This work is based on the chaining of workload and algorithms from image analysis, data science, and artificial intelligence. It can be arranged for practical purposes in the following order:
1. UAV-data acquisition
2. Plant cataloging and extraction
3. Digital plant scoring
4. Map generation

As relevant Python packages, it was used in addition to TensorFlow for classification, Matplotlib and Seaborn for visualization, Rasterio and Geopandas for managing georeferenced data and images. For applying filters and working with images, Scikit-image, Scikit-learn, and OpenCV were used.

2.6 Plant cataloging

Identifying the georeferenced location of the plants in the field is required to analyze images at the plant level or plant instance. Therefore, this work proposes the use of generated images from flights in early crop stages, preferably before canopy closure, as implemented by Günder et al. (2022). In the first stage, the elaborated algorithm individually analyzes these images with filtering and computer vision techniques. Later, the images are connected by aligning and pattern recognition methods. This additionally enables the recognition of seeding lines and the filtering of off-line weed. As a result, the position of individual plants was retrieved at multiple points, allowing to identify each plant's centroid coordinates, and saving them to GIS compatible files. As following step, by using centroid coordinates, RGB composite images can be created of individual plants at different time points and in a large scale. These images were used in the training process of the model. Figure 3 shows schematically the cataloging procedure.
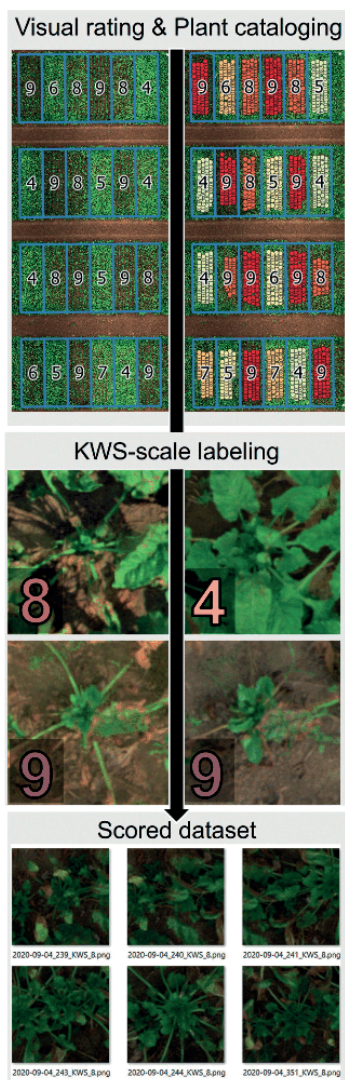

Fig. 3: Scheme of the algorithm for plant cataloging including orthorectification, row detection and weed discrimination

41

Agriculture/Landwirtschaft

2.7 Digital plant scoring of testing field

When plants are cataloged and RGB composite images are created, predictions take place using modeled CNN. Every categorical output is embedded in the respective plant centroid coordinate, and this is the principal procedure to create georeferenced application maps. Considering this, the testing of the model has been run in the corresponding trial. The first two missions were used to detect the plants, and the remaining eight missions from July onwards were used for scoring. Class 0, which corresponded to small plants, was arbitrarily assigned to class 1 if they appeared before July 15 and class 9 if they appeared after that date. To determine the metrics of the results, the average of the results in the same georeferenced area, where the experts carried out the scoring, was calculated first. For this purpose, a buffer area was delimited to cover approximately scored ten to twenty plants.
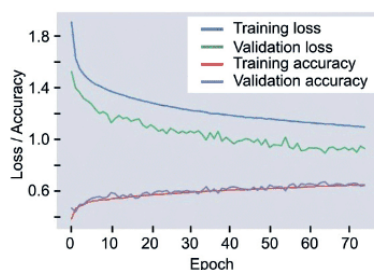

Fig. 4: Loss and accuracy history of training step for lenet CNN model

3 Results and discussion

During training, the best training loss in the validating set was 0.9265 and its accuracy 0.6426 (Fig. 4). The normalized confusion matrix for each class for the validation set (20% of the total training set) is shown in Figure 5A. Generally, classification performance is inaccurate with a slight deviation to under- and overestimate the class level in one unit distance, especially for classes between 3 to 6. This effect may be due to the significant heterogeneity in the development of symptoms and the different resistance mechanisms to keep the foliage healthy of the two varieties from the training field, making it challenging to sort the correct class. Additionally, due to their higher density in the training field in comparison to testing field, the overlapping of leaves does not allow the complete observation of the entire leaf mass of each plant and can also influence the performance. It is believed that when neighbor plants are healthier than the centroid plant, a tendency to underestimate could take place. The opposite effect is expected when neighbor plants present more severe symptoms. Furthermore, it should also be noted that the weather conditions and sky conditions during image acquisition could have a significant influence on the results. Balancing training steps with data containing sunny and cloudy sky conditions must be considered in future studies. This phenomenon was also observed by Barreto et al. (2021).

In the testing experiment, 49 plants were automatically detected and then directly analyzed with the trained model, and the results obtained are displayed in Figure 5B; here, the error between neighboring classes showed a slight increase. There was also a clear difference in performance for classes 3 and 7, being the last with better results. Such differences may be caused due to the diverse development in the symptomatic. Since it was inoculated at sowing date, the symptoms appear on the leaves closer to the ground. On the other side, the training trial has been inoculated by row closure, which
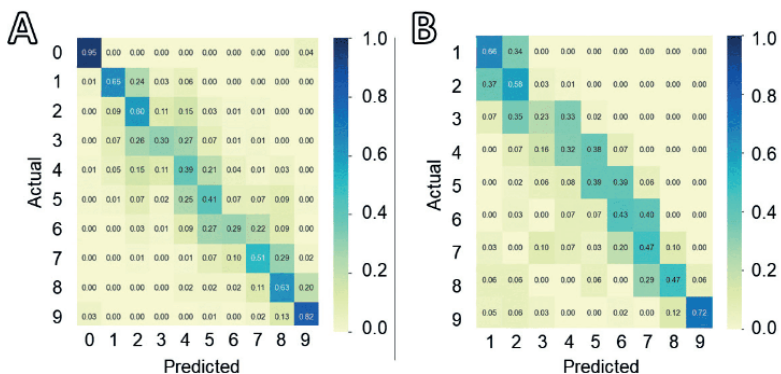

Fig. 5: Normalized confusion matrix of the analyzed model on validation dataset (A) and testing dataset (B)

increases the presence of diseased leaves in the most aerial part causing error in classification for class 3. The increase or decrease of classes must be analyzed in-depth to find a method that improves the precision of the analysis. Battilani et al. (1990) suggest a class reduction based on a relationship with the DS percentage, along with Smith and Martin (1978) whose describes a scale of 10 classes. Shane (1992) describes the magnitudes of the scale of 9 classes, and that of more classes; an important point to note is that the KWS scale only describes classes 1, 3, 5, 7, and 9 leaving the classification of the intermediate classes to interpolation and interpretation by experts. Therefore, selecting the appropriate number of classes for detecting CLS symptoms with aerial images should also be analyzed in-depth.

Additionally, Shane (1992) and Vereijssen et al. (2003) highlighted the lack of precision of categorical scales to determine low intensities of the disease. To overcome this drawback, a classification analysis at the pixel level and leaf segmentation in those low classes could be necessary to increase the accuracy of the detections. Integrating this work to improve precision at low infection levels may be of great interest in future work. In the same order, the difference in flight height may have generated a distortion even though a pixel size rescaling was performed so that both experiments have the same GSD. Future work should be focused on determining the best GSD for this method.

Once all the plants of the testing field have been analyzed, it is possible to render them on maps. Thus, Figure 6 shows three flights in a time series mapped in a heatmap manner, the least affected plants being marked with light red tones and the most affected in the darkest red scale. In this figure, the field dynamics are visualized, the inoculated areas are detected, and the spread of CLS is visible in time.

Thus, it is possible to determine the DI for the whole experiment for each flight date, obtaining the total number of plants and the number of diseased plants. It is also possible to determine DI following the same method used for IPM. It is determined for 100 plants chosen in a transect in a field and counting the diseased. For example, Figure 7 shows the calculation of the two methods for the date of July 28, 2020; all plants with a value greater or equal to 2 were considered diseased. For the 100 plants, the DI was 58%, and for all detected plants was 60%.

4   Conclusion

It can be concluded that the combination of UAV imagery with deep learning systems is a valuable instrument to determine parameters for CLS control on the field. This technology can reduce the very laborious work of monitoring and thereby improve the georeferenced fungicide application and contribute to time- and eco-efficiency in sugar beet production.
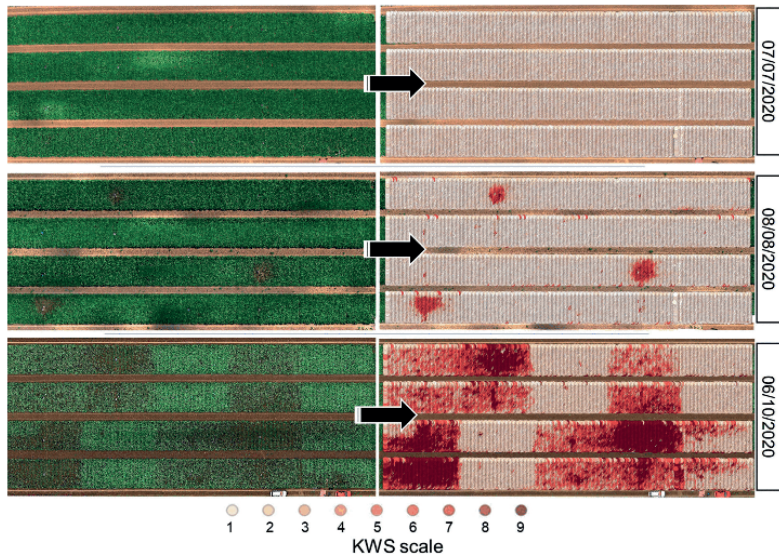

Fig. 6: Time-series orthomosaics presented as RGB composite (left) and CNN prediction (right) including category correction to emulate KWS scale (1–9, light red to dark red)
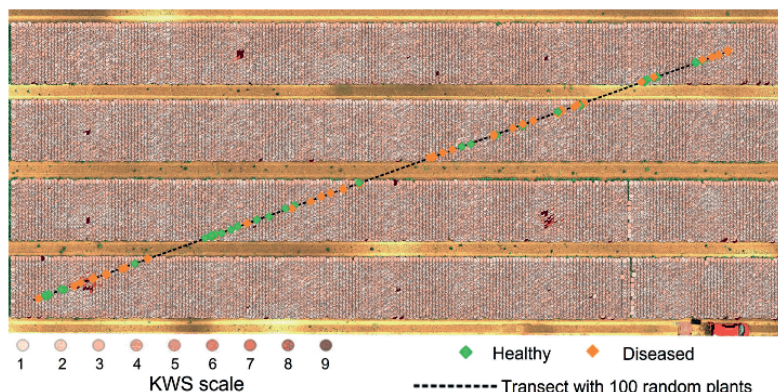
Fig. 7: Image classification of 100 selected plants by July 28, 2020 according to the KWS scale (1–9, light red to dark red). In green and orange colour randomly selected plants, in orange plants considered diseased with a disease severity class of at least 2

Plant cataloging has proven to be a handy tool for plant tracking through the growing season and generating annotations for training deep learning models.

Increasing the depth of the trained model is possibly the key to model detection improvement. Also, higher image resolution and thus generating a great number of high-quality annotations helps to obtain better results. Additionally, it is essential to take advantage of the production and development of cameras and UAVs.

Generated maps can serve as a basis for application maps in practical cultivation or the evaluation of variety performance in variety trials. This output will be "the first step" to provide decision making for practical agriculture or breeding based on UAV imagery in the coming years.

Acknowledgments

References

Barreto A., Lottes P., Ispizua Yamati F.R., Baumgarten S., Wolf N.A., Stachniss C., Mahlein A.-K., Paulus S. (2021): Automatic UAV-based counting of seedlings in sugar-beet field and extension to maize and strawberry, *Computers and Electronics in Agriculture 191*, 106493; DOI: 10.1016/j.compag.2021.106493

Battilani P., Beltrami G., Meriggi P., Ponti I., Rossi A., Rossi V., Rosso F., Tugnoli V., Zocca A. (1990): Nuovi indrizzi di difesa anticercosporica, *L'Informatore Agrario 46*, 53–70

Booth J.C., Sullivan D., Askew S.A., Kochersberger K., McCall D.S. (2021): Investigating targeted spring dead spot management via aerial mapping and precision-guided fungicide applications, *Crop Sci. 61 (5)*, 3134–3144; DOI: 10.1002/csc2.20623

Dammer K.-H., Hamdorf A., Ustyuzhanin A., Schirrmann M., Leithold P., Leithold H., Volk T., Tackenberg M. (2015): Zielflächenorientierte, präzise Echtzeit-Fungizidapplikation in Getreide, *Landtechnik 70 (2)*, 31–43; DOI: 10.15150/LT.2015.2657

Görlich F., Marks E., Mahlein A. K., König K., Lottes P., Stachniss C. (2021): UAV-Based Classification of Cercospora Leaf Spot Using RGB Images, *Drones 5 (2)*, 34; DOI: 10.3390/drones5020034

Gummert A., Ladewig E., Varrelmann M., Kenter C., Märländer B. (2018): *Leitlinien des integrierten Pflanzenschutzes im Zuckerrübenanbau*, https://www.nap-pflanzenschutz.de/fileadmin/SITE_MASTER/content/IPS/Integrierter_Pflanzenschutz/Leitlinien_IPS/Leitlinie_IPS_zuckerruebe.pdf

Günder M., Ispizua Yamati F.R., Kierdorf J., Roscher R., Mahlein A.-K., Bauckhage C. (2022): Agricultural Plant Cataloging and Establishment of a Data Framework from UAV-based Crop Images by Computer Vision, *Preprint arXiv:2201.02685v1* [cs.CV] 8 Jan 2022, submitted to GigaScience

Jay S., Comar A., Benicio R., Beauvois J., Dutartre D., Daubige G., Li W., Labrosse J., Thomas S., Henry N., Weiss M., Baret F. (2020): Scoring Cercospora Leaf Spot on Sugar Beet: Comparison of UGV and UAV Phenotyping Systems, *Plant phenomics 2020*, ID 9452123; DOI: 10.34133/2020/9452123

Khan J., Del Rio L.E., Nelson R., Khan M.F.R. (2007): Improving the Cercospora Leaf Spot Management Model for Sugar Beet in Minnesota and North Dakota, *Plant Dis. 91 (9)*, 1105–1108; DOI: 10.1094/PDIS-91-9-1105

Lecun Y., Boser B., Denker J.S., Henderson D., Howard R.E., Hubbard W., Jackel L.D. (1989): Backpropagation Applied to Handwritten Zip Code Recognition, *Neural Computation 1 (4)*, 541–551; DOI: 10.1162/neco.1989.1.4.541

Mahlein A.-K. (2016): Plant Disease detection by imaging sensors – Parallels and specific demands for precision agriculture and plant phenotyping, *Plant Dis. 100 (2)*, 241–251; DOI: 10.1094/PDIS-03-15-0340-FE

44

Rosebrock A. (2017): *Image classification with Keras and deep learning*, https://www.pyimagesearch.com/2017/12/11/image-classification-with-keras-and-deep-learning; Thursday, December 23, 2021

Shane W.W. (1992): Impact of Cercospora Leaf Spot on Root Weight, Sugar Yield, and Purity of *Beta vulgaris*, *Plant Dis. 76 (8)*, 812; DOI: 10.1094/PD-76-0812

Smith G.A., Martin S.S. (1978): Differential Response of Sugarbeet Cultivars to Cercospora Leaf Spot Disease, *Crop Sci. 18 (1)*, 39–42; DOI: 10.2135/cropsci1978.0011183X001800010011x

Vereijssen J., Schneider J., Termorshuizen A., Jeger, M. (2003): Comparison of two disease assessment methods for assessing Cercospora leaf spot in sugar beet, *Crop Prot. 22 (1)*, 201–209; DOI: 10.1016/S0261-2194(02)00146-1

Weiland J., Koch G. (2004): Sugarbeet leaf spot disease (*Cercospora beticola* Sacc.), dagger. *Mol. Plant Pathol. 5 (3)*, 157–166; DOI: 10.1111/j.1364-3703.2004.00218.x

Wolf P.F.J., Verreet J.A. (2009): Empirical-deterministic prediction of disease and losses caused by Cercospora leaf spots in sugar beets, *Journal für Kulturpflanzen 61(5)*, 168–177

Authors' addresses: *Facundo R. Ispizua Yamati*[1]*; *Abel Barreto*[1]; *Maurice Günder*[2]; *Christian Bauckhage*[2]; *Anne-Katrin Mahlein*[1],

1 Institute of Sugar Beet Research (IfZ), Holtenser Landstraße 77, 37079 Göttingen, Germany;

2 Institute for Computer Science III, University of Bonn, Friedrich-Hirzebruch-Allee 5, 53115 Bonn, Germany;

* Corresponding author: Ispizua@ifz-goettingen.de

Supplementary materials

Table 4-1. Performance of pipeline for multiclass image classification based on the KWS scale prediction and visual scoring

KWS scale[a]	Frequency[b]	Precision	Recall	Specificity	F1
1	0.47	0.87	0.66	0.93	0.75
2	0.06	0.15	0.59	0.79	0.23
3	0.10	0.46	0.23	0.97	0.31
4	0.09	0.40	0.32	0.96	0.35
5	0.04	0.24	0.39	0.96	0.30
6	0.02	0.28	0.43	0.97	0.34
7	0.03	0.35	0.47	0.95	0.40
8	0.06	0.74	0.47	0.98	0.57
9	0.12	0.92	0.72	0.99	0.81

[a] Class 1, represents the absence of symptoms of Cercospora leaf spots; class 3, when leaf spots are present on old leaves, 5 when leaf spots merge to form necrotic areas; class 7 is assigned when the oldest leaves died, and the disease progresses to the internal leaves, and class 9 applies to the total death of the foliage. [b] In total 5842 images were evaluated with the same distribution as the training set.

CHAPTER 5: Pixel-wise disease quantification - Manuscript III

Disease Incidence and Severity of Cercospora Leaf Spot in Sugar Beet Assessed by Multispectral Unmanned Aerial Images and Machine Learning

Abel Barreto[1]*, Facundo Ramón Ispizua Yamati[1], Mark Varrelmann[1], Stefan Paulus[1] and Anne-Katrin Mahlein[1]

[1] Institute of Sugar Beet Research (IfZ), Holtenser Landstraße 77, 37079 Göttingen, Germany

*Corresponding author: barreto@ifz-goettingen.de

Disease Incidence and Severity of Cercospora Leaf Spot in Sugar Beet Assessed by Multispectral Unmanned Aerial Images and Machine Learning

Abel Barreto,[1] Facundo Ramón Ispizua Yamati, Mark Varrelmann, Stefan Paulus, and Anne-Katrin Mahlein

Institute of Sugar Beet Research, 37079 Göttingen, Germany

Abstract

Disease incidence (*DI*) and metrics of disease severity are relevant parameters for decision making in plant protection and plant breeding. To develop automated and sensor-based routines, a sugar beet variety trial was inoculated with *Cercospora beticola* and monitored with a multispectral camera system mounted to an unmanned aerial vehicle (UAV) over the vegetation period. A pipeline based on machine learning methods was established for image data analysis and extraction of disease-relevant parameters. Features based on the digital surface model, vegetation indices, shadow condition, and image resolution improved classification performance in comparison with using single multispectral channels in 12 and 6% of diseased and soil regions, respectively. With a postprocessing step, area-related parameters were computed after classification. Results of this pipeline also included extraction of *DI* and disease severity (*DS*) from UAV data. The calculated area under disease progress curve of *DS* was 2,810.4 to 7,058.8%·days for human visual scoring and 1,400.5 to 4,343.2%·days for UAV-based scoring. Moreover, a sharper differentiation of varieties compared with visual scoring was observed in area-related parameters such as area of complete foliage (A_F), area of healthy foliage (A_H), and mean area of lesion by unit of foliage ($A_{\bar{L}/F}$). These advantages provide the option to replace the laborious work of visual disease assessments in the field with a more precise, nondestructive assessment via multispectral data acquired by UAV flights.

Keywords: automatic scoring, digital surface model, multiclass classification, partial least squares discriminant analysis, support vector machine radial, time-series, unmanned aerial vehicle

Cercospora leaf spot (CLS) is one of the most widespread foliar diseases in sugar beet. This disease is caused by the fungus *Cercospora beticola* Sacc. And, under moderate to high disease pressure, yield losses of up to 50% of recoverable sucrose were reported for infected fields (Shane and Teng 1992). For disease management, protectant and systemic fungicides from the group of ethylene bisdithiocarbamate, benzimidazoles, quinone outside inhibitors, and demethylation inhibitors have mainly been used. The extensive use of these fungicide groups led to the appearance of resistant isolates of *C. beticola* over recent years (Rangel et al. 2020).

New generations of resistant sugar beet from the recent breeding process are important pillars of CLS management and, at the same time, reduce the chance of emergence of fungicide-resistant strains (Vogel et al. 2018). Resistant varieties mainly present three advantages: (i) minimal yield penalty even under low infection pressure, (ii) opportunity to increase ecoefficiency of sugar beet production by reduced fungicide application, and (iii) reduction of the risk of increased inoculum potential and stronger epidemics in the following years (Wolf and Verreet 2002). CLS-resistant sugar beet can only be achieved by continuous breeding of new varieties. A crucial parameter to determine quantitative resistance in a sugar beet variety is disease severity (*DS*) (Nutter et al. 1991), representing the damage of

photosynthetic leaf area. Additional but less-used parameters such as lesion size, lesion numbers, or sporulation rate were also reported as relevant to identify CLS-resistant varieties (Feindt et al. 1981; Leucker et al. 2016; Rossi et al. 2000). Another important parameter for CLS control is disease incidence (*DI*) (Nutter et al. 1991). In the field, most of the systemic fungicides are applied at certain threshold values of *DI*. This control measure avoids economic losses in terms of yield in monitored regions (Wolf and Verreet 2002).

The assessment of these parameters requires a time-demanding visual scoring in the field by experts (Bock et al. 2020, 2021; Nutter 1990). Visual scoring and the role of experts for disease diagnosis is crucial but, at the same time, it is the bottleneck in the breeding process and for disease control (De Coninck et al. 2012; Mahlein 2016). Experts are highly qualified to identify typical symptoms of CLS such as tan to gray-colored circular spots (3 to 5 mm) by canopy closure. Necrotic areas develop after initial tissue collapse and they are also quantified as CLS damage during visual scoring (Weiland and Koch 2004). Under severe epidemics and before harvesting, experts are trained to differentiate new leaf growth emerging from middle collapsed leaves during scoring. Multispectral cameras attached to an unmanned aerial vehicle (UAV) constitute a monitoring system that, together with an appropriate image-processing pipeline, can solve the mentioned drawbacks of visual scoring by human experts regarding bias and limitations regarding workload (Bock et al. 2020). Multispectral UAV systems also exhibit several benefits for disease detection in comparison with satellite or aerial remotesensing imaginary, regarding (i) flexibility of operation, (ii) high spatial resolution, and (iii) acquisition of data on demand (Deng et al. 2018; Jay et al. 2018). Since the first study to evaluate CLS with multispectral, ground-based nonimaging data (Steddom et al. 2005), enormous progress in sensor technology and analysis algorithms from machine learning (ML) have taken place (Mahlein et al. 2018). The analysis of RGB and multispectral images by thresholding, quantification of vegetation indices, ML, as well as deep learning approaches have been reported to detect and quantify CLS in more recent works (Görlich et al. 2021; Jay et al. 2020; Mahlein et al. 2013; Ziya et al. 2018). Key aspects for image-based CLS quantification were mentioned by Jay et al. (2020). In this work, spot density or the number of spots per leaf area and the healthy region of image perspective, named as normalized green fraction,

---

48

were found to be the most relevant parameters for scoring CLS. From these two parameters, the green fraction was the most robust and consistent parameter over time whereas, quantitatively, the spot density presents the disadvantage of an abrupt drop as the necrotic area expands around the first lesions. Jay et al. (2020) calculated from UAV images the area under disease progress curve (AUDPC) (Madden et al. 2007) and, for future works and for better performance, recommended standardizing image resolution and considering the changing light conditions during a flight mission for radiometric calibration. The present study provides significant improvements for time-series analysis of multispectral UAV data acquired in a variety trial. To rate quantitative CLS resistance of two differing sugar-beet varieties, AUDPC$_{DS}$ together with yield loss were used. The digital surface model (DSM), an available but not previously used output from photogrammetry, was included in the analysis to implement a robust workflow. The aims of the study were to (i) propose an ML classification model and a pixelwise approach to detect CLS-diseased tissue of sugar beet by multispectral UAV imagery; (ii) apply the advantages of multispectral and DSM features to improve classification; (iii) formulate a pipeline to assess DS, DI, and relevant parameters from multispectral images for monitoring disease development; and (iv) identify principal differences between UAV-based and expert human scoring.

Materials and Methods

Experimental field

In 2019, a CLS variety trial was conducted near Göttingen, Germany (51°33'3.9″ N, 9°54'0.6″ E). The trial was arranged with two sugar beet varieties and three fungicide strategies in a two-factorial block design with three blocks or repetitions (Fig. 1). The three fungicide strategies were control with fungicide, inoculated with fungicide, and inoculated without fungicide (see the fungicide regime in Supplementary Table S3). Two varieties of sugar beet (*Beta vulgaris* subsp. *vulgaris*) were selected from the national variety list of the German Federal Plant Variety Office (Bundessortenamt 2017) and, for better description in this study, assigned as "susceptible" and

"resistant" according to resistance properties against the fungus *Cercospora* (registration identifier numbers 3012 and 2444) (Bundessortenamt 2017). Additional information about the varieties is specified in Supplementary Table S1. Sugar beet plants were sown on 9 April in six-row plots with an area of 21.6 m^2. At row closure (14 June 2019), plots of inoculated treatments were infected by hand with CLS-diseased, air-dried sugar beet leaf material at 4 g m^{-2}, produced as described by Imbusch et al. (2021). Fungicide application started at the onset of occurrence of first lesions of CLS diseases and was repeated if symptoms recurred following the local management practices. In total, four applications took place (Supplementary Table S3). At harvest, root yield and quality were determined. The beet roots were weighed after washing and processed to beet brei. The brei samples were analyzed for sucrose, potassium, sodium, and amino-nitrogen content according to standardized procedures. The key indicators of variety performance, white sugar yield (WSY) and loss of WSY due to CLS (WSY$_{loss}$), were calculated from root yield and quality parameters according to German standard equations (Märländer et al. 2003). This experiment was repeated in 2020 with slight modifications: one additional repetition and less disease pressure by changing the inoculated with fungicide level by control without fungicide; and, in 2021, extended with three further varieties than in seasons 2019 to 2020.

Disease assessment

Visual scoring of CLS as ground truth was carried out simultaneously to UAV flights (Supplementary Table S2). Symptoms were quantified as a mean value of the plot by assessing middle leaves in percentage, estimating a representative infected from total leaf area (Wolf and Verreet 2002). The determination of DI was also conducted at plant level (DI-plant). In total, 75 plants were randomly selected per treatment and inspected for CLS symptoms. Average percentage of infected plants delivered the DI-plant score (Wolf and Verreet 2002).

Technical specifications, flight mission, and photogrammetry

A quad copter (DJI Inspire 2; Da-Jiang Innovations Science and Technology Co., Ltd.) was used as a UAV platform to carry the
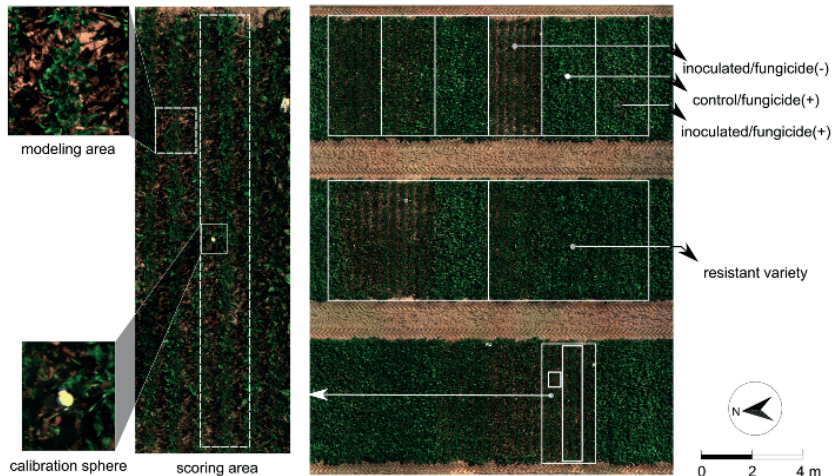

Fig. 1. Composed RGB image of experimental field on 21 August 2019 under sunny conditions. Specification of areas for modeling and scoring, and location of calibration sphere for digital surface model (DSM) features within the plot (left). Distribution of experimental treatments, fungicide strategies, and variety (right).

multispectral imaging sensor (RedEdge-M; MicaSense, Inc.) to map the area of study. The camera provides three visible spectral bands of 475 ± 20 nm (BLUE), 560 ± 20 nm (GREEN), 668 ± 10 nm (RED), and two near-infrared spectral bands of 840 ± 40 nm (NIR) and 717 ± 10 nm (REDEDGE). For time-series overlaying and accurate georeferencing, ground control points were installed in the field corner points and identified as markers on the images for coordinate correction. Images were captured in flight missions within 3 h of local solar noon, with a flight time of 19 min. The flight mission included a forward overlap of 70%, a lateral overlap of 70%, a flight speed of 0.4 m/s, and a flight altitude of 5 m above ground level, delivering an average ground sample distance (GSD) of 4.1 mm for multispectral orthomosaic images. The monitoring campaign started 1 day before inoculation with C. beticola (13 June 2019). In total, 14 missions were completed under diverse weather conditions (Supplementary Table S2). Radiometric calibration was implemented in R software (version 3.5.3) (R Core Team 2020), considering specifications recommended by MicaSense. For this step, the gray reference panel (RP02-1701160-SC) was employed for spectral correction. As the first step of radiometric calibration, raw images were converted to radiance to account for image capture metadata such as gain, exposure setting, and vignette effects. Afterward, the radiance images were converted to reflectance to account for the time-dependent factor calculated from captured gray panel images before the start and after UAV landing. Output reflectance images were stitched using the software Agisoft Metashape Professional (version 1.6.4, build 10732, 64 bit; Agisoft LLC, St. Petersburg, Russia) for stitching of reflectance images. Multispectral orthomosaic in reflectance values were exported as well as the respective digital elevation model from the photogrammetry procedure in the WGS84 coordinates system.

Defining feature types

Five types of features were considered to support ML models: simple vectorization of single bands (SB), determination of vegetation indices (VIs), features related to DSM (DSM$_f$), a feature for quantifying shaded regions as index (SH), and a feature type that includes resolution (RE) of multispectral orthomosaic images and DSM. VI features included six selected indices: difference between red and blue band (D_{678500}) (Merzlyak et al. 1999), modified chlorophyll absorption in reflectance index 2 (MCARI$_2$) (Haboudane 2004), MCARIOSAVI (Main et al. 2011), modified soil adjusted vegetation index 2 (MSAVI$_2$) (Qi et al. 1994), modified simple ratio (MSR) (Chen 1996), and green vegetation index (GVI) (Bannari et al. 1995). Calculation of individual VIs is specified in Table 1. Calculation of SH feature is based on previous studies which highlighted the effect of the environment and passive illumination on the detection of CLS (Görlich et al. 2021; Jay et al. 2020). Therefore, shaded areas were quantified using the normalized saturation-value difference index (NSVDI) as proposed by Ma et al. (2008), which transforms multispectral reflectance values to the hue-saturation-value color system and considers the saturation (S) and value (V) for calculation, as shown in equations 1 and 2:

$$V = max(R_{BLUE}, R_{GREEN}, R_{RED}) \tag{1}$$

$$S = \{ [max(R_{BLUE}, R_{GREEN}, R_{RED}) - min(R_{BLUE}, R_{GREEN}, R_{RED})] \} / [max(R_{BLUE}, R_{GREEN}, R_{RED})] \tag{2}$$

Then, the index was determined as follows:

$$NSVDI = (S - V)/(S + V) \tag{3}$$

To obtain DSM features, we consider the smallest surface or pixel of the orthomosaic digital surface model as the plane enclosed by four pixels; $z_{i,j}$, $z_{i+1,j}$, $z_{i,j+1}$, and $z_{i+1,j+1}$, where $z_{i,j}$ is the altitude at a pixel with row i, column j position. As mentioned in Corripio (2003) and for a regular pixel of GSD value of l, the x, y, z components of the vectors along the neighbor pixels are defined as:

$$\begin{cases} a = (l, 0, \Delta z_a), \ with \ \Delta z_a = z_{i+1,j} - z_{i,j} \\ b = (0, l, \Delta z_b), \ with \ \Delta z_b = z_{i,j+1} - z_{i,j} \\ c = (-l, 0, \Delta z_c), \ with \ \Delta z_c = z_{i,j+1} + z_{i+1,j+1} \\ d = (0, -l, \Delta z_d), \ with \ \Delta z_d = z_{i+1,j} - z_{i+1,j+1} \end{cases} \tag{4}$$

Considering this, the normal vector image ($n_{i,j}$) can be calculated as follows:

$$n_{i,j} = \frac{a \times b}{2} + \frac{c \times d}{2} = \frac{1}{2} \begin{vmatrix} \vec{i} & \vec{j} & \vec{k} \\ l & 0 & \Delta z_a \\ 0 & l & \Delta z_b \end{vmatrix} + \frac{1}{2} \begin{vmatrix} \vec{i} & \vec{j} & \vec{k} \\ -l & 0 & \Delta z_c \\ 0 & -l & \Delta z_d \end{vmatrix} \tag{5}$$

The determinant image of $n_{i,j}$ can be interpreted as the surface area (A, where $A = |n_{i,j}|$), and the division of $n_{i,j}$ by $|n_{i,j}|$ can deliver the image n_u containing a pixelwise unitary vector normal to surface:

$$n_u = n_{ij}/|n_{ij}| \tag{6}$$

Qu (2018) mentioned the principles for quantitative reflectance, which varies at specific wavelength and is ruled by incidence and viewing geometries of the light source, surface observed, and the spectral sensor. This is the reason to calculate the angle of incidence between the canopy surface and light source (θ_s) in this study; and we considered the slope (ζ) (angle between surface and normal to horizontal) as the closest angle to the viewing angle. Our argumentation is based on the dynamic of the UAV system to acquire images during the flight mission. The slope can be calculated with a dot product of the normal vector the terrain (Z_u, where $Z_u = 0 \vec{i} + 0 \vec{j} + 1 \vec{k}$) and n_u as follows:

$$\zeta = arccos(Z_u \cdot n_u) \tag{7}$$

Table 1. Vegetation indices and computation of multispectral bands[a]

Vegetation index	Computation	Literature
D_{678500}	$R_{RED} - R_{BLUE}$	Merzlyak et al. (1999)
MCARI$_2$	$\frac{1.5[2.5(R_{800} - R_{670}) - 1.3(R_{800} - R_{550})]}{\sqrt{(2R_{800} + 1)^2 - (6R_{800} - 5\sqrt{R_{670}}) - 0.5}}$	Haboudane (2004)
MCARIOSAVI	$\frac{R_{820}/R_{670} \cdot R_{700} - 0.2(R_{820}/R_{550} \cdot R_{670})(R_{820}/R_{670})}{1.16(R_{800} - R_{670})/(R_{800} + R_{670} + 0.16)}$	Main et al. (2011)
MSAVI$_2$	$\frac{2R_{800} + 1 - \sqrt{(2R_{800} + 1)^2 - 8(R_{800} - R_{650})}}{2}$	Qi et al. (1994)
MSR	$\frac{\frac{R_{800}}{R_{650}} - 1}{\sqrt{\frac{R_{800}}{R_{670}}} + 1}$	Chen (1996)
GVI	$-0.283R_{GREEN} - 0.660R_{RED} + 0.577R_{REDEDGE} + 0.388R_{NIR}$	Bannari et al. (1995)

[a] D_{678500} = difference between red and blue band. MCARI$_2$ = modified chlorophyll absorption in reflectance index 2. MCARIOSAVI = vegetation index derived from MCARI and OSAVI, MSAVI$_2$ = modified soil adjusted vegetation index 2, MSR = modified simple ratio, and GVI = green vegetation index. R_x represents a spectral band expressed in reflectance. NIR = near-infrared.

50

If we consider the sun as the light source, the angle of incidence between the sun and the canopy cover surface (θ_x) can be determined:

$$\theta_t = arccos(S_a \cdot n_g) \tag{8}$$

Finally, because of RE features and observations of the relative heterogeneous values of resolution obtained by the monitoring system (Supplementary Table S2), and based on the recommendations of Jay et al. (2020), the resolution in GSD from each multispectral orthomosaic (m) and their respective DSM (l) were considered as additional features. An overview of calculated features is provided in Supplementary Figure S1.

Labeling

In all, 100 image patches (approximately 105 by 205 pixels) were labeled pixelwise for the modeling stage. Of these, 60 image patches were considered for training and 40 for testing. Pixelwise annotation included four classes: "diseased" for areas affected by CLS, "healthy" for apparently healthy leaf tissue, "soil" for soil regions, and "other" for any other region that does not belong to the aforementioned classes (see Supplementary Fig. S1).

Modeling

The objective of this step was to identify the most relevant ML methods to solve the four-class task. High computing time for training and unbalanced class distribution (Fig. 2A) led to a reduction of sampled pixels for testing various ML methods. Over 1 million pixel values were reduced to 15,000 samples by down-sampling

guided by the lowest pixel frequency in Figure 2B. In total, five ML methods were tested and compared: K-nearest neighbors (KNN), partial least squares discriminant analysis (PLS-DA), random forest (RF), the support vector machine linear (SVML), and the support vector machine radial (SVMR). All methods used included repeated cross-validation, resampling of training data, and optimized model parameterization according to Barreto et al. (2020). Aiming for complete feature reduction, the contribution of individual feature type performance was evaluated. Six classifiers were trained using the best method identified in the previous step. The reference classifier used only SB features. For the next four classifiers, additional feature types such as VI, SH, and DSM$_f$ were added to SB features for training. Finally, we trained a classifier based only on VI features. After evaluating feature type reduction, the optimized pipeline was established. The pipeline starts with radiometric calibration and photogrammetric processing of raw images, resulting in the multispectral orthomosaic and DSM. RE features of both photogrammetry outputs are stored (m,l) and, from the multispectral orthomosaic, reflectance values of all five channels are directly extracted and vectorized (SB). VI and SH features are calculated and vectorized in the same way; ζ and θ, or DSM features were determined from DSM, following equations 7 and 8. All feature types fed the best-performing multiclass classifier (PLS-DA); the output class was reshaped in a binary matrix (H'); and, by a healthy foliage cover lower than 40% ($FC_h < 40\%$) (Table 2), a second classifier was activated for classifying pixel values as other,

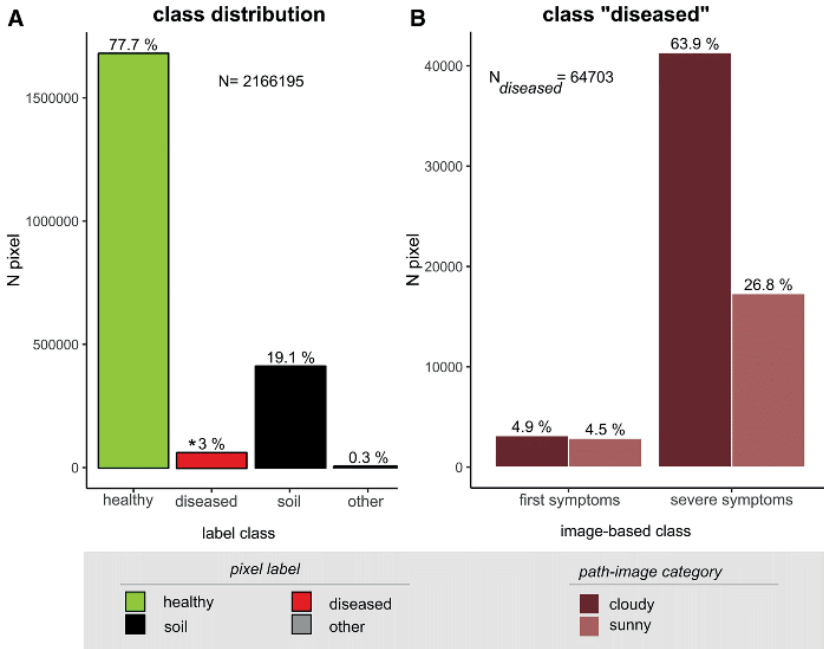**Fig. 2.** Distribution of pixels. **A,** Class distribution of pixelwise image-based annotation of training dataset. **B,** Additional annotation of pixels from class "diseased" (*) based on "first symptoms" of Cercospora leaf spot (until 15% of disease severity), and "severe symptoms" (more than 15% of disease severity) at different ambient light conditions. N represents the total number of pixels evaluated.

soil, diseased, or healthy. Outputs of these two classifiers were segmented or split into four binary masks, as shown in the following example for diseased class:

$$D_{i,j} = \begin{cases} 1, & \text{if } output_{i,j} \in \text{"diseased"} \\ 0, & \text{else} \end{cases} \qquad (9)$$

As a next step, masks were merged following operation 1: $D_{i,j} = OR_{i,j}(D', D'')$ and operation 2: $M_{i,j} = \{M' \in O', S', H'\backslash M' - AND_{i,j}(M', D)\}$. The final output consists of four images: $O_{i,j}$, $S_{i,j}$, $D_{i,j}$, and $H_{i,j}$, assigned to classes other, soil, diseased, or healthy, respectively. An overview of the complete pipeline is shown in Figure 3B.

Postprocessing, UAV-parameter definition, and automatic scoring

Considering the scoring area (Fig. 1) and to achieve at least 100 samples per plot ($n = 34$), we used 34 individual objects per plot ($n = 34$), called instances, to run our pipeline. An individual instance (I_n) is a circle with a radius of 5 cm. Scoring instances were randomly distributed across the plot, avoiding instance overlapping. In a following postprocessing step, CLS clusters were determined considering the dynamic development of diseased regions from single spots to necrotic tissue (Jay et al. 2020). For this, a cluster (C_{cls}) was extracted form the output image mask D (Fig. 3C) by labeling eight connected cluster pixels (He et al. 2017). DS for an individual instance (I) was determined as follows:

$$DS_I = \left\{ \left[\sum_i \sum_j D_I \times A_I \right] \Big/ \left[\sum_i \sum_j \{D_I + H_I\} \times A_I \right] \right\} \times 100 \qquad (10)$$

The plotwise DS (DS_{UAV}) was defined as the average of all ds_I belonging to the evaluation area of a plot:

$$DS_{UAV} = \frac{\sum_{n=1}^{n} DS_{I_n}}{n} \times 100\% \qquad (11)$$

To determine DI, it is necessary to define an affected or diseased unit (d_o) as mentioned by Nutter et al. (1991); in our case, a diseased instance. We defined an instance as diseased, based on Nutter et al. (1991), if at least one lesion was present or if the pixel summation in

$D_{I,i}$ was different from zero (at least one CLS cluster). The total number of d_{uUAV} in a plot or for a treatment was determined as follows in algorithm 1:

Algorithm 1: Counting of diseased instances (d_{uUAV})

Result: d_{uUAV}
1   $d_{uUAV} \leftarrow 0$
2   **for** $n \in \{1,...,n\}$ **do**
3   **if** $\sum D_{In} \neq 0$ **then**
4        $d_{nUAV} \leftarrow d_{uUAV} + 1$
5   end
6   end

Considering this, DS_{UAV} was calculated as:

$$DI_{UAV} = \{d_{uUAV}/n\} \times 100\% \qquad (12)$$

At this stage of image postprocessing, from a wide choice to compute parameters, we focused additionally on calculating the following parameters (mathematically defined in Table 2): foliage cover (FC), cover of healthy foliage (FC_h), cover of diseased foliage (FC_d), area of foliage (A_F), area of healthy foliage (A_H), area of diseased foliage (A_D), DS (cover based, ds_I), number of clusters (c), number of clusters per unit of foliage area (c_F), mean cluster area ($A_{\bar{c}}$), mean cover cluster per unit of foliage cover ($C_{\bar{c}/F}$), and mean area of cluster by unit of foliage area ($A_{\bar{c}/F}$).

Temporal analysis for parameters

In accordance with Madden et al. (2007), AUDPC was calculated for UAV- and expert-based parameters using equation 13. Our first assessment was considered on 13 June, 1 day before inoculation.

$$\text{AUDPC} = \sum_a^{b-1} \frac{(y_a + y_{a+1})}{2} \times (t_{o+1} - t_o) \qquad (13)$$

where b = number of assessment times, a = assessment time, y = acquired parameter from UAV or visual scoring, and t = days before or after inoculation.

Statistics

After checking the absence of outliers, normal distribution of variables, linearity, and homoscedasticity of AUDPCs for parameters,

Table 2. Definition for parameters inside instance

Parameter	Abbreviation	Formula
Area of diseased foliage	A_D	$\sum_i \sum_j D_I \times A_I$
Area of foliage	A_F	$\sum_i \sum_j \{D_I + H_I\} \times A_I$
Area of healthy foliage	A_H	$\sum_i \sum_j H_I \times A_I$
Cover of diseased foliage	FC_D	$\frac{\sum D_{I_i}}{\sum I_i} \times 100\%$
Cover of healthy foliage	FC_H	$\frac{\sum_i \sum_j H_I}{\sum I} \times 100\%$
Disease severity (cover based)	ds_I	$\frac{\sum_i \sum_j D_I}{\sum_i \sum_j D_I + H_I} \times 100\%$
Mean cluster area	$A_{\bar{c}}$	$\frac{\sum \sum D_b \times A_b}{c}$
Mean cover cluster per unit of foliage cover	$C_{\bar{c}/F}$	$\frac{\sum \sum D_I}{c} \times \frac{1}{\sum \sum D_I + H_I}$
Mean area of cluster by unit of foliage area	$A_{\bar{c}/F}$	$\frac{\sum \sum D_I \times A_I}{c} \times \frac{1}{\sum \sum \{D_I + H_I\} \times A_I}$
Number of clusters	c	c
Number of clusters per unit of foliage area	c_F	$\frac{c}{\sum \sum \{D_I + H_I\} \times A_I}$
Foliage cover	FC	$\frac{\sum \sum \{D_I + H_I\}}{\sum \sum I} \times 100\%$

52

Spearman's correlation coefficient (r_s) was calculated to determine the degree of linear correlation and whether significant differences existed between DS_{UAV} and expert-based DS in percentage terms. Statistical analysis was carried out with the "agricolae" package in R software. Analysis of variance (ANOVA) for a randomized complete block factorial design was used to determine the significance of

variety and fungicide factor. For evaluation of quantitative resistance, a two-sample t test was performed to WSY_{loss} and $AUDPC_{DS}$ (inoculated with fungicide) to compare significant mean differences of the susceptible and resistant varieties. For each treatment, no posthoc evaluation was done because of the simplicity of the two-varieties trial field design.
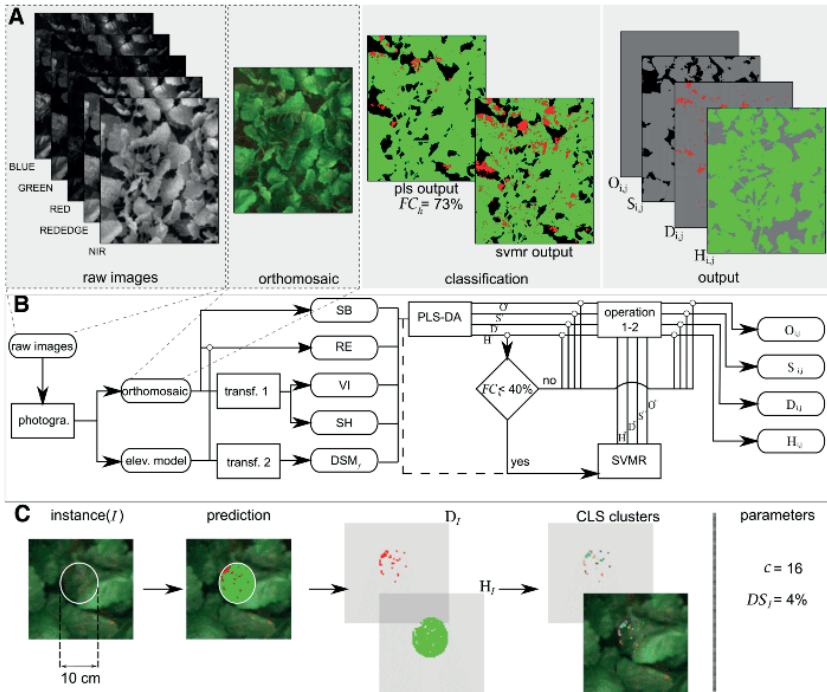

Fig. 3. Image processing flowchart of multispectral unmanned aerial vehicle (UAV) images. A, Overview of input imagery, photogrammetry, and classification results, as well as final output of pipeline. B, Flowchart for multispectral UAV imagery from raw images to multiclass-segmented binary outputs for classes "other", "soil", "diseased", and "healthy". Abbreviations SB, RE, VI, SH, and DSM$_t$ are addressed to single bands, resolution, vegetation indices, shadow, and digital surface model feature types, respectively. Operation 1: $D_{i,j} = OR_{i,j}(D', D'')$ and operation 2: $M_{i,j} = \{M' \in O', S', H'|M' - AND_{i,j}(M', D)\}$. C, Determination of number of clusters (c) and disease severity (DS) for an individual instance with circular form of 10 cm in diameter in projection to soil.

Table 3. Performance of models and pipeline for classification of pixelwise multiclass segmentation[a]

Method[b]	Acc	Diseased			Healthy			Soil			Other		
		Prec	Rec	F1	Prec	Rec	F1	Prec	Rec	F1	Prec	Rec	F1
PLS-DA	**85.8**	24.2	25.5	24.8	**82.1**	**89.4**	**85.6**	62.1	83.0	71.0	67.3	84.2	74.8
SVML	83.1	22.3	35.9	27.5	81.1	84.8	82.9	59.4	85.4	70.1	53.1	90.1	66.9
SVMR	82.0	**28.1**	**73.0**	40.5	82.9	84.0	83.4	60.1	74.6	66.6	37.1	96.4	53.6
RF	81.7	25.1	68.8	36.8	83.6	84.6	84.1	62.5	71.2	66.6	22.0	97.7	36.0
KNN	76.0	19.2	69.8	30.1	82.7	77.7	80.1	53.6	69.5	60.6	30.7	94.9	46.4
Pipeline	86.3	33.3	62.2	43.4	94.9	92.1	93.5	70.3	66.4	68.3	77.6	84.0	80.6

[a] Acc = accuracy, Prec = precision, and Rec = recall. Numbers in bold indicate the best performance overall classes; and the methods with relevant performance metrics for classes "diseased" and "healthy".
[b] PLS-DA, SVML, SVMR, RF, and KNN are abbreviations for partial least squares discriminant analysis, support vector machine linear, support vector machine radial, random forest, and k-nearest neighbor method, respectively.

Results

ML methods and multiclass performance

The PLS-DA method showed the highest overall classification accuracy in the test dataset (85.8%) (Table 3) and the highest F1 score for the classes healthy, soil, and other. An F1 score between 1 and 6% higher was observed compared with the rest of the classifiers for the most frequent class, healthy (Table 3; Fig. 2). A disadvantage of the PLS-DA method in terms of precision and recall was observed in the class diseased. The SVMR method performed better in classification of diseased pixels from precision and recall scores (28 and 73%, respectively). This method presented clear advantages in terms of F1 scores, yielding up to 16% higher precision-recall balance in comparison with the PLS-DA method. The RF method had a similar but lower F1 score in the diseased class and less overall accuracy than the SVMR method, while the SVML and KNN methods were neither the best for the multiclass task in terms of accuracy nor presented advantages for detecting diseased pixels. The proposed pipeline combines advantages of the best-performing classifiers. The pipeline showed the best performance in precision for the healthy class, better

F1 score in the class diseased, and a slight improvement of the overall accuracy compared with single classifiers.

Dynamic of feature type for performance contribution

The area under the curve (AUC) values from the precision-recall (PR) curve is shown in Figure 4 and used to understand the dynamic of the contribution of each class to the overall performance. For this aim, SB features were taken as reference and, by individually adding each feature type, a comparison of performance was feasible through AUC values. The class healthy showed a high classification performance for all combinations in general (AUC close to 1). A slightly better performance was observed for all feature combinations that included VI features (VI-, SB-VI-, and SB-VI-SH-DSM$_r$-RE features). For the class diseased, all feature types showed a better performance than single bands. VI and SH features contributed the most to performance after the all features classifier, followed by DSM and RE features. For classes healthy, diseased, soil, and other, the best classification performance was obtained using the PLS method with all features. An increase in AUC values of 1, 12, 6, and 2%, respectively, for each class is observed compared with the reference model (SB features).
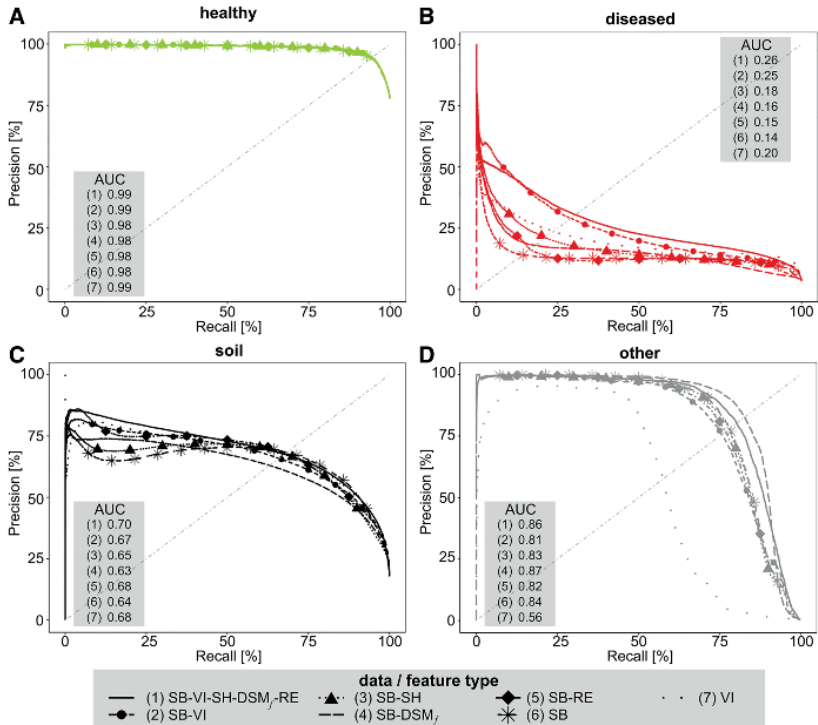
Fig. 4. Area under the curve (AUC) for Precision-Recall curve from partial least squares discriminant analysis classifiers. Abbreviations SB, RE, VI, SH, and DSM$_r$ are addressed to single bands, resolution, vegetation indices, shadow, and digital surface model feature types, respectively. Comparison of diverse feature types to contribute in performance in the **A,** healthy; **B,** diseased; **C,** soil; and **D,** other classes.

54

Only two cases were observed with lower performance than the reference: by adding DSM and RE features for the classes soil and other, respectively. Although the PR curve was not evaluated for the SVMR method, it is relevant to mention the results of the available analysis of feature importance for both classifiers, as well as the individual behavior of features belonging to DSM and RE. RE features showed low importance values in all four classes (0 to 4%); both m and l contributed 0% in the class soil. From DSM_{fs} individual relevance was observed as well: slope (ζ) had a range of importance in all classes of 3 to 18% for the PLS-DA classifier and 2 to 67% for the SVMR classifier; this feature affected principally the classes diseased and healthy. Angle of incidence between the canopy surface and light source (θ_s) showed only a low contribution, with an importance range from 1 to 9 and 0 to 3% for the PLS-DA and SVMR classifier, respectively.

Epidemiological development of *DS* and scoring comparison

Development of *DS* scoring for expert-based and UAV-based data for the treatment inoculated without fungicide is shown in Figure 5A.

In the susceptible variety, the exponential phase of *DS* was observed from the middle of July until the beginning of August. The resistant variety showed a later and longer exponential increase from the middle of August until the end of September. In all experimental treatments, $AUDPC_{DS}$ values obtained from expert scores were in a range from 2,810.4 to 7,058.8%.days, while UAV-based values were generally lower, in a range from 1,400.5 to 4,343.2%.days. Susceptible and resistant varieties showed clear differences in the $AUDPC_{DS}$ values. Emphasizing quantitative resistance and observing the fungicide strategy with highest disease pressure (inoculated without fungicide), UAV scores for susceptible and resistant genotypes were 4,343.2 and 2,403.3%.days, respectively; likewise, expert scores were 7,058.8 and 4,874.8%.days (Fig. 5A). Moreover, mean values of $AUDPC_{DS}$ were significantly different between the tested varieties and for both expert and UAV assessments (two-sample t test, $P \leq 0.05$). *DS* development of the inoculated with fungicide and noninoculated with fungicide treatment is shown in Supplementary Figure S3A and B.
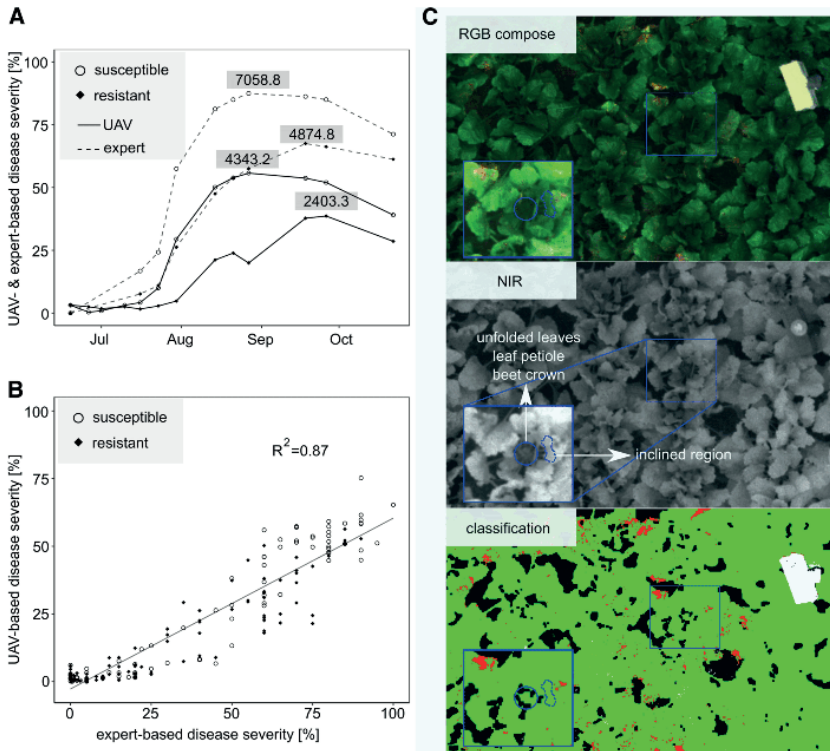
Fig. 5. A, Dynamic of disease severity (DS) based on unmanned aerial vehicle (UAV)- and expert-based scores (in gray boxes, area under disease progress curve values in %.days) and **B,** degree of relationship of both scores based on UAV scores. Symbols: r_S = Spearman's rank correlation coefficient, asterisks (***) = significant at the $P \leq 0.001$ level, slope = 0.63, and intercept = −2.7. **C,** RGB compose, near-infrared (NIR)-band image, and result of classification of a scored field region; identification of regions for explaining underestimation of UAV-based DS scores.

After evaluation of normal distribution, the nonparametric correlation test delivered a Spearman's correlation coefficient (r_s) of 0.91, with a strong correlation of expert and UAV scores ($P \leq 0.01$) (Fig. 5B).

In the case of DI scoring, UAV-based values showed a strong decrease from the first monitoring date to the end of June and beginning of July, as shown in Figure 6A for the inoculated treatment. The minimum value of DI coincides in time with the maximum values for the cover of healthy foliage (Fig. 6B). Under the highest disease pressure, the susceptible variety reached the maximum DI score by the end of July, 2 weeks earlier than the maximum DS score (Fig. 5A). In
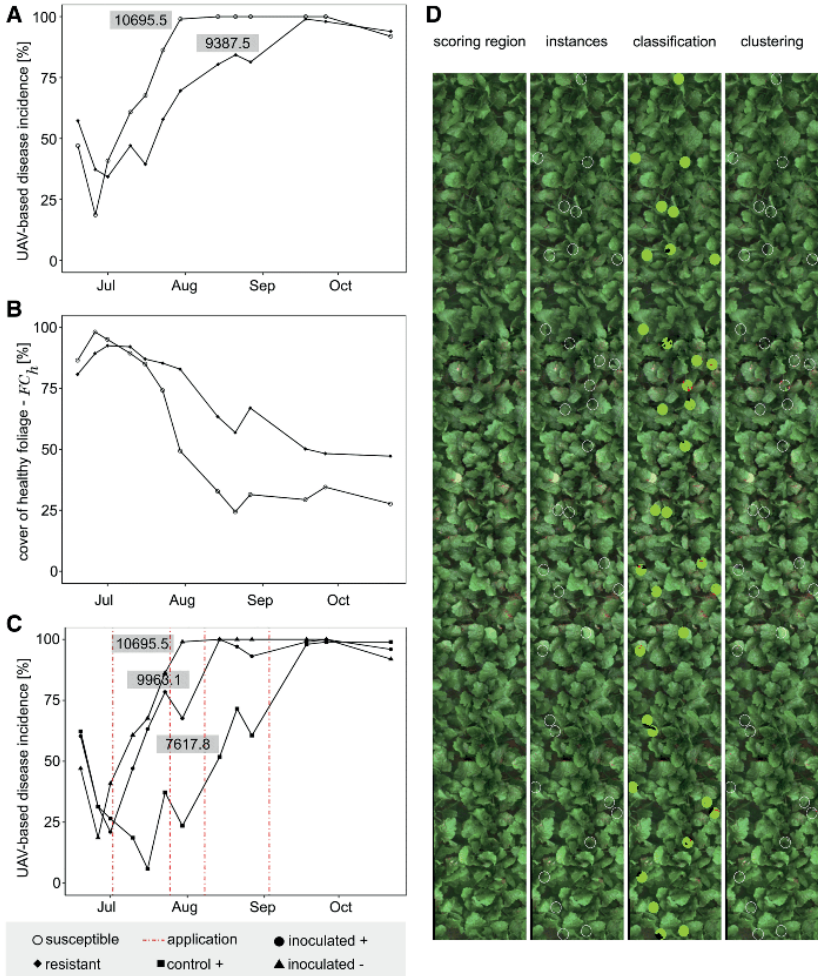
Fig. 6. Disease incidence (DI) based on unmanned aerial vehicle (UAV) scoring. Development of DI **A,** between varieties under the highest disease pressure; **B,** foliage cover of healthy vegetation; and **C,** susceptible variety within all fungicide strategies. Symbols + or − indicate presence or absence, respectively, of fungicide application. In gray boxes, area under disease progress curve values in %.days. **D,** Determination of DI after selecting a scoring region, identification of 34 instances, multiclass prediction, and clustering inside a plot for susceptible variety and inoculated without fungicide application on 10 July 2019.

contrast, the resistant variety reached the highest DI value simultaneously with the highest DS value. Within fungicide levels, a peculiar zig-zag behavior was observed for the noninoculated fungicide-applied treatment (Fig. 6B). Three local minima were observed at the middle of July, end of July, and end of August, 14, 5, and 19 days after fungicide application, respectively. A similar behavior was observed in the inoculated fungicide-applied treatment with two local minima. AUDPC$_{DI}$ values for the DI_{UAV} parameter in all treatments ranged from 7,617.8 to 10,695.9% days, and individual plotwise scores from UAV and experts were significantly correlated (r_s 0.59, $P \leq 0.01$). The behavior of UAV-based DI curve for the two additional fungicide levels is shown in Supplementary Figure S3C and D.

ANOVA and quality parameters

Fungicide strategy was the only significant factor that affected root yield, sucrose content, and WSY (Table 4). The variety and combined effect variety-fungicide did not affect quality parameters. WSY$_{loss}$ due to CLS was 32.6 and 47.1% for the resistant and susceptible variety, respectively. Mean values were significantly different (two-sample t test, $P \leq 0.05$) and complement AUDPC$_{DS}$ for quantitative resistant between both varieties.

ANOVA of AUDPC from expert-based and UAV-based scores of parameters DS and DI were similar and showed that DS was significantly affected by the variety and fungicide factor (Table 4), whereas DI was only affected by fungicide strategy. The top three F values for the factor fungicide were also $A_{C/F}$, A_c, and the parameter $C_{C/F}$. In general, all expert-based and UAV-based parameters were significantly affected by the factor fungicide. In the same mode, A_F, A_H, and $A_{C/F}$ present the highest F values and are the most significant parameters for the factor variety.

Discussion

Precision, recall, and specificity for disease detection

We noticed on the images a typical characteristic of the so-called "real-world" cases of imbalanced multiclass data. Facing imbalance,

a robust classification over all classes is achieved with the help of high precision (Gautheron et al. 2019). The proposed pipeline can fulfill this condition for the best results (Table 3). As a single classifier, the PLS-DA method delivered the best results for the multiclass task. Supremacy of the classifier is mainly observed in the high precision and high recall value of the most frequent class, healthy (Fig. 2). PLS is a linear method originally designed for regression; however, it is possible to use it for classification by implementing a discrimination function (Barker and Rayens 2003; Liland and Indahl 2009). In the past, PLS-DA showed advantages for disease detection in spectroscopy. Gold et al. (2020) obtained the best performance with PLS-DA by comparing three classification methods for a multiclass task. In their work, plant leaves were assessed, and nonimaging spectral information from 400 to 2,400 nm was used to classify potato late blight disease in four different disease stages. For a two-class task, Barreto et al. (2020) also found the best performance with a PLS-DA classifier to discriminate healthy and diseased sugar beet plants affected with Rhizoctonia root rot disease. In their review, Lee et al. (2018) attributed the popularity of PLS-DA in chemometrics to characteristics of spectral data: a high number of samples, a high number of variables, and a tendency of collinearity among the variables. SVMR was the best method to classify CLS-affected regions in our study, because a lower false-positive (FP) rate than for PLS-DA concerning the discrimination of diseased pixels was found. Classes soil and healthy were observed around two-third less in SVMR than in the PLS-DA classifier. This led us to infer that a nonlinear decision boundary can perform a better classification of diseased pixels (Ghosh et al. 2019). Our pipeline combined advantages of both classifiers, achieving a high recall but low precision for the class diseased.

Despite the good overall accuracy of 86.3%, the imbalance in class distribution in the dataset has to be critically considered. Moreover, the class diseased was relatively underrepresented. In a previous study for image-based classification of CLS-diseased regions, Görlich et al. (2021) came to precision and recall values similar to those in our pipeline (33 and 67%). According to Maxim et al. (2014), a methodology with high recall is fit for disease detection

Table 4. Analysis of variance results for quality, visual rating, and unmanned aerial vehicle (UAV) parameters

Parameter	F value[c]			
	Block	Variety	Fungicide	Variety-fungicide
Quality[a]				
Root yield (RY)	0.6	0.3	9.7**	2.0
Sucrose content (SC)	2.6	3.0	12.1**	1.6
White sugar yield (WSY)	4.2	3.4	12.7**	2.0
Expert[b]				
Disease severity (DS-leaf)	0	5.7*	15.8***	1.3
Disease incidence (DI-plant)	0.1	0.3	4.7*	0.3
UAV[b]				
Area of foliage (A_F)	0	22.4***	10.1**	0.9
Area of healthy foliage (A_H)	0.8	18**	13.1**	1.0
Mean area of cluster by unit of foliage area ($A_{C/F}$)	6.5*	14.9**	15.3***	1.3
Disease severity (ds-cover based)	1.8	13.9**	10.9**	1.6
Disease severity (DS_{UAV}-area based)	1.8	13.7**	10.9**	1.6
Mean cover cluster per unit of foliage cover ($C_{C/F}$)	6.1*	13.6**	13.8**	1.3
Cover of healthy foliage (FC_H)	1.6	9.5*	11.0**	1.7
Number of clusters per unit of foliage area (c_F)	2.3	7.9*	7.4**	2.7
Foliage cover (FC)	0.8	7.4*	8.0**	1.8
Cover of diseased foliage (FC_d)	1.7	6.1*	8.6**	0.6
Mean cluster area (A_C)	4.6	5.3*	15.1***	1.9
Area of diseased foliage (A_D)	1.4	4.7	7.7**	0.6
Number of clusters (c)	1.4	2.8	6.7*	1.9
Disease incidence (DI_{UAV})	2.2	0.2	7.3**	1.0

[a] Plotwise quality parameters.

[b] Plotwise area under disease progress curve parameters.

[c] Degrees of freedom of 1, 1, 2, and 2; for block, variety, fungicide, and variety–fungicide factor levels. Asterisks *, **, and *** indicate significant at the $P \leq$ 0.05, 0.01, and 0.001 levels.

because pixels labeled as diseased are correctly classified as this class (Maxim et al. 2014). Nevertheless, under low precision and high recall, the key parameter "specificity" was not reported until now. Specificity is the ability of the classifier to designate nonaffected regions correctly and is based on the FP rate (Maxim et al. 2014). Our pipeline shows a specificity in the class diseased of 95% (calculated from Supplementary Table S2), which is a robust number for classification. This number signifies that 95% of pixels belonging to classes healthy, other, and soil are not classified as diseased (Akobeng 2007). For a hypothetical case of high precision and low recall, the classifier would present poor detection results due to a high false-negative (FN) rate, where most of the labeled diseased pixels would be misclassified as healthy, soil, or other. FN results labeled healthy are mainly chlorotic tissue surrounding CLS lesions as an indirect effect before necrosis (Baranski et al. 2005; Mahlein et al. 2013). FN of class soil is the main constraint of the classifier and pipeline; here, harvest residues of the previous crop used as mulch are commonly classified as diseased regions, which is probably caused by the spectral similarity of collapsed leaves after severe CLS infestation. This constraint is the main reason for using the condition of "$FC_b < 40\%$" to reduce the FN rate of the SVMR in the final pipeline.

Influence of feature type reduction on performance

Based on the presented results and the complexity of the recorded object, individual instead of complete feature type reduction is recommended in the PLS-DA model. Although the contribution of VI in the SVMR classifier was not evaluated, SVMR place the D_{678500}, MSR, and $MCARIOSAVI$ index within the top five variables for the class diseased (Supplementary Table S4). D_{678500} and $MCARIOSAVI$ are vegetation indices with high sensitivity to changes of chlorophyll content (Daughtry et al. 2000; Merzlyak et al. 1999), while MSR is reported to correlate strongly with the leaf area index and the fraction of photosynthetically active radiation absorbed by the canopies (Chen 1996). The SH feature or $NSVDI$ is also a crucial variable for the classification, shown by its place in the top five in the importance ranking for the classes healthy, diseased, and other (Supplementary Table S4). This emphasizes the relevance of quantifying light conditions and shaded regions during the analysis of multispectral UAV-based images. Loss of information and corrupted biophysical parameters are the principal constraints of shaded regions in vegetation (Aboutalebi et al. 2018; Zarco-Tejada et al. 2004; Zhang et al. 2015). The effect of RE features on overall performance is still unclear. This study presented relative homogeneous resolution values ($m = 3.6$ to 5.2 mm) in comparison with the past work of Jay et al. (2020) (9.0 to 23.0 mm). Technical limitations in terms of sensor resolution and CLS spot size do not allow testing a wider resolution range. From the used DSM_b motivated by the quantitative reflectance theory (Qu 2018), ξ is the most relevant angular variable for both classifiers. The angle between sensor and object surface is crucial for the diseased and healthy class according to this study. Furthermore, for future models classifying CLS infection, it is recommended to drop θ_s computation due to poor contribution to the overall performance.

Comparison of expert and automatic scoring

As mentioned by Bock et al. (2021), DS can be expressed in multiple metrics and is used to rate a disease quantitatively by using a numeric scale. This means that CLS can be rated by the description of symptoms, as Jay et al. (2020) did in their work, or DS can be rated by the proportion of diseased foliage area, as presented in this work. Our results confirm that the latter type of DS metric can be calculated by a pixelwise approach with a high correlation to visual scores. However, the slope of 0.63 from linear regression indicates that the UAV scoring estimates only a low percentage of actual DS. This tendency to underestimate DS can be explained by the UAV imaging perspective from nadir (Fig. 5C). The pipeline includes healthy middle leaves, unfolded new leaves, and petioles, whereas experts consider only the middle leaves as the object of assessment. Inclined leaves should also contribute to the underestimation due to a mixed-pixel effect of healthy and diseased labeled samples (Bohnenkamp et al.

2019; Thomas et al. 2018). The present work presents the computing of DS (Fig. 5A) using elemental parameters as c and $A_{c/F}$ (Supplementary Fig. S4A and B), allowing a better understanding of disease development. Curves describe a first increase in the number of CLS clusters followed by an increase of the area of those clusters. We observed that, in terms of number of clusters, the susceptible variety presents the highest number of local maximums during the season (Supplementary Fig. S4A); nevertheless, the parameter $A_{t/F}$ shows potential to identify resistance with significant differentiation of varieties (Table 4). The present study proposed a pipeline to determine DI considering the principles of Nutter et al. (1991). Specimens to evaluate for the disease were the complete plant (expert) and the defined instance (UAV). The exponential phase of UAV-based DI took place 2 to 3 weeks earlier than the exponential phase of DS, showing the potential for creating application maps by georeferencing a scoring area. In the relationship between UAV and visual scoring for values of DI, the degree of correlation is lower compared with results of DS. Wolf and Verreet (2002) showed the differences of assessing DI for plant and leaves; here, the plant-based development reached the maximal DI values earlier than leaf-based visual assessments. The proposed DI_{UAV} also achieves the maximal score later than the plant-based human estimations. For this reason, we recommend performing visual scoring on a leaf scale in future studies, because we expect this modification to increase the degree of correlation with the UAV assessment.

A zig-zag development was observed in all experimental treatments with fungicide application but not in treatments without fungicide. Beyond the fungicide treatment, the zig-zag effect can be further explained with the nadir perspective of UAV imaging, the growth rate of sugar beet during the vegetation period, and the disease pressure. From June to July, sugar beet plants display the highest growth rate of leaves in the season (Kenter et al. 2006), which can be seen in the development of healthy foliage cover (Fig. 6B). After applying fungicide, new unfolded leaves remain healthy with this protective effect and are recorded with the multispectral sensor, decreasing the number of diseased units. The same effect is observed for the second and third application (Fig. 6C) but, after the fourth application at the beginning of September, no decrease of DI was observed, and this coincides with the lowest leaf growth rate, where values are very close to 0 g of leaf in dry matter (grams per square meter per day) from September until harvesting. A lower number of local minimum and a slight decrease in DI values were observed after fungicide applications to the inoculated plots. We attribute this smoother behavior of the DI curve to high disease pressure exerted by the pathogen. Finally, computing DI presents inaccurate values during low foliage cover. This effect is attributed to classifier performance as discussed before, where harvest residues of previous crops are misclassified as diseased foliage. Here, an approach for instance segmentation at the leaf organ will decrease inaccuracy of classifiers and largely reduce the computing time for a pixelwise approach.

Contribution of DSM to the library of parameters and variety differentiation

The principal advantage of using DSM to calculate parameters for disease quantification is the area of the surface (A). A higher differentiation between the varieties is observed by comparing area-based and cover-based parameters. This highlights the potential of area-based parameters to deliver more precise variety differentiation. For example, A_H presents a higher degree of significance in the factor variety than FC_H. The same effect is observed between A_F and FC, as well as $A_{c/F}$ and their foliage cover version ($C_{c/F}$). The density of lesions or, as we called them in this work, the number of clusters, is a type of metric to quantify DS according to Bock et al. (2021). In this work, it was found that, by counting the number of lesions, segmentation of regions (including foliage, soil, and others) makes a difference for evaluating resistance. Information in Table 4 corroborates this statement. When a parameter to quantify CLS lesions by unsegmented area (c) is compared with a parameter with segmented foliage surface (c_F), the factor variety becomes relevant. A similar

58

effect could be observed when comparing the expert-based and UAV-based DI parameters because diseased specimens are being counted ignoring the quantity of foliage. Jay et al. (2020) also mentioned the relevance of lesion density and the cover of healthy foliage to monitor the development of CLS. However, the effects of variety and fungicide strategy were not specified. Lastly, it was demonstrated in the present study that three parameters based on area, including A_F, A_H, and the lesion-based DS metric $A_{\bar{0}/F}$, can deliver a stronger variety differentiation than the well-known DS parameter. The computing of those parameters is easy to extract from the analysis of UAV monitoring data.

Jay et al. (2020) mentioned the disadvantages of multispectral UAV monitoring regarding low-resolution images when compared with high-resolution, robot-based RGB images. This work shows that, when resolution is not a limiting factor, the same parameters can be extracted by both approaches even under the passive illumination of UAV monitoring.

Advantages of automated UAV scoring for determination of resistance and potential improvements

The present work successfully establishes a pipeline to process multispectral UAV images for a pixelwise detection of CLS disease in field trials. Strength and weaknesses were discussed with the help of the PR curves and the analysis of confusion matrix. Advantages in the use of DSM were highlighted, especially by contributing to the differentiation of resistance for sugar beet varieties. DSM allows calculation of a new branch of parameters to describe DS and the CLS development. DS and DI were calculated in diverse metrics according to the last recommendation of Bock et al. (2021). UAV-based DI showed a potential use for creating application maps due to earlier sensitivity for CLS quantification than DS. Improvements of this parameter can be achieved by the segmentation at leaf level and, in future studies, a test for integrated management of CLS has to be conducted. Finally, by comparing the performance of visual scoring and automatic UAV-based scoring, both results came in the same direction and, as mentioned before, differentiation of resistance properties between varieties is sharper from UAV-scoring than the human visual scoring. Considering the arguments exposed, we conclude that multispectral UAV systems are potential tools to determine the resistance of new sugar beet varieties under field conditions. Here, it was proven that the technology can replace the very laborious work of visual scoring by supplying efficiently trustful parameters, thereby accelerating the breeding process itself. The presented approach can be transferred to agricultural practice for decision making in integrated pest management.

Literature Cited

Aboutalebi, M., Torres-Rua, A. F., Kustas, W. P., Nieto, H., Coopmans, C., and McKee, M. 2018. Assessment of different methods for shadow detection in high-resolution optical imagery and evaluation of shadow impact on calculation of NDVI, and evapotranspiration. Irrig. Sci. 37:407-429.

Akoheng, A. K. 2007. Understanding diagnostic tests 1: Sensitivity, specificity and predictive values. Acta Paediatr. 96:338-341.

Bannari, A., Morin, D., Bonn, F., and Huete, A. R. 1995. A review of vegetation indices. Remote Sens. Rev. 13:95-120.

Baranski, R., Baranska, M., and Schulz, H. 2005. Changes in carotenoid content and distribution in living plant tissue can be observed and mapped in situ using NIR-FT-Raman spectroscopy. Planta 222:448-457.

Barker, M., and Rayens, W. 2003. Partial least squares for discrimination. J. Chemometr. 17:166-173.

Barreto, A., Paulus, S., Varrelmann, M., and Mahlein, A.-K. 2020. Hyperspectral imaging of symptoms induced by *Rhizoctonia solani* in sugar beet: Comparison of input data and different machine learning algorithms. J. Plant Dis. Prot. 127:441-451.

Bock, C., Barbedo, J. G. A., Del Ponte, E. M., Bohnenkamp, D., and Mahlein, A.-K. 2020. From visual estimates to fully automated sensor-based measurements of plant disease severity: Status and challenges for improving accuracy. Phytopathol. Res. 2:9.

Bock, C., Pethybridge, S. J., Barbedo, J. G. A., Esker, P. D., Mahlein, A.-K., and Ponte, E. M. D. 2021. A phytopathometry glossary for the twenty-first century: Towards consistency and precision in intra- and inter-disciplinary dialogues. Trop. Plant Pathol. 47:14-24.

Bohnenkamp, D., Behmann, J., and Mahlein, A.-K. 2019. In-field detection of yellow rust in wheat on the ground canopy and UAV scale. Remote Sens. 11:2495.

Bundessortenamt. 2017. Beschreibende Sortenliste Getreide, Mais Öl- und Faserpflanzen, Leguminosen, Rüben, Zwischenfrüchte 2017.

Chen, J. M. 1996. Evaluation of vegetation indices and a modified simple ratio for boreal applications. Can. J. Rem. Sens. 22:229-242.

Corripio, J. G. 2003. Vectorial algebra algorithms for calculating terrain parameters from DEMs and solar radiation modelling in mountainous terrain. Int. J. Geogr. Inf. Syst. 17:1-23.

Daughtry, C., Walthall, C., Kim, M., de Colstoun, E., and McMurtrey, J. 2000. Estimating corn leaf chlorophyll concentration from leaf and canopy reflectance. Remote Sens. Environ. 74:229-239.

De Coninck, B. M., Amand, O., Delauré, S. L., Lucas, S., Hias, N., Weyens, G., Mathys, J., de Bruyne, E., and Cammue, B. P. 2012. The use of digital image analysis and real-time PCR fine-tunes bioassays for quantification of Cercospora leaf spot disease in sugar beet breeding. Plant Pathol. 61:76-84.

Deng, L., Mao, Z., Li, X., Hu, Z., Duan, F., and Yan, Y. 2018. UAV-based multispectral remote sensing for precision agriculture: A comparison between different cameras. ISPRS J. Photogramm. Remote Sens. 146:124-136.

Feindt, F., Mendgen, K., and Heitefuss, R. 1981. Feinstruktur unterschiedlicher Zellwandreaktionen im Blattparenchym anfälliger und resistenter Rüben (*Beta vulgaris* L.) nach Infektion durch *Cercospora beticola* Sacc. J. Phytopathol. 101:248-264.

Gautheron, T., Habrard, A., Morvant, E., and Sebban, M. 2019. Metric learning from imbalanced data. Pages 923-930 in: 2019 IEEE 31st Int. Conf. Tools with Artificial Intelligence (ICTAI).

Ghosh, S., Dasgupta, A., and Swetapadma, A. 2019. A study on support vector machine based linear and non-linear pattern classification. Pages 24-28 in: 2019 Int. Conf. Intelligent Sustainable Systems (ICISS).

Gold, K. M., Townsend, P. A., Herrmann, I., and Gevens, A. J. 2020. Investigating potato late blight physiological differences across potato cultivars with spectroscopy and machine learning. Plant Sci. 295:110316.

Görlich, F., Marks, E., Mahlein, A.-K., König, K., Lottes, P., and Stachniss, C. 2021. UAV-based classification of Cercospora leaf spot using RGB images. Drones (Basel) 5:34.

Haboudane, D. 2004. Hyperspectral vegetation indices and novel algorithms for predicting green LAI of crop canopies: Modeling and validation in the context of precision agriculture. Remote Sens. Environ. 90:337-352.

He, L., Ren, X., Gao, Q., Zhao, X., Yao, B., and Chao, Y. 2017. The connected component labeling problem: A review of state-of-the-art algorithms. Pattern Recognit. 70:25-43.

Imbusch, F., Liebe, S., Erven, T., and Varrelmann, M. 2021. Dynamics of Cercospora leaf spot disease determined by aerial spore dispersal in artificially inoculated sugar beet fields. Plant Pathol. 70:853-861.

Jay, S., Baret, F., Dutartre, D., Malatesta, G., Héno, S., Comar, A., Weiss, M., and Maupas, F. 2018. Exploiting the centimeter resolution of UAV multispectral imagery to improve remote-sensing estimates of canopy structure and biochemistry in sugar beet crops. Remote Sens. Environ. 231:1-17.

Jay, S., Comar, A., Benicio, R., Beauvois, J., Dutartre, D., Daubige, G., Li, W., Labrosse, J., Thomas, S., Henry, N., Weiss, M., and Baret, F. 2020. Scoring Cercospora leaf spot on sugar beet: Comparison of UGV and UAV phenotyping systems. Plant Phenomics 2020:1-18.

Kenter, C., Hoffmann, C. M., and Märländer, B. 2006. Effects of weather variables on sugar beet yield development (*Beta vulgaris* L.). Eur. J. Agron. 24:62-69.

Lee, L. C., Liong, C. Y., and Jemain, A. A. 2018. Partial least squares discriminant analysis (PLS-DA) for classification of high-dimensional (HD) data: A review of contemporary practice strategies and knowledge gaps. Analyst (Lond.) 143:3526-3539.

Leucker, M., Mahlein, A.-K., Steiner, U., and Oerke, E.-C. 2016. Improvement of lesion phenotyping in *Cercospora beticola* sugar beet interaction by hyperspectral imaging. Phytopathology 106:177-184.

Liland, K. H., and Indahl, U. G. 2009. Powered partial least squares discriminant analysis. J. Chemometr. 23:7-18.

Ma, H., Qin, Q., and Shen, X. 2008. Shadow segmentation and compensation in high resolution satellite images. Pages 1036-1039 in: IGARSS 2008-2008 IEEE Int. Geosci. Remote Sens. Symp. 2.

Madden, L. V., Hughes, G., and van den Bosch, F. 2007. Temporal analysis I: Quantifying and comparing epidemics. Pages 63-116 in: The Study of Plant Disease Epidemics. American Phytopathological Society. St. Paul, MN. U.S.A.

Mahlein, A.-K. 2016. Plant disease detection by imaging sensors—Parallels and specific demands for precision agriculture and plant phenotyping. Plant Dis. 100:241-251.

Mahlein, A.-K., Kuska, M., Behmann, J., Polder, G., and Walter, A. 2018. Hyperspectral sensors and imaging technologies in phytopathology: State of the art. Annu. Rev. Phytopathol. 56:535-558.

Mahlein, A.-K., Rumpf, T., Welke, P., Dehne, H. W., Plümer, L., Steiner, U., and Oerke, E. C. 2013. Development of spectral indices for detecting and identifying plant diseases. Remote Sens. Environ. 128:21-30.

Main, R., Cho, M. A., Mathieu, R., O'Kennedy, M. M., Ramoelo, A., and Koch, S. 2011. An investigation into robust spectral indices for leaf chlorophyll estimation. ISPRS J. Photogramm. Remote Sens. 66:751-761.

Märländer, B., Hoffmann, C., Koch, H. J., Ladewig, E., Merkes, R., Petersen, J., and Stockfisch, N. 2003. Environmental situation and yield performance of the sugar beet crop in Germany: Heading for sustainable development. J. Agron. Crop Sci. 189:201-226.

Maxim, L. D., Niebo, R., and Utell, M. J. 2014. Screening tests: A review with examples. Inhal. Toxicol. 26:811-828.

Merzlyak, M. N., Gitelson, A. A., Chivkunova, O. B., and Rakitin, V. Y. 1999. Non-destructive optical detection of pigment changes during leaf senescence and fruit ripening. Physiol. Plant. 106:135-141.

Nutter, F., Jr. 1990. Remote sensing and image analysis for crop loss assessment. Pages 93-105 in: Crop Loss Assessment in Rice. International Rice Research Institute, Manila, Philippines.

Nutter, F., Jr., Teng, P., and Shokes, F. 1991. Disease assessment terms and concepts. Plant Dis. 75:1187-1188.

Qi, J., Chehbouni, A., Huete, A. R., Kerr, Y. H., and Sorooshian, S. 1994. A modified soil adjusted vegetation index. Remote Sens. Environ. 48:119-126.

Qu, Y. 2018. Sea surface albedo. Pages 163-185 in: Comprehensive Remote Sensing, vol. 5. S. Liang, ed. Earth Systems and Environmental Sciences. Elsevier, Amsterdam, The Netherlands.

R Core Team (2020). R: A Language and Environment for Statistical Computing. Foundation for Statistical Computing, Vienna, Austria.

Rangel, L. I., Spanner, R. E., Ebert, M. K., Pethybridge, S. J., Stukenbrock, E. H., de Jonge, R., Secor, G. A., and Bolton, M. D. 2020. Cercospora beticola: The intoxicating lifestyle of the leaf spot pathogen of sugar beet. Mol. Plant Pathol. 21:1020-1041.

Rossi, V., Battilani, P., Chiusa, G., Giosuè, S., Languasco, L., and Racca, P. 2000. Components of rate-reducing resistance to Cercospora leaf spot in sugar beet: Conidiation length, spore yield. J. Plant Pathol. 82:125-131.

Shane, W., and Teng, P. 1992. Impact of Cercospora leaf spot on root weight, sugar yield, and purity of Beta vulgaris. Plant Dis. 76:812-820.

Steddom, K., Bredehoeft, M. W., Khan, M., and Rush, C. M. 2005. Comparison of visual and multispectral radiometric disease evaluations of Cercospora leaf spot of sugar beet. Plant Dis. 89:153-158.

Thomas, S., Behmann, J., Steier, A., Kraska, T., Muller, O., Rascher, U., and Mahlein, A.-K. 2018. Quantitative assessment of disease severity and rating of barley cultivars based on hyperspectral imaging in a non-invasive, automated phenotyping platform. Plant Methods 14:45.

Vogel, J., Kenter, C., Holst, C., and Märländer, B. 2018. New generation of resistant sugar beet varieties for advanced integrated management of Cercospora leaf spot in central Europe. Front. Plant Sci. 9:222.

Weiland, J., and Koch, G. 2004. Sugarbeet leaf spot disease (Cercospora beticola Sacc.). Mol. Plant Pathol. 5:157-166.

Wolf, P. F. J., and Verreet, J. A. 2002. An integrated pest management system in Germany for the control of fungal leaf diseases in sugar beet: The IPM sugar beet model. Plant Dis. 86:336-344.

Zarco-Tejada, P. J., Miller, J. R., Morales, A., Berjón, A., and Agüera, J. 2004. Hyperspectral indices and model simulation for chlorophyll estimation in open-canopy tree crops. Remote Sens. Environ. 90:463-476.

Zhang, L., Sun, X., Wu, T., and Zhang, H. 2015. An analysis of shadow effects on spectral vegetation indexes using a ground-based imaging spectrometer. IEEE Geosci. Remote Sens. Lett. 12:2188-2192.

Ziya, A., Mehmet, M. O., and Yusuf, Y. 2018. Determination of sugar beet leaf spot disease level (Cercospora beticola Sacc.) with image processing technique by using drone. Curr. Invest. Agric. Curr. Res. 5:669-678.

60

Supplementary materials

Glossary

A	Surface area.
A_D	Surface area of diseased foliage.
A_F	Surface area of complete foliage.
A_H	Surface area of healthy foliage.
$A_{\bar{c}/F}$	Mean surface area of CLS cluster by unit of foliage area.
$C_{\bar{c}/F}$	Mean cover of CLS cluster by unit of foliage cover.
DI	Disease incidence.
DS	Disease severity.
D_{678500}	VI called "difference between RED and BLUE band".
FC	Foliage cover.
FC_d	Cover of diseased foliage.
FC_h	Cover of healthy foliage.
GVI	Green vegetation index.
I	Individual instance.
$MCARIOSAVI$	$MCARIOSAVI$ index.
$MCARI_2$	Modified chlorophyll absorption in reflectance index 2.
$MSAVI_2$	Modified soil adjusted vegetation index 2.
MSR	Modified simple ratio index.
$NSVDI$	Normalized saturation-value difference index.
θ_s	Angle of incidence between the canopy surface and light source.

ζ	Slope or angle between surface and normal to horizontal.
c	Number of clusters.
c_F	Number of clusters per unit of foliage area.
ds_I	Cover based disease severity at I level.
l	Resolution in GSD of DSM.
m	Resolution in GSD of multispectral orthomosaic.
AUC	Area under the curve.
AUDPC	Area under disease progress curve.
CLS	Cercospora leaf spot.
DMIs	Demethylation Inhibitors.
DSM	Digital surface model.
DSM_f	Abbreviation for DSM features.
GSD	Ground sample distance.
KNN	K-nearest neighbors.
ML	Machine learning.
PLS-DA	Partial least squares discriminant analysis.
PR	Precision-recall.
QoIs	Quinone outside Inhibitors.
RE	Abbreviation for resolution features.
RF	Random forest.
RI	Registration identifier.
SB	Abbreviation for single bands features.
SH	Abbreviation for shadow feature or $NSVDI$.

SVML	Support vector machine linear.
SVMR	Support vector machine radial.
UAV	Unmanned aerial vehicle.
VI	Vegetation index and abbreviation for VI features.
WSY	White sugar yield.
WSY$_{loss}$	Loss of white sugar yield.

Table 5-1. In Manuscript III as Table S1, properties of susceptibility to *Cercospora beticola*, yield and quality according to national variety list (Bundessortenamt 2017)

Variety	RI	Susceptibility to *Cescospora beticola*	RY	WSY	SC	K + Na	AmN
susceptible	3012	5	5	6	6	2	5
resistant	2444	3	6	6	6	4	5

value of 1: parameter is missing or very low developed, value of 5: parameter is moderately developed, value of 9: parameter is very strongly developed. RI, registration identifier of the German Federal Variety Office Bundessortenamt; RY, root yield; WSY, white sugar yield; SC, sucrose content; K + Na, concentration of potassium plus sodium; AmN, amino-nitrogen concentration.

Table 5-2. In Manuscript III as Table S2, technical specifications of UAV flights

Date	m	l	Sky	S_u
13th June	3.6	14.4	sunny	$-0.67\vec{\imath} + 0.25\vec{\jmath} + 0.70\vec{k}$
19th June	4.3	17.0	sunny	$0.44\vec{\imath} + 0.39\vec{\jmath} + 0.81\vec{k}$
26th June	5.2	20.8	sunny	$0.56\vec{\imath} + 0.32\vec{\jmath} + 0.76\vec{k}$
1st July	4.2	16.8	sunny	$0.43\vec{\imath} + 0.39\vec{\jmath} + 0.81\vec{k}$
10th July	4.0	15.8	cloudy	$0.53\vec{\imath} + 0.36\vec{\jmath} + 0.77\vec{k}$
16th July	4.0	16.0	cloudy	$0.41\vec{\imath} + 0.43\vec{\jmath} + 0.81\vec{k}$
23rd July	4.1	16.5	sunny	$0.31\vec{\imath} + 0.48\vec{\jmath} + 0.82\vec{k}$
30th July	4.0	16.1	sunny	$0.44\vec{\imath} + 0.46\vec{\jmath} + 0.77\vec{k}$
14th August	4.1	16.6	sunny	$-0.27\vec{\imath} + 0.57\vec{\jmath} + 0.77\vec{k}$
21st August	3.8	15.3	sunny	$0.39\vec{\imath} + 0.57\vec{\jmath} + 0.72\vec{k}$
27th August	4.5	18.2	sunny	$0.46\vec{\imath} + 0.57\vec{\jmath} + 0.68\vec{k}$
18th September	3.4	13.5	sunny	$0.57\vec{\imath} + 0.62\vec{\jmath} + 0.54\vec{k}$
26th September	4.2	16.9	cloudy	$0.36\vec{\imath} + 0.74\vec{\jmath} + 0.56\vec{k}$
22nd October	4.4	17.7	cloudy	$0.56\vec{\imath} + 0.75\vec{\jmath} + 0.35\vec{k}$

where m and l are the ground sample distance (GSD) in mm from the multispectral orthomosaic and the digital elevation model respectively. S_u is the unit vector of the trial field in the direction of the sun.

Table 5-3. In Manuscript III as Table S3, fungicide applications and specifications

Application date	Rate	Product	Active substance	Group
2nd July	0.6 liter/Ha	Duett Ultra	Thiophanat-Methyl, Epoxiconazol	benzimidazole,DMIs
25th July	0.6 liter/Ha	Duett Ultra	Thiophanat-Methyl, Epoxiconazol	benzimidazole,DMIs
8th August	1.0 liter/Ha	Amistar	Azoxystrobin	QoIs
3rd September	1.0 liter/Ha	Rubric	Epoxiconazol	DMIs

Table 5-4. In Manuscript III as Table S4, top 5 variables according to class importance for the PLS-DA- and SVMR-classifier

	Healthy		Diseased		Soil		Other	
place	PLS-DA	SVMR	PLS-DA	SVMR	PLS-DA	SVMR	PLS-DA	SVMR
1	$MCARI_2$	MSR	$MCARI_2$	$BLUE$	NIR	D_{678500}	$MCARI_2$	$BLUE$
2	$MSAVI_2$	$MCARI_2$	$MSAVI_2$	D_{678500}	$REDEDGE$	MSR	$BLUE$	$NSVDI$
3	$GREEN$	$MSAVI_2$	$REDEDGE$	$NSVDI$	$MSAVI_2$	$MCARIOSAVI$	$MSAVI_2$	MSR
4	$NSVDI$	$BLUE$	NIR	MSR	$MCARI_2$	$MCARI_2$	$NSVDI$	$GREEN$
5	$BLUE$	RED	$GREEN$	$MCARIOSAVI$	GVI	$MSAVI_2$	D_{678500}	RED
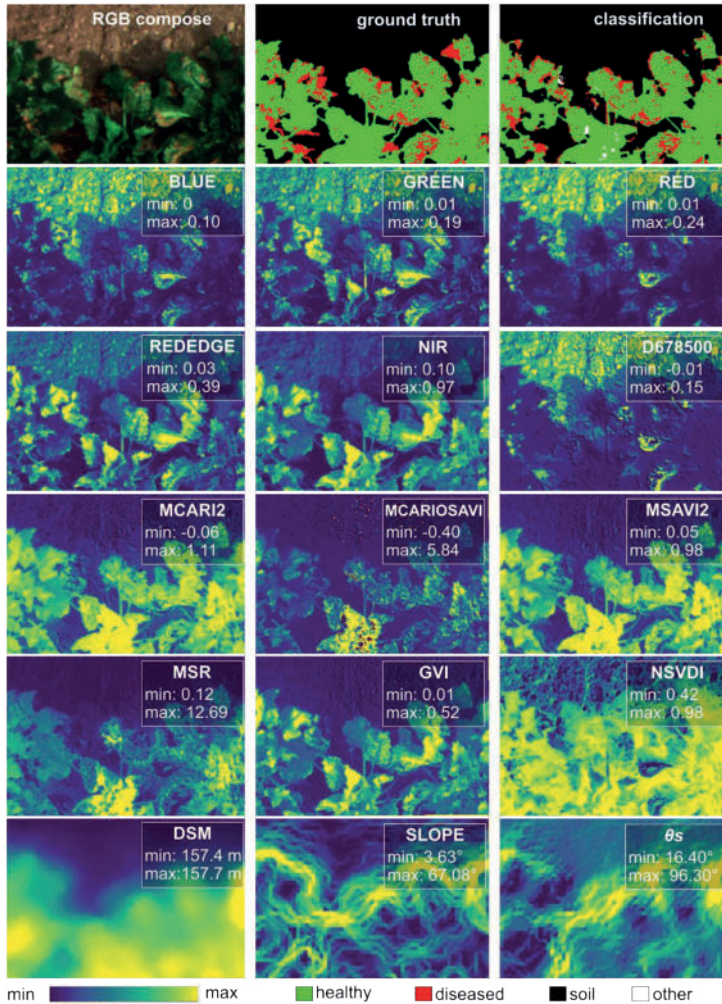
Figure 5-1. In Manuscript III as Figure S1, input variables and features, including classification output and ground truth image under sunny condition with low cloud presence. Assessment of 14th August. Identified outliers by frequency were not considered in the color scale: 5% trimming discards, percentile between the 2.5th and 97.5th percentile of the variable distribution.

A PLS-DA

		prediction			
	class	diseased	other	healthy	soil
reference	diseased	12880	135	2643	34835
	other	120	4744	153	614
	healthy	22610	610	934840	87225
	soil	17656	1560	21929	200613

B SVMR

		prediction			
	class	diseased	other	healthy	soil
reference	diseased	36858	443	1041	12151
	other	69	5426	43	93
	healthy	55173	4182	878215	107715
	soil	39261	4576	17499	180422

C pipeline

		prediction			
	class	diseased	other	healthy	soil
reference	diseased	31393	43	7681	11376
	other	121	4728	185	597
	healthy	26392	186	962716	55991
	soil	36345	1138	43722	160553

Figure 5-2. In Manuscript III as Figure S2, confusion matrix to segment the multiclass task for the (A) PLS-, and (B) SVMR-classifier, and (C) the proposed pipeline.
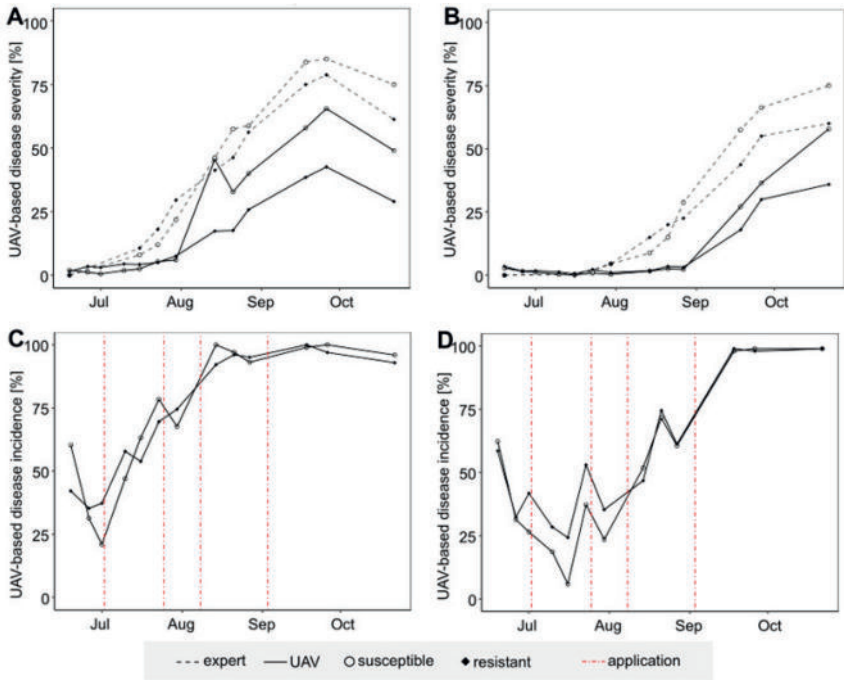
Figure 5-3. In Manuscript III as Figure S3, development of disease severity based on UAV-scores of area data for the treatment inoculated with fungicide (A) and the non-inoculated treatment with fungicide (B). UAV scores for the disease incidence parameter, (C) inoculated with fungicide, and (D) non-inoculated with fungicide treatment.
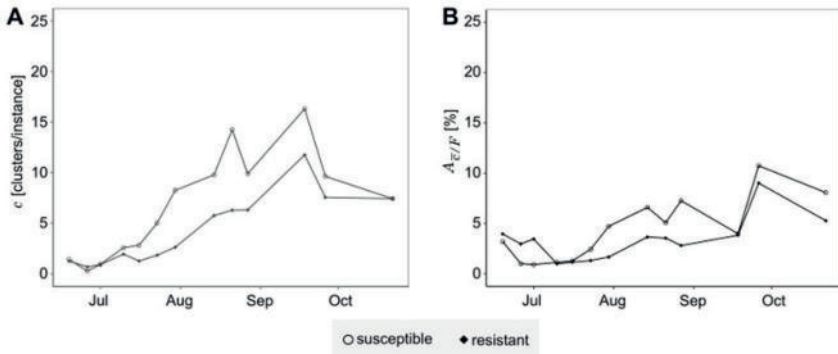
Figure 5-4. In Manuscript III as Figure S4, development of (A) number of CLS clusters per evaluated instance (c) and (B) area of cluster by unit of foliage area in percentage ($A_{\bar{c}/F}$) based on UAV-scores for the inoculated with fungicide treatment.

CHAPTER 6: Leaf segmentation as scoring unit - Manuscript IV

Data Augmentation for Mask-Based Leaf Segmentation of UAV-Images as a Basis to Extract Leaf-Based Phenotyping Parameters

Abel Barreto[1]*, Lasse Reifenrath[2], Richard Vogg[2], Fabian Sinz[2] and Anne-Katrin Mahlein[1]

[1]* Institute of Sugar Beet Research (IfZ), Holtenser Landstraße 77, 37079, Göttingen, Lower Saxony, Germany

[2] Department of Computer Science, University of Göttingen, Holtenser Landstraße 77, 37079 Göttingen, Germany

*Corresponding author: barreto@ifz-goettingen.de

Author contributions

TECHNICAL CONTRIBUTION

Check for updates

Data Augmentation for Mask-Based Leaf Segmentation of UAV-Images as a Basis to Extract Leaf-Based Phenotyping Parameters

Abel Barreto[1] · Lasse Reifenrath[2] · Richard Vogg[2] · Fabian Sinz[2] · Anne-Katrin Mahlein[1]

Abstract

In crop protection, disease quantification parameters such as disease incidence (DI) and disease severity (DS) are the principal indicators for decision making, aimed at ensuring the safety and productivity of crop yield. The quantification is standardized with leaf organs, defined as individual scoring units. This study focuses on identifying and segmenting individual leaves in agricultural fields using unmanned aerial vehicle (UAV), multispectral imagery of sugar beet fields, and deep instance segmentation networks (Mask R-CNN). Five strategies for achieving network robustness with limited labeled images are tested and compared, employing simple and copy-paste image augmentation techniques. The study also evaluates the impact of environmental conditions on network performance. Metrics of performance show that multispectral UAV images recorded under sunny conditions lead to a performance drop. Focusing on the practical application, we employ Mask R-CNN models in an image-processing pipeline to calculate leaf-based parameters including DS and DI. The pipeline was applied in time-series in an experimental trial with five varieties and two fungicide strategies to illustrate epidemiological development. Disease severity calculated with the model with highest Average Precision (AP) shows the strongest correlation with the same parameter assessed by experts. The time-series development of disease severity and disease incidence demonstrates the advantages of multispectral UAV-imagery in contrasting varieties for resistance, as well as the limits for disease control measurements. This study identifies key components for automatic leaf segmentation of diseased plants using UAV imagery, such as illumination and disease condition. It also provides a tool for delivering leaf-based parameters relevant to optimize crop production through automated disease quantification by imaging tools.

Keywords Mask R-CNN · Leaf segmentation · UAV · Plant disease · Sugar beet

1 Introduction

Imaging sensors attached to unmanned aerial vehicles (UAVs) are systems that currently revolutionize the way to monitor agricultural fields [1]. Agricultural management practices are feasible after analysis of high spatial and temporal resolution images, allowing decision making at the right place, with the right intensity, and at the right time. The list of practical applications of UAV-systems starts with the area of plant breeding and phenotyping, and has further applications for plant protection, yield prediction, growth vigor, nutrient status, weed detection and drought stress. Moreover, UAV-systems support precision agriculture because crop production is optimized by maintaining or increasing yield, while reducing environmental impact and resources for pest, water and nutrient management [2].

Disease quantification is a common visual scoring activity for plant breeding and decision making in plant

✉ Abel Barreto
barreto@ifz-goettingen.de

Lasse Reifenrath
reifenrathlasse@gmail.com

Richard Vogg
vogg@cs.uni-goettingen.de

Fabian Sinz
sinz@cs.uni-goettingen.de

Anne-Katrin Mahlein
mahlein@ifz-goettingen.de

1 Institute of Sugar Beet Research, Holtenser Landstraße 77, Göttingen 37079, Lower Saxony, Germany

2 Department of Computer Science, University of Göttingen, Goldschmidtstraße 7, Göttingen 37077, Lower Saxony, Germany

⚛ Springer

protection nowadays. This activity must be executed several times over vegetation development by appropriately trained staff or experts [3]. The most established parameters for quantification are disease incidence (*DI*) and disease severity (*DS*) [4, 5]. For phenotyping *DI* and *DS* in sugar beets, experts collect a representative number of sugar beet leaves, which are assessed for presence or absence of symptoms, and for determining the degree of damage [6]. According to Reynolds et al. [7], phenotyping work like visual scoring represents the major proportion of costs in experimental trials. Variability and repeatability of collected data is also an issue in field assessments: "Inter-rater" errors occur when different experts are involved in phenotyping at various key disease development stages. The high manpower requirement associated with this error source is a disadvantage for extensive experimental fields. Similarly, other factors negatively influence the variability and repeatability of observations, including the effect of noise, heat, exhaustion or time allocated for an assessment [5]. All those factors emphasize the limitations of visual scoring methods and motivate the development of innovative and automated UAV-based imaging approaches for quantification of plant diseases [8–11].

In the past, studies used RGB and multispectral UAV-systems for disease quantification in sugar beet fields. Jay et al. [8] and Görlich et al. [9] segment limits of plot regions from RGB and multispectral orthomosaic images to calculate *DS* in variety trials. Similarly, a pipeline by Günder et al. [12] to segment individual plants, was extended for an application in disease quantification of Cercospora leaf spot (CLS) to classify infested plants according to their disease categories [10]. Circular regions within a plot are considered for an automated analysis of multispectral images to calculate *DI*, *DS*, and additional parameters such as area of foliage, area of healthy foliage, number of lesions and mean area of lesion by unit of foliage [11]. Whether circular-, plant-, or plot-based regions, this image-based scoring shows robustness to calculate *DS*. Nevertheless, *DI* is an aspect to improve: Barreto et al. [11] highlight the disadvantages of delimiting scoring in circle regions within a plot. False positive pixel classification of non-diseased regions leads to inaccurate quantification of diseased units for *DI*. Visualization of scored multispectral images shows that the principal reason of disease misclassification is the pixel quantification of harvest residues of previous crop laying on soil regions. This highlights a potential application of leaf segmentation because image-regions with high misclassification rate are removed from determining *DI*. While leaf segmentation could also contribute to *DS*, this has not been tested yet.

Image-based leaf phenotyping requires detecting and delineating a representative number of leaves for a later parameter calculation. Sugar beet canopy is a complex structure of non-uniform leaves. Individual leaves are positioned with extreme overlap, mutual occlusion, at different heights and diverse orientation. Moreover, leaf appearance is dynamic, either by natural develop stages and senescence, or by exogenous factors like diseases. Leaves change in size, and color from green to yellow, by degradation of chlorophyll content, and later from yellow to brown when necrotic tissue dominates the canopy. At last, weather conditions play also role. UAV monitoring activities must be able to cope with cloudy and sunny sky conditions if farmers are to obtain an on-time decision. Furthermore, shaded regions caused by passive illumination have to be considered for image-based individual leaf segmentation.

To solve the task of leaf identification and segmentation from UAV-data, adequate data analysis approaches are required. This task can potentially be automated by deep learning models in computer vision, more specifically instance segmentation [13]. Unfortunately, the main limitation of deep learning models in agriculture is the need for a high number of labeled images [14]. In the context of UAV-data of agricultural fields, labeling individual leaves in real images is time intensive, making this work the bottleneck for the availability of labeled data.

In this paper, we make two main contributions: (i) we address the challenge of leaf segmentation from multispectral UAV-based images with a limited number of labeled images. We evaluate augmentation approaches including basic image manipulation and copy-paste techniques to create a data set of adequate size for training instance segmentation models (Mask R-CNN). For this specific aim, we consider recommendations as described by Kurnichov et al. [15] using a copy-paste data augmentation approach for banana plantain and arabidopsis images. We identify the best model by testing performance under diverse disease and illumination conditions. (ii) We apply our best leaf segmentation model to large orthomosaic images, and integrate Mask R-CNN into a pipeline to extend the number of parameters for disease quantification beyond the circle-based parameters. Lastly, we apply the pipeline in a variety trial and evaluate the performance by comparing expert with automated scored data of *DS* collected in time-series.

2 Modeling Leaf Segmentation

2.1 Field Monitoring and Methodology

The monitoring campaign took place from 2019 to 2021 in four locations [11, 16]. We use multispectral UAV-systems: a DJI Inspire 2 with a 5-channel multispectral sensor, Micasense RedEdge-M; and a DJI Matrice 210 with a 6-channel sensor variant, Micasense Altum. To get high resolution images, flight missions were planned to deliver a ground sample distance (GSD) between 2.5 and 4.1 mm. We truncate and calibrate the raw images from

digital numbers to reflectance according to Barreto et al. [11]. For the photogrammetry, we use the software Agisoft Metashape Professional for stitching of truncated multi-channel images, and export the output as orthomosaic. We generate image patches to cover a field area of 1.28×1.28 m and scale these to 512×512 px by resampling (Fig. 1a). We use five and six channel re-scaled arrays for defining RGB composite images from reflectance values by using $V = \max(\lambda_{BLUE}, \lambda_{GREEN}, \lambda_{RED})$, and the following formulae:

$$r = \frac{\lambda_{RED}}{V}^{0.7}, \quad g = \frac{\lambda_{GREEN}}{V}^{0.7}, \quad b = \frac{\lambda_{BLUE}}{V}^{0.7} \tag{1}$$

Data augmentation: Manual data labeling is a very difficult and time-consuming task, particularly for sugar beet images which have highly overlapping leaves with almost identical colors. We compare five strategies (see Fig. 1b) to generate sufficient training data while keeping the labeling efforts within reasonable bounds. First, we completely label every leaf in 100 images (512 × 512 pixels) containing healthy and diseased sugar beet plants under sunny and cloudy light conditions. In total, the images contain 2951 leaves without occlusion and we split the individual leaves 80/20 into training and validation set. Eighteen additional completely labeled images serve as a hold-out test set to evaluate the performance of different models. For the background, we select 758 background UAV-images (without sugar beet plants), containing different field conditions such as: diverse soil humidity, weed pressure and soil tillage.

We use the training data and background images in four of five data augmentation strategies (I–V). For all strategies the data sets contain 10,000 images (training to validation ratio of 8000 to 2000). For strategy I we use a copy-paste augmentation technique. For this, we paste 70–140 randomly selected segmented leaves onto randomly selected background images. We use image flipping, scaling and brightness shift to transform each leave image before pasting it to the background. Likelihood and transformation factor are specified in Table 1. Strategies II to IV are mixed strategies. We combine the copy-paste method described above with the inclusion of 100 fully labeled images. Additionally, we include 100 fully labeled images and apply basic manipulation methods, such as flipping, rotation, channel shift, cropping, and brightness adjustment (Table 1). For strategy II, we use the 100 original images and created 4900 copy-paste images. Subsequently, we augment the whole set two times with simple augmentations to obtain 10,000 images. Strategy III uses the 100 original images along with 1900 copy-paste images. We augment this dataset with basic transformations five times. In the case of Strategy IV, we employ 100 original images and 100 copy-paste images, subjecting them to fifty rounds of basic augmentations. The last

strategy (V) relies solely on basic manipulation, with each original image augmented 100 times.

Training: For instance segmentation, we use a Mask R-CNN architecture [17] with a ResNet-101 backbone for ROI (region of interest) prediction. We train the models on four RTX 5000 GPUs running in parallel with two images per batch (batch size = eight images) and use the adapted Mask R-CNN implementation for Tensorflow 2.0 [17] with modules Cudnn 7.6.5.32−10.2, cuda 10.1.243 and Tensorflow 2.2.0. Before training, we specify the classes "leaf" and "background". We put the number of ROIs to train per image from 200 up to 256 and anchors to train per image from 256 up 512. We initialize our models with weights pretrained on the COCO data set [13]. Training the model for one step takes about 22 s. Since we make 500 steps per epoch we get a training time of three hours for one epoch. Mask R-CNN implements a multi-task loss, $\mathcal{L} = \mathcal{L}_{cls} + \mathcal{L}_{box} + \mathcal{L}_{mask}$, to balance correct class predictions, accurate bounding boxes and exact masks. In this study, we trained all models for 50 epochs based on the available computational resources. During the first 25 epochs, the learning rate is kept at 0.001, then changed to 0.0001 until the end of the training.

Evaluation and metrics: We group test set images in six categories based on illumination conditions (cloudy and sunny), as well as the degree of disease damage (healthy, medium and severe). We evaluate the performance of the models with precision, recall and average precision (AP). Precision measures how many of our predicted leaves are actually leaves, while recall evaluates how many of the actual true leaves are detected by the model. Precision and recall depend on a threshold measuring intersection over union (IoU) between a predicted and a ground truth leave. We set this threshold to 50% for precision and recall. This means that to accept a prediction as correct it needs to overlap at least to 50% with a ground truth leave. The second hyperparameter is the confidence score threshold describing how confident the model must be to use the leave prediction. In this paper, we compare values of 0.5 and 0.75 for the confidence score (CS).

For AP, we measure precision and recall for all possible confidence thresholds and plot them in a curve. The area under this curve is the AP. It is large when the true predictions come with high confidence values and there are few false positives.

2.2 Instance Leaf Segmentation

Augmentation for leaf segmentation: In this section we compare the five augmentation strategies for leaf segmentation in diseased sugar beet plants. In Table 2 the AP, precision and recall under two confidence scores CSs are compared. In all approaches, by increasing the CS value, the number of false negative or missed leaves will increase. In contrast

to recall, precision increases with higher CS. Increasing CS from 0.50 to 0.75 yields between 6% to 12% better precision results. The advantages of models with CS of 0.50 was reflected on a higher AP in comparison to models with 0.75 CS. Overall, the best AP was found in the model of strategy V with a value of 0.31. This strategy consist of augmenting fully labeled images only using simple techniques to increase the train and validation set to 10,000 images. Considering the study of Kuznichov et al. [15], and our findings based on the precision values obtained from strategy I in Table 2, we confirm that copy-paste augmentation strategy can serve as alternative for training Mask RCNN models for

leaf segmentation. However, it is worth noting that the most efficient approach might be achieved by employing basic augmentation techniques. A reason for this behavior can be potentially attributed to the number of leaves and their relatively low resolution, which characteristics of small object detection and segmentation tasks. Two-stage detectors such as Mask R-CNN have been observed to exhibit a 50% drop in detection performance for small objects compared to larger ones [18, 19]. Difficulty to distinguish object from background, lack of well-trained features due to limited object information (number of pixels), object occlusion and truncation, are the principal challenges of two-stage detectors for

Algorithm 1 Implementation of sliding window prediction for large images

1: **procedure** LEAFSEG(I, W, s, o)
    ▷ I: RGB orthomosaic image
    ▷ W: weights of trained Mask R-CNN model
    ▷ s: vector with dimensions of window/image to predict
    ▷ o: overlap pixels between windows

2:    $m, n \leftarrow I_{m,n}$ ▷ Get number of rows and columns (m, n)
3:    $I_{leaf}, I_c \leftarrow \emptyset_{m,n}$ ▷ Creating empty matrices
4:    $centers \leftarrow \emptyset$
5:    $stepSize \leftarrow s[1] - o$
6:    $c, c_x, c_y \leftarrow 0$
7:    $P_{masks[1], s[2]} \leftarrow false$
8:    $P_{mask}[(o + 1) : (s[1] - o - 1), (o + 1) : (s[2] - o - 1)] \leftarrow true$
9:    $Nwin_x \leftarrow (m/stepSize)_{[ceiling]}$
10:    $Nwin_y \leftarrow (n/stepSize)_{[ceiling]}$
11:    **for** $x \leftarrow 1 : Nwin_x$ **do**   ▷ Cut the large image into patches
12:        **for** $y \leftarrow 1 : Nwin_y$ **do**
13:            $a \leftarrow s[1]/2 + c_x$
14:            $b \leftarrow s[2]/2 + c_y$
15:            $centers \leftarrow centers \cup a, b$
16:            $c_x, c_y \leftarrow c_x, c_y + stepSize$
17:            $c \leftarrow c + 1$
18:            $I_c[a - s[1]/2, b - s[2]/2] \leftarrow c$
19:            $I_c[a + s[1]/2, b - s[2]/2] \leftarrow c$
20:            $I_c[a + s[1]/2, b + s[2]/2] \leftarrow c$
21:            $I_c[a - s[1]/2, b + s[2]/2] \leftarrow c$
22:        **end for**
23:    **end for**
24:    **for** $w \leftarrow 1 : c$ **do**   ▷ Mask R-CNN prediction for single windows
25:        $lim_x \leftarrow \{min_x(which(I_c = w)), max_x(which(I_c = w))\}$
26:        $lim_y \leftarrow \{min_y(which(I_c = w)), max_y(which(I_c = w))\}$
27:        $P \leftarrow I[lim_x, lim_y, 3]$ ▷ 3D array of image patch
28:        $L_1, .., L_k \leftarrow Prediction(W, P) \in \{leaf\}$
29:        $L \leftarrow \{L_1, .., L_k\}[which(\{L_1, .., L_k\} \cap P_{mask})]$ ▷ Intersect only with non-overlapping center of patch P_{mask}
30:        $I_{leaf}[lim_x[1] : lim_x[2], lim_y[1] : lim_y[2]] \leftarrow L$
31:    **end for**
32: **end procedure**

Table 1 Operations, likelihood and change factor for image transformation used in copy-paste and simple augmentation techniques

Technique	Operation	Likelihood	Factor
Copy-paste	Flipping[a]	1.0	Degree range: 0 to 159°
	Scaling[a]	1.0	Scale range: 0.5 to 1.0
	Brightness shift[a]	1.0	Factor: 0.7 to 1.1
Simple	Horizontal flip[b]	0.4	–
	Vertical flip[b]	0.4	–
	Rotation[b]	0.4	Rotation angles: 90, 180, 270°
	Channel shift[b]	0.6	Shift range: -10 to +10
	Cropping[b]	0.7	Cropping range: 1 to 40%
	Brightness shift[b]	0.5	Factor: 0.8 to 1.5

a= transformation applied to single leaves, and b= transformation applied to entire patch image

quantifying small objects [18]. At this stage, when limited amount of information is a constraining factor, image context becomes relevant. Visual objects often appear within specific environments and may coexist with related objects [20]. The incorporation of contextual information in the datasets gradually increases from strategy I to V (Table 2), consequently enhancing the AP scores. The epidemiological development of the leaf disease and the nadir UAV-perspective by imaging should be an example of image context for the used data augmentation techniques, because specific environmental conditions and coexist with other related objects are not emulated. A previous study demonstrated that enhancing the performance of small object detection is attainable by incorporating additional image information (1 mm GSD) and utilizing simplified conditions. More specifically, when recording images of sugar beet plants prior to canopy closure and in the absence of disease pressure, with fewer leaves, no overlapping, and no leaf senescence, the use of Mask R-CNN yielded an AP value of 0.413 [21].

Environmental conditions for segmenting diseased leaves: We test on data sets with categories "cloudy" and "sunny" separately to further explain the performance of a

Table 3 Performance of model from strategy V in test set considering patch-based image annotation for two light conditions and three disease severity stages
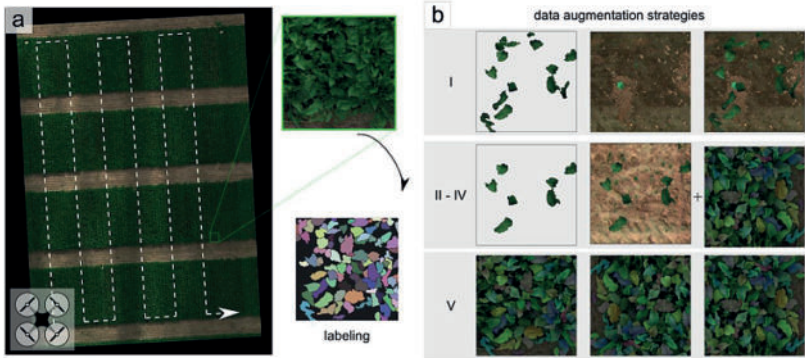
		Healthy	Middle	Severe	Average
Cloudy	AP	0.315	0.350	0.354	**0.339**
	Precision	0.741	0.670	0.701	0.704
	Recall	0.380	0.441	0.436	0.419
Sunny	AP	0.304	0.265	0.242	**0.270**
	Precision	0.680	0.535	0.528	0.581
	Recall	0.399	0.404	0.350	0.384
Average	AP	**0.309**	**0.307**	**0.298**	0.305
	Precision	0.710	0.602	0.615	0.642
	Recall	0.390	0.423	0.393	0.402

The Average Precision (AP) performance for each disease severity stage or light condition is individually highlighted in bold

Table 4 Definition of parameters inside leaf instance

Parameter	Abbreviation	formula
Leaf area	A_l	$\sum_i \sum_j A_L$
Leaf slope	ζ_l	$\dfrac{\sum_i \sum_j \zeta_L}{i \times j}$
Diseased leaf area	A_D	$\sum_i \sum_j D_L \times A_L$
Healthy leaf area	A_H	$\sum_i \sum_j H_L \times A_L$
Disease severity (cover based)	ds_l	$\dfrac{\sum_i \sum_j D_L}{\sum_i \sum_j D_L + H_L} \times 100\%$
Disease severity (area based)	DS_l	$\dfrac{\sum_i \sum_j D_L \times A_L}{A_l} \times 100\%$
Number of clusters	c	c
Average cluster area	$A_{\bar{c}}$	$\dfrac{\sum_i \sum_j D_L \times A_L}{c}$

Mask R-CNN leaf segmentation model under two different environmental illumination conditions. For this evaluation,

Table 2 Error metrics of Mask R-CNN models for augmentation strategies I to V considering two confidence scores for prediction in the test set

		Strategy	I	II	III	IV	V
CS	0.50	AP	0.036	0.161	0.251	0.297	**0.305**
		Precision	0.377	0.457	0.568	0.623	0.642
		Recall	0.064	0.249	0.336	0.384	0.402
	0.75	AP	0.015	0.102	0.162	0.183	0.162
		Precision	0.436	0.581	0.695	0.726	0.723
		Recall	0.022	0.139	0.201	0.221	0.200

The model with the highest Average Precision (AP) is highlighted in bold

CS confidence score

Fig. 1 a Experimental field trial with flight mission, RGB composite orthomosaic, and labeling of image patches (left). **b** Data augmentation following five strategies an (I) exclusively copy-paste technique, (II–IV) combination of copy-paste and simple techniques, and (IV) exclusively simple techniques

the best model in terms of AP (strategy V) was analyzed in Table 3 for all six categories. Data recorded under sunny illumination conditions is the principal source for decrease of performance. UAV-images of sunny days drop in AP of 7% against cloudy and diffuse illumination. However, the question still remains as to whether the drop in performance is primarily influenced by false positive or false negative detections. A more detailed analysis of additional metrics, such as precision, reveals that this parameter experiences a more significant decrease in performance compared to the AP, while the recall remains relatively constant (resulting in a 12.3% decrease in precision). We conclude that analyzing images recorded under sunny illumination conditions increases the number of false positives or objects incorrectly detected as leaves. Illumination is an image condition that affects intra-class variation. This variation drastically impacts the performance of object detection deep learning approaches, because object appearance change in brightness and shading [22]. Furthermore, the effect of degree of disease damage is not clearly visible (Table 3). Future research will need to evaluate this last phenomena seeking the practical application of segmentation. Additionally, apart from the RGB composite, the removed multispectral channels ($\lambda_{REDEDGE}$, λ_{NIR}, and $\lambda_{I,WIR}$) from original multispectral orthomosaics needs to be evaluated within alternative representations for false color composite images to determine possible improvement of leaf instance segmentation of infected fields. Finally, with the increased availability of computational resources for the training step, it is necessary

to evaluate early stopping for achieving optimal leaf instance segmentation results.

3 Application of Leaf Segmentation for Parameter Extraction

3.1 Methodology for Disease Quantification in Variety Trial

We explore the potential of leaf segmentation for monitoring field experiments in a variety trial in 2021 near Göttingen, Germany. The goal of this experiment was to quantify resistance against the disease Cercospora leaf spot (CLS). We arranged a plot-trial with five sugar beet varieties and two fungicide strategies in a two-factorial block design with four blocks or repetitions. The two fungicide strategies are: control with fungicide, and inoculated without fungicide. The registration identifiers of the five sugar beet varieties *Beta vulgaris* L. ssp. *vulgaris* (A–E) are: 3012, 2444, 3290, 3316 and 3706 respectively. Selected varieties belong to the national variety list of the German Federal Plant Variety Office (Bundessortenamt) [23].

Disease assessment: We carry out visual scoring of *DS* of CLS as ground truth simultaneously to the UAV flights, and quantify symptoms as an average value of the plot by assessing middle leaves in percentage estimating a representative infected from total leaf area [6]. The assessment is conducted at leaf level. In total, we randomly sample 100
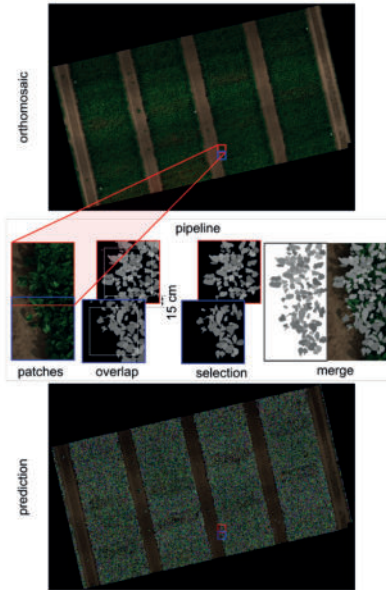
Fig. 2 Pipeline sliding windows for Mask R-CNN prediction of large orthomosaic images, considering an overlap between windows of 15 cm

leaves (25 leaves/plot) per treatment and inspect them for CLS symptoms.

Prediction on large images: Orthomosaic images from UAV-imagery outrun current GPUs capacity for prediction. To extend the model application to a large image from a complete mapped field, we use a sliding windows procedure (Fig. 2). For this purpose and as proposed by Machefer et al. [24], we crop the RGB composite orthomosaic image (I) in patches with an overlap (15 cm or 60 px, o) between neighbours. We use the segmentation model to predict leave instances sequentially on each patch; and eliminate instances with 100% cover in the overlap region. After selection, we reconstruct the remaining leaves in a new orthomosaic image (I_{leaf}). Algorithm 1 shows the procedure.

Instance segmentation for leaf parameter extraction: The availability of I_{leaf} increases the potential for extraction of plant phenotyping parameters. In this study, we propose the integration of this output to a pipeline for pixel-wise classification and extraction of disease-relevant parameters as

specified by Barreto et al. [11]. The new pipeline starts with radiometric calibration and photogrammetric processing of raw images resulting in the multispectral orthomosaic and the digital surface model (DSM). Then, we create a RGB composite orthomosaic image as specified in Sect. 2.1 (Fig. 3a). In the next step, prediction of large image takes place to deliver the I_{leaf} output (Fig. 3b). We calculate image features of multispectral orthomosaic and DSM and store them for later feeding them to two multiclass classifiers, a partial least squares discriminant analysis (PLS-DA), and a support vector machine radial (SVMR). At this level each pixel (Z) is assigned one of four classes, "other", "soil", "diseased", "healthy". This results in a binary array of four layers or images: $O_{i,j}$, $S_{i,j}$, $D_{i,j}$, and $H_{i,j}$, assigned to the four classes respectively. The overlay of any of those outputs with an instance L ($L \in I_{leaf}$) returns four outputs with the delimited instance region: O_L, S_L, D_L, and H_L (Fig. 3c). The binary image D_L is relevant for disease quantification; therefore, clusters (c) can be extracted from D_L (Fig. 3c) by labeling eight connected cluster pixels [25].

Considering the image area (A_L) and image slope (ζ_L) as calculated features from DSM within an instance L [11, 26], we calculate the leaf-based parameters with the formulae in Table 4. These parameters are: leaf area (A_l), leaf slope (ζ_l), diseased leaf area (A_D), healthy leaf area (A_H), disease severity (cover based, ds_l), disease severity (area based, DS_l), number of clusters (c), and mean cluster area ($A_{\overline{c}}$).

Automatic scoring at plot level: Some parameters can not be directly determined from one instance, but they require a sample of instances within a field area. In field trials, this sampling takes place within a plot. A representative sampling for monitoring diseases normally consists of taking 100 leaves for scoring per plot [6]. In the same way, we can express the parameters mentioned in Table 4 as an average within the field area. Moreover, we can calculate the relevant parameter DI in a plot-based manner. To determine DI, it is necessary to define an affected or diseased unit as mentioned by [11, 27, 28]. In the past, we defined an instance as diseased if at least one lesion was present or if the pixel summation in D was greater or equal than one cluster ($c \geq 1$). We can also define a diseased unit with another parameter such as ds_l. Similarly, it is possible to establish threshold values to order diseased leaves (Fig. 6a).

3.2 UAV Parameter for Disease Quantification

Leaf segmentation for disease severity: We compare the disease quantification parameter, DS from UAV-based and expert-based sources in Fig. 4. Figure 4a and b show a parabolic behavior of the UAV-based DS for models with the lowest and the highest AP (strategy I and V). This behaviour presents a maximum value of UAV-based DS at 40% of the ground truth data, and seems to be a limit for the automatic

Fig. 3 Prediction of disease quantification parameters by application ▶ of leaf segmentation. **a** RGB composite of diseased plants, **b** segmentation of leaves, and **c** multiclass pixel-classification and parameter extraction of leaf instances as healthy region (H_L), diseased region (D_L), and number of clusters within a leaf (c)

calculation of leaf-based *DS*. By evaluating the proportion of variance in linear regression (r^2) between both *DS*s, we observe slightly better results in the linear regression model of the UAV-based data from strategy V compared to strategy I. Moreover, there are no clear differences between models with CS of 0.50 or 0.75.

We attribute this parabolic relationship of UAV-based *DS* to the image context and the combined effect from nadir UAV perspective and the new leaf growth emerging of a typical severe epidemics of CLS [29]. The nadir perspective of UAV record mainly above-located leaves which are under severe epidemics and covered by healthy new leaves. This entails special advantage of visual scoring because from a side perspective heavy diseased and small leaves are quantified with high *DS* values [30], while low *DS* values are delivered from UAV-based scores by quantifying healthy new leaves.

To mitigate the effect of image context by analyzing less disease development stages, in Fig. 4c and d were deleted all data with high expert-based values (*DS* higher than 40%). In general, values of r^2 increase significantly after data deletion. Here, the model with the highest AP (strategy V) shows a clear advantage against model of strategy I. In addition, the model with CS of 0.75 performs slightly better than the model with CS of 0.50. A possible solution against this image context challenge is to introduce a new class of leaf instances for leaves with damage higher than 40% in order to give priority to the detection of this morphological different leaves.

Epidemiological development of disease quantification parameters: In this section we show one of the principal applications of leaf segmentation for parameter extraction and plant phenotyping of variety trials for resistance quantification. As described in Sect. 3.1, we work with the experimental design with five varieties and two fungicide strategies. In Fig. 5, we show the development of each genotype during the complete period for disease monitoring with average values of DS_l, A_l, and c. We compare the development of DS_l in Fig. 5a and b for the control with fungicide and inoculated without fungicide variants. Here we see the effect of disease pressure by applications of fungicide, where the control with fungicide variant keeps all varieties healthy until the beginning of September (Fig. 5a). We further observe resistant characteristics of a genotype with high disease pressure. In Fig. 5b, variety A shows the most
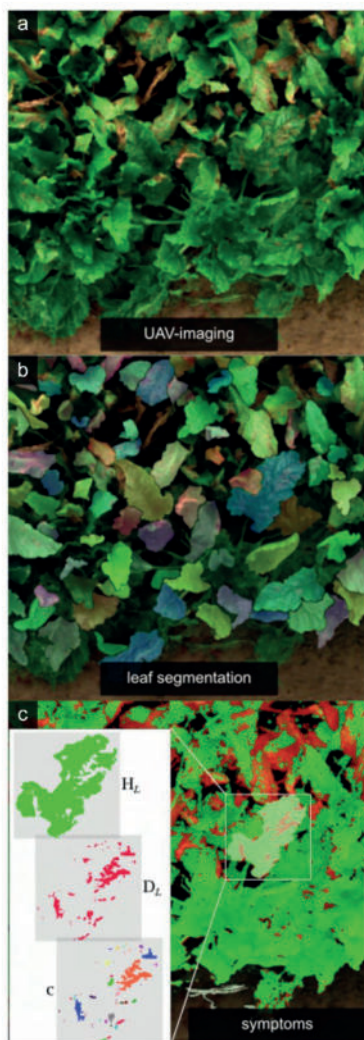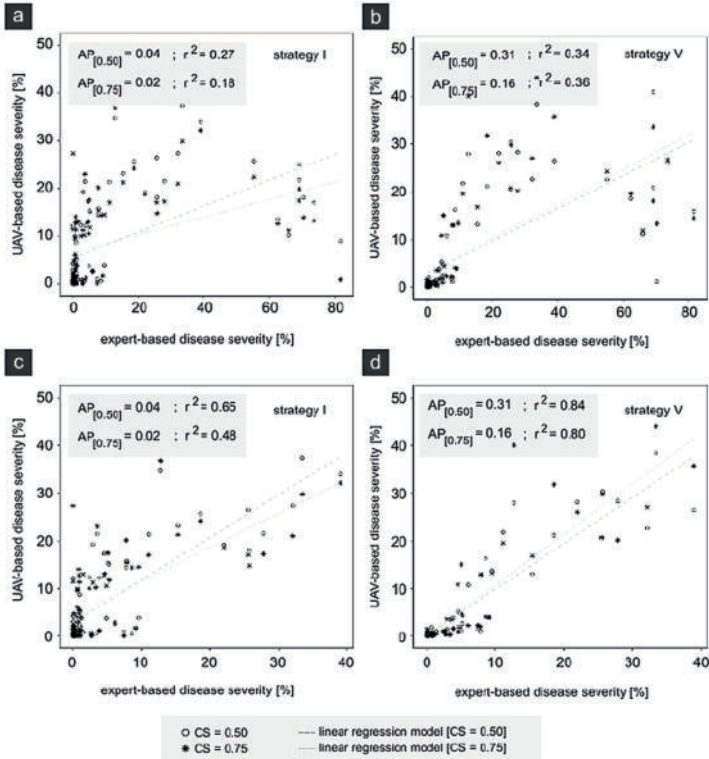
Fig. 4 Relationship of unmanned aerial vehicle (UAV)- and expert-based scores for confidence scores (CS) of 0.50 and 0.75 in two monitoring dates of experimental test field. Comparison of all ground-truth values for model in data augmentation **a** strategy I and **b** strategy V. Comparison for ground truths lower than 40 % in **c** strategy I and **d** strategy V. Monitoring dates: 17th and 31st August 2021

susceptible characteristics, and variety E presents apparently the highest tolerance against CLS. The leaf area is also affected by the genotype and disease pressure (Fig. 5c and d). In Fig. 5c we see that variety C presents the smallest A_l until mid August, while varieties D and E show the biggest A_l during the complete monitoring period. A_l is further affected by disease pressure. UAV-monitoring is a new way to describe resistance (Fig. 5d), where an accumulative value of leaf area highlights the resistance of a genotype. Figure 5e and f show the development of c, where we observe similar properties for disease quantification as with DS_l. The shape

for instance should influence the relevance of c for disease quantification. In our past contribution [11], we calculate c from a circle shape instance and do not find relevance for disease quantification and variety differentiation for resistance. However, using leaf form instances from our instance segmentation model, we are able to contrast variety quantitative resistance.

UAV-parameters for plant protection measure: In Germany, thresholds of DI are the principal indicators for plant protection measures, avoiding losses in sugar beet cultivation [6]. On the field and for the case of CLS, leaves
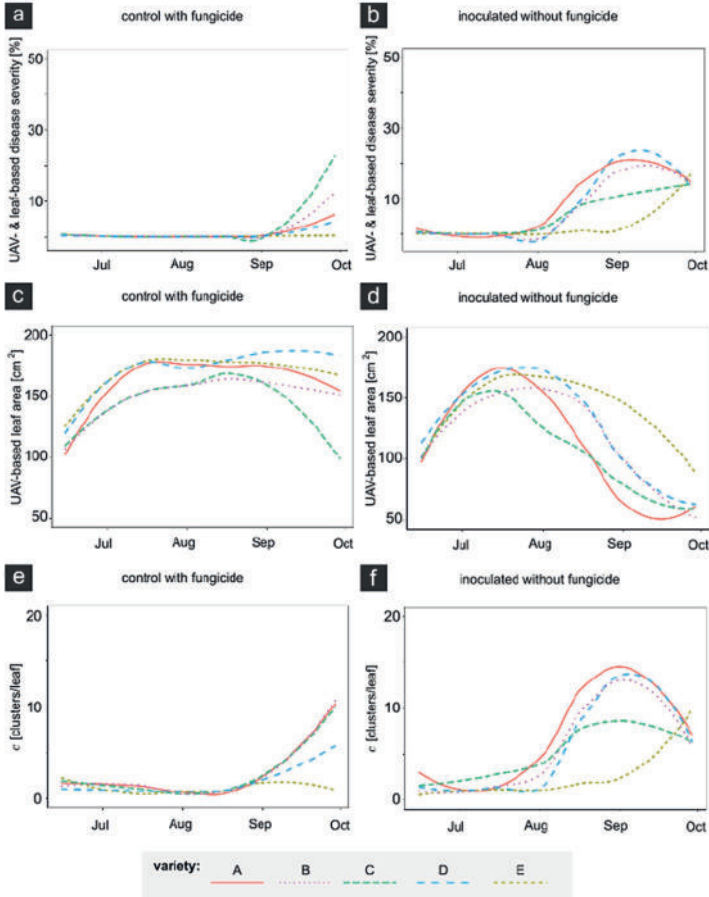
Fig. 5 Development within fungicide strategies and five sugar beet varieties of leaf-based disease quantification parameters: disease severity (**a**, **b**), leaf area (**c**, **d**), and number of clusters per leaf (**e**, **f**). A total of 100 leaves were used for each treatment level. Curves were smoothed using locally estimated scatterplot method

are ordered as "diseased" when at least one CLS spot is present on a sampled middle leaf. To implement an automatic scoring approach, an accurate and robust detection of single spots is compulsory. However, current pixel-wise UAV-based image processing approaches are far from 100% level of precision and recall [9, 11]. This disadvantage makes the automatic definition of a diseased unit a challenge due to the risk of false positives if the criteria

Fig. 6 Decision making based on disease incidence (*DI*). **a** Criteria ▶ for defining a diseased unit based by thresholding c or ds_l parameter. **b** Development of *DI* curve based on diverse threshold magnitudes individually for c and ds_l parameters. **c** Development of UAV-based and expert-based parameters. A total of 100 leaves were used for the treatment level in time-series (variety B and control with fungicide). Curves were smoothed using locally estimated scatterplot method

"$c \geq 1$" is considered, because of the wrong classification of healthy regions as diseased increases. However, this criterium is easy to adapt to different disease quantification parameters in image-processing approaches (e.g. by using c or ds_l) and diverse threshold values (Fig. 6a). We emulate possible time-series developments of *DI* with four different threshold values that defines a diseased unit ("diseased" $if\{c \mid ds_l \geq 1, 5, 10, 25\}$ number of clusters or %). In Fig. 6b we observe that *DI* based on c parameter has a slightly advantage in comparison with *DI*s based on ds_l criteria, due to the early exponential phase in *DI* curve. Nevertheless, *DI* with the most sensible definition criteria of "diseased" ("diseased" if $\{c \geq 1\}$) shows the disadvantage of the inaccurate pixel-wise approach, delivering high values of *DI* at the begin of July when the pathogen was just inoculated, with false positive detections. This inaccuracy can lead to a wrong decision for disease control. The alternative to this problem is to fix a higher threshold value to define a diseased unit avoiding possible emergence of false positives as observed in criteria $\{c \geq 5, 10, 25\}$. However, this decision shifts the exponential phase of *DI* to a later point in time, making this adaptation not suitable for practical use.

In Fig. 6c, we visualize the development of expert-based and UAV-based parameters. We observe that *DS* from expert-based and our leaf segmentation UAV-based data stay close together. This demonstrates that multispectral UAV-imaging for an automatic *DS* assessment under field conditions is feasible. However, in the case of *DI*, the expert ratings show an early exponential phase in the curve in July, while UAV-based scoring with a criteria "$c \geq 5$" presents an exponential phase two months later than the experts. The performance of UAV-based *DI* parameter can be improved with a higher precision and recall for detecting diseased regions. However, we suspect there is a technical gap in the case of CLS for multispectral VISNIR UAV-imaging comparison to expert evaluation. We believe that this is due to restricted view of nadir perspective of UAV-based images in comparison to the possibility of the expert to sample middle and old sugar beet leaves individually, where first symptoms are observed [31].
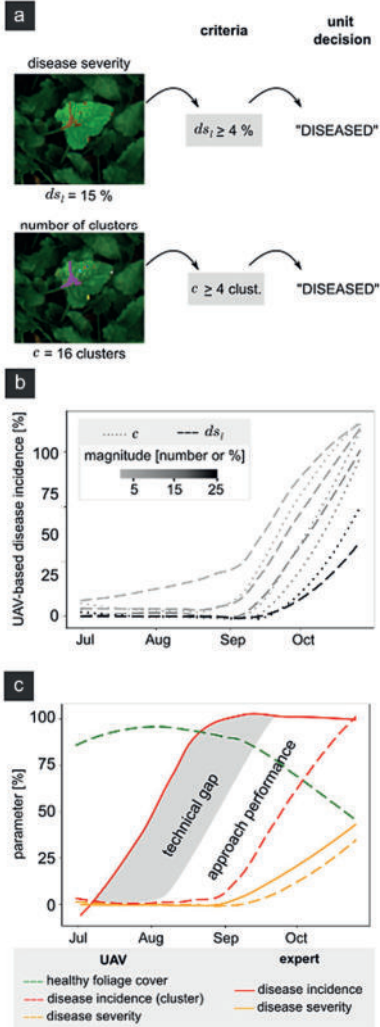
4 General Discussions, Further Work and Conclusion

In this work we give an overview of the complexity of modeling a leaf segmentation approach for UAV-images under field condition. For practical use, automatic leaf segmentation should provide robustness. This includes good performance under diverse illumination conditions, for a high number of genotypes, and considering the epidemiological development of infested plants. This requires a high number of annotated images for modeling one plant–pathogen interaction.

Mask R-CNN models with a good AP performance deliver more accurate disease quantification parameters according to our results in comparison with models with a low AP. Leaf-based phenotyping parameters are relevant tools to describe epidemiological development of sugar beet genotypes under diverse disease pressure. Accumulated $A_l\bar{O}$ over the complete monitoring season should differentiate genotypes for resistance against leaf diseases.

Instance form, whether circle or leaf, should influence the relevance of respective parameters to differentiate genotypes. To graph this statement, we evaluate the case for c parameter from our past contribution [11], where circle-form c showed no significance for the genotype factor, while a leaf-form c presents a potential for resistance differentiation (Fig. 5c).

One of the principal limits for monitoring and scoring leaf diseases in field experiments is the necessity of a high number of trained personal. An automatic UAV-based scoring offers the chance to eliminate human error proper from individual scoring increasing the efficiency of collecting data.

The potential application of multispectral UAV-imaging and leaf-based parameters for disease management has to be analyzed in future studies. Although we mention the possible technical gap for UAV-based DI, we have to consider the potential of dividing a mapped field in mini plots for calculating DI, to make an individual and geo-referenced decision in large mapped fields. Reduction of fungicide use is an important step towards sustainable sugar beet production. This reduction is feasible through site-specific applications guided by geo-referenced and accurate UAV-based DI's as indicators for decision-making.

In conclusion, our experiments show basic image augmentation techniques to be more efficient than the computationally expensive copy-paste augmentation approach for training the leaf segmentation Mask R-CNN on UAV-images in our resource constraint setting. We demonstrate that a leaf-segmentation Mask R-CNN model can be integrated in a pipeline to extract leaf-based parameters of monitored fields. Advantages and limitations from calculated parameters are identified and critically discussed.

Moreover, geo-referenced decision making and site-specific application needs to be addressed by future research. Although we evaluate only the case of CLS disease, the present pipeline for leaf-based parameter extraction can be transferred to agricultural practice and can support decision making in plant breeding for resistance and integrated disease management. Overall, we demonstrate that UAV-based monitoring of sugar beet fields followed by proper post-processing, can output reliable information that increases efficiency by replacing the very laborious work of visual scoring.

Appendix A Supplementary information

UAV	Unmanned aerial vehicle
CLS	Cercospora leaf spot
DSM	Digital surface model
DI	Disease incidence
DS	Disease severity
AP	Average precision
ROI	Region of interest
ML	Machine learning
IoU	Intersection over union
CS	Confidence score
GSD	Ground sample distance
A	Surface area
ζ_L	Image slope or angle between surface and normal to horizontal within a leaf instance
ζ_l	Average slope or angle between surface and normal to horizontal within a leaf instance
PLS-DA	Partial least squares discriminant analysis
SVMR	Support vector machine radial
L	Individual leaf instance
A_L	Image surface area within leaf instance
A_l	Surface area within leaf instance
$A_{\bar{c}}$	Average cluster area within leaf instance
A_H	Surface area of healthy foliage within leaf instance
A_D	Surface area of diseased foliage within leaf instance
ds_l	Cover based disease severity within leaf instance
DS_l	Area based disease severity within leaf instance
W	Trained weights for leaf segmentation Mask R-CNN model
c	Number of clusters

Declarations

References

1. Aasen H, Honkavaara E, Lucieer A, Zarco-Tejada PJ (2018) Quantitative remote sensing at ultra-high resolution with UAV spectroscopy: a review of sensor technology, measurement procedures, and data correction workflows. Remote Sens. https://doi.org/10.3390/rs10071091

2. Maes WH, Steppe K (2019) Perspectives for remote sensing with unmanned aerial vehicles in precision agriculture. Trends Plant Sci 24(2):152–164. https://doi.org/10.1016/j.tplants.2018.11.007

3. Vereijssen J, Schneider JHM, Termorshuizen AJ, Jeger MJ (2003) Comparison of two disease assessment methods for assessing Cercospora leaf spot in sugar beet. Crop Prot 22(1):201–209. https://doi.org/10.1016/S0261-2194(02)00146-1

4. Madden LV, Hughes G, van den Bosch F (2007) Temporal analysis I: quantifying and comparing epidemics. In: The Study of Plant Disease Epidemics, pp 63–116

5. Bock C, Barbedo JGA, Del Ponte EM, Bohnenkamp D, Mahlein A-K (2020) From visual estimates to fully automated sensor-based measurements of plant disease severity: status and challenges for improving accuracy. Phytopathol Res 2(1):9. https://doi.org/10.1186/s42483-020-00049-8

6. Wolf PFJ, Verreet JA (2002) An integrated pest management system in Germany for the control of fungal leaf diseases in sugar beet: the IPM sugar beet model. Plant Dis 86(4):336–344. https://doi.org/10.1094/pdis.2002.86.4.336

7. Reynolds D, Baret F, Welcker C, Bostrom A, Ball J, Cellini F, Lorence A, Chawade A, Khafif M, Noshita K, Mueller-Linow M, Zhou J, Tardieu F (2019) What is cost-efficient phenotyping?

8. Jay S, Comar A, Benicio R, Beauvois J, Dutartre D, Daubige G, Li W, Labrosse J, Thomas S, Henry N, Weiss M, Baret F (2020) Scoring Cercospora leaf spot on sugar beet: Comparison of UGV and UAV phenotyping systems. Plant Phenomics 2020, 1–18. https://doi.org/10.34133/2020/9452123

9. Görlich F, Marks E, Mahlein A-K, König K, Lottes P, Stachniss C (2021) UAV-based classification of Cercospora leaf spot using RGB images. Drones 5(2). https://doi.org/10.3390/drones5020034

10. Yamati FRI, Barreto A, Günder M, Bauckhage C, Mahlein A-K (2022) Sensing the occurrence and dynamics of cercospora leaf spot disease using UAV-supported image data and deep learning. Sugar Industry, 79–86. https://doi.org/10.36961/si28345

11. Barreto A, Ispizua Yamati FR, Varrelmann M, Paulus S, Mahlein A-K (2022) Disease incidence and severity of Cercospora leaf spot in sugar beet assessed by multispectral unmanned aerial images and machine learning. Plant Disease

12. Günder M, Ispizua Yamati FR, Kierdorf J, Roscher R, Mahlein A-K, Bauckhage C (2022) Agricultural plant cataloging and establishment of a data framework from UAV-based crop images by computer vision. GigaScience 11 https://academic.oup.com/gigascience/article-pdf/doi/10.1093/gigascience/giac054/44118901/giac054.pdf. https://doi.org/10.1093/gigascience/giac054. giac054

13. He K, Gkioxari G, Dollár P, Girshick R (2018) Mask R-CNN

14. Danielczuk M, Matl M, Gupta S, Li A, Lee A, Mahler J, Goldberg K (2019) Segmenting Unknown 3D Objects from Real Depth Images using Mask R-CNN Trained on Synthetic Data. In: 2019 International Conference on Robotics and Automation (ICRA), pp. 7283–7290 (2019). https://doi.org/10.1109/ICRA.2019.8793744

15. Kuznichov D, Zvirin A, Honen Y, Kimmel R (2019) Data Augmentation for Leaf Segmentation and Counting Tasks in Rosette Plants. In: Proceedings of the IEEE/CVF Conference on Computer Vision and Pattern Recognition (CVPR) Workshops

16. Barreto A, Lottes P, Ispizua Yamati FR, Baumgarten S, Wolf NA, Stachniss C, Mahlein A-K, Paulus S (2021) Automatic UAV-based counting of seedlings in sugar-beet field and extension to maize and strawberry. Comput Electron Agric 191:106493. https://doi.org/10.1016/j.compag.2021.106493

17. Abdulla W (2017) Mask R-CNN for object detection and instance segmentation on Keras and TensorFlow. Github

18. Leng J, Ren Y, Jiang W, Sun X, Wang Y (2021) Realize your surroundings: Exploiting context information for small object detection. Neurocomputing 433:287–299. https://doi.org/10.1016/j.neucom.2020.12.093

19. Chen C, Liu M-Y, Tuzel O, Xiao J (2017) R-cnn for small object detection. In: Lai, S.-H., Lepetit, V., Nishino, K., Sato, Y. (eds.) pp. 214–230. Springer, ???

20. Tong K, Wu Y, Zhou F (2020) Recent advances in small object detection based on deep learning: A review. Image Vis Comput 97:103910. https://doi.org/10.1016/j.imavis.2020.103910

21. Weyler J, Magistri F, Seitz P, Behley J, Stachniss, C (2022) In-field phenotyping based on crop leaf and plant instance segmentation, 2725–2734

22. Liu L, Ouyang W, Wang X, Fieguth P, Chen J, Liu X, Pietikäinen M (2020) Deep learning for generic object detection: A survey. Int J Comput Vision 128:261–318. https://doi.org/10.1007/s11263-019-01247-4

23. Bundessortenamt (2022): Getreide, Mais, Öl- und Faserpflanzen. In: Beschreibende Sortenliste, p. 369

24. Machefer M, Lemarchand F, Bonnefond V, Hitchins A, Sidiropoulos P (2020) Mask R-CNN refitting strategy for plant counting and

sizing in uav imagery. Remote Sensing 12(18):23. https://doi.org/10.3390/RS12183015

25. He L, Ren X, Gao Q, Zhao X, Yao B, Chao Y (2017) The connected-component labeling problem: A review of state-of-the-art algorithms. Pattern Recogn 70:25–43. https://doi.org/10.1016/j.patcog.2017.04.018

26. Corripio JG (2003) Vectorial algebra algorithms for calculating terrain parameters from DEMs and solar radiation modelling in mountainous terrain. Int J Geogr Inf Sci 17(1):1–23. https://doi.org/10.1080/713811744

27. Nutter F Jr, Teng P, Shokes FM (1991) Disease assessment terms and concepts. Plant Dis 75:1187–1188. https://doi.org/10.1094/PD-75-1187

28. Bock CH, Pethybridge SJ, Barbedo JGA, Esker PD, Mahlein A-K, Ponte EMD (2021) A phytopathometry glossary for the twenty-first century : towards consistency and precision in intra- and inter-disciplinary dialogues. Tropical Plant Pathology. https://doi.org/10.1007/s40858-021-00454-0

29. Weiland J, Koch G. (2004) Sugarbeet leaf spot disease (Cercospora beticola Sacc.). Molecular Plant Pathology 5(3), 157–166 . https://doi.org/10.1111/j.1364-3703.2004.00218.x

30. Woo HR, Kim HJ, Lim PO, Nam HG (2019) Leaf senescence: Systems and dynamics aspects. Annu Rev Plant Biol 70:347–376. https://doi.org/10.1146/annurev-arplant-050718-095859

31. Rangel LI, Spanner RE, Ebert MK, Pethybridge SJ, Stukenbrock EH, de Jonge R, Secor GA, Bolton MD (2020) Cercospora beticola: The intoxicating lifestyle of the leaf spot pathogen of sugar beet. Mol Plant Pathol 21(8):1020–1041. https://doi.org/10.1111/mpp.12962

CHAPTER 7: Site-specific fungicide application based on automated scoring - Manuscript V

Abel Barreto[1] and Anne-Katrin Mahlein[1]

[1]Institute of Sugar Beet Research (IfZ), Holtenser Landstraße 77, 37079, Göttingen, Lower Saxony, Germany

7.1. Abstract

Plant diseases often exhibit a non-uniform distribution within agricultural fields, and site-specific disease control management can capitalize on this spatial variability to reduce fungicide consumption and provide economic benefits. This study aims to compare the effectiveness of uniform and site-specific crop protection measures in managing the spread of Cercospora leaf spot, a foliar disease in sugar beet cultivation. Site-specific management is achieved by utilizing application maps generated from Unmanned Aerial Vehicle (UAV) and multispectral imagery, which are processed to determine disease quantification parameters. The study also evaluates the distance to inoculated zones and fungicide consumption to gain insights into disease epidemiology and control efficiency, respectively. Results show that conducting geo-referenced and UAV-based disease assessments allows for earlier disease control measures compared to visual scoring by humans. There were no significant differences in yield and quality parameters between uniform and site-specific fungicide management. The distance to the inoculation zone played a significant role in disease incidence and lesion numbers, highlighting its importance in implementing those UAV parameters in effective control measures. Surprisingly, site-specific fungicide management required a higher application rate compared to uniform management. Future research should focus on establishing UAV-based thresholds for accurate site-specific disease control and exploring the potential of precision crop protection principles to optimize modern sugar beet production.

Keywords: application map, disease incidence, decision-making, UAV, Cercospora leaf spot, sugar beet

7.2. Introduction

The productiveness of crop is predominantly influenced by entviromental factors, which can cause stress responses in crops. In this context, plant pathogens are considered biotic stress factors that cause plant disease and can heavily harm the productiveness of crops. Plant diseases, often exhibit a patchy distribution within agricultural cultivated fields (Hillnhütter *et al.*, 2011). However, current disease management practices rely on conventional methods that involve the uniform application of pesticides, including fungicides, resulting in undesired of over- and under-dosing across the entire field. To effectively address the heterogeneity of disease occurrence on field, a potential solution is the partition of agricultural fields into smaller areas for more targeted decision-making units (Oerke *et al.*, 2010). Site-specific fungicide application is a promising in reducing fungicide consumption and optimizing crop production, thereby offering potential economic benefits (Maes and Steppe, 2019). Nevertheless, despite its potential advantages, site-specific fungicide management approaches are often neglected due to the lack of suitable technology for practical application for preventive and curative use (Oerke *et al.*, 2010).

In the last years, site-specific fungicide applications have gained considerable attention as a preventive fungal disease management approach, particularly for the cultivation of cereal crops. Numerous studies have explored this technique, which revolves around the optimization of fungicide doses based on crop biomass (Dammer *et al.*, 2008; Ehlert and Dammer, 2006; Tackenberg *et al.*, 2016). Deflection angle and multispectral imaging sensors were primarily utilized on acquiring geographic information and providing data for both off-line and on-line decision support systems. Site-specific and preventive systems have demonstrated the potential in reducing fungicide use from 8% to 23% in comparison to uniform fungicide application with no differences in yield performance (Ehlert and Dammer, 2006; Tackenberg *et al.*, 2016). Another approach of preventive site-specific fungicide application involves leveraging satellite historical imagery and recurrent disease occurrence patterns across multiple years. For instance, in annual or perennial crops such as cotton, the use of color-infrared composite images and prescription maps to guide sprays has resulted in a reported 43% reduction in fungicide use (Yang, 2020). While preventive site-specific fungicide application has demonstrated a reduction of fungicide

usage, the exploration of spatial disease development poses a significant challenge for implementing another kind of site-specific management, curative site-specific applications (Thiessen and Heege, 2013).

Imaging Unmanned Aerial Vehicle (UAV) systems have the capability to assess the disease development on fields by collecting data that contributes to the generation of detailed disease detection maps. Additionally, they play a crucial role in aiding the development of curative site-specific disease control strategies (Maes and Steppe, 2019; Mahlein *et al.*, 2018). Modern Imaging UAV systems utilize high-resolution multispectral technology, which provides detailed canopy information in the visual and near-infrared spectral range, allowing field mapping under natural light conditions (Barreto *et al.*, 2023; Ispizua Yamati *et al.*, 2022; Jay *et al.*, 2020). By capturing images and employing appropriate analysis routines, UAV systems offer a non-destructive assessment tool that delivers valuable disease intensity parameters, including disease severity (DS) (Barreto *et al.*, 2023) and disease incidence (DI) (Barreto *et al.*, 2022), which are obtained through automated post-processing steps. Furthermore, disease incidence serves as a reliable indicator for determining the optimal timing of fungicide applications in a curative response for foliar diseases (Wolf and Verreet, 2002).

In sugar beet cultivation, Cercospora leaf spot (CLS) possess a significant threat to productivity and is caused by the fungus *Cercospora beticola* Sacc. (Jones and Windels, 1991; Rangel *et al.*, 2020; Skaracis *et al.*, 2010). The integrated management of CLS is the standard agricultural practice to minimize the risk of pathogen resistance to fungicide and to ensure productivity (Cioni *et al.*, 2014; Gummert and Ladewig, 2012; Jones and Windels, 1991; Wolf and Verreet, 2002). However, in cases where integrated measures such as crop rotation and resistant cultivars fail, curative applications serve as a last resort to safeguard sugar production in terms of both quantity and quality (Hoffmann, 2010). Decision-making tools for curative fungicide application are based on disease development and use epidemic thresholds as indicators which are expressed in DI (Lang, 2005; Wolf and Verreet, 2002). Similarly, utilizing multispectral information obtained from UAV-based systems allows the determination of georeferenced DI values, offering an alternative decision support system for site-specific CLS management (Barreto *et al.*, 2022; Oerke *et al.*, 2010).

The aim of this research was to: (I) adapt an automatic scoring approach for disease assessment that utilizes circle- and leaf-based parameters for disease quantification to a field experiment inoculated with *C. beticola*; (II) to generate fungicide application maps using threshold values derived from UAV-based disease incidence (DI) data. (III) to evaluate the influence of the distance of inoculation zone and two types of fungicide management (site-specific and uniform) on UAV-based disease quantification, yield, and quality parameters; and (IV) to determine the efficacy of fungicide application in terms of fungicide consumption to understand the effectiveness of site-specific and uniform CLS management.

7.3. Material and methods

Experimental field

In year 2022, an experimental field study on CLS was carried out in Göttingen, Germany (51°33'18.6"N 9°54'01.4"E). The experiment was designed to investigate the effects of two fungicide strategies on the distance to the inoculation zone by using a randomized two-factorial design with three repetitions (see top part of Figure 7-1). The fungicide strategies employed were a uniform fungicide management based on the recommendation for the management of leaf diseases described by Gummert and Ladewig (2012); and a site-specific fungicide management. The uniform fungicide strategy was performed by tractor-based spraying, while the site-specific fungicide strategy was performed by a portable sprayer for manual application. Inoculation zones were delimited in circular regions with a diameter of 2 m. These regions were inoculated 12 days after sowing with effectively 4g per m^2 CLS-infected sugar beet air-dried leaf material. In the following lines, the inoculation zones will also be referred to as hotspots. Inoculation was done in circular regions with a diameter of 2 m by hand, and. Seeking the stratification of automatic scoring, every plot was subsample in 50 miniplots (arrangement of 5 rows and 10 columns). The second factor of the experimental design was determined by measuring the distance between the center of each miniplot to the center of the hotspot. During harvest, the root yield and quality were assessed in 12 miniplot within each plot (see top part of Figure 7-1). The beets were washed, weighed, and processed into beet brei. The brei samples were analyzed for sucrose, potassium, sodium, and amino-nitrogen content using standardized procedures. Lastly, white sugar yield (WSY) was calculated based on

root yield and quality parameters, following German standard equations (Märländer *et al.*, 2003).
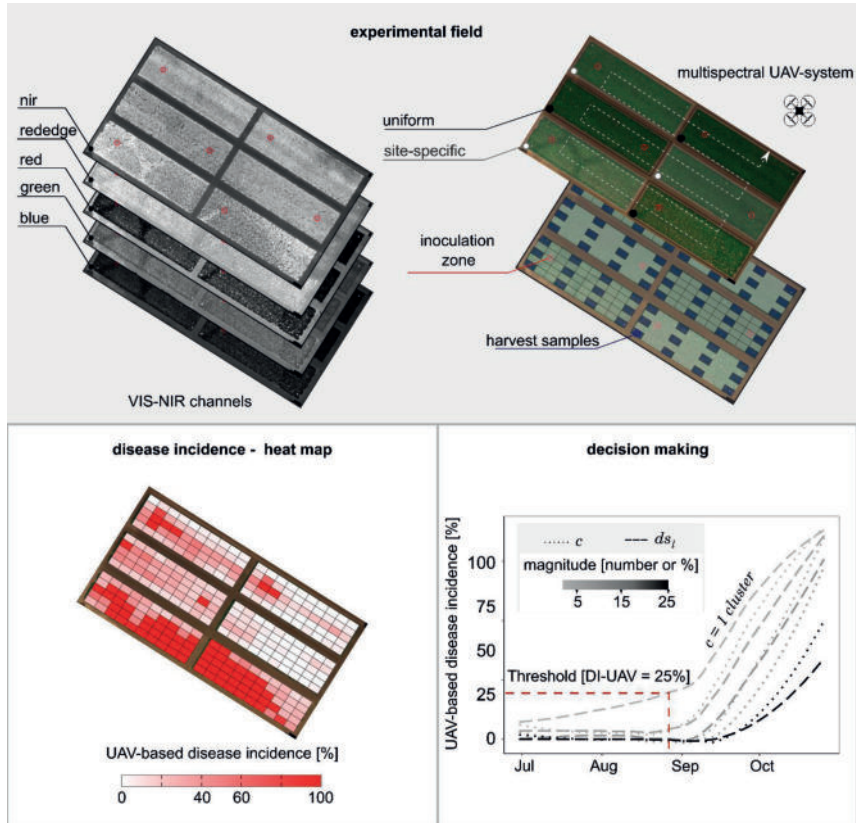
**Figure 7-1.** Multispectral and RGB-composite orthomosaic image of experimental field trial and visualization of fungicide management levels (uniform and site-specific); inoculation zones (hotspots); and miniplots to harvest (top). Down-left: heat map of georeferenced UAV- and leaf-based disease incidence (DI_{leaf}). Down-right: threshold value for automatic scoring based on disease incidence using image-based leaves instances.

Monitoring season

Two types of monitoring approaches were employed to facilitate decision-making regarding fungicide application: a UAV-based and an expert-based monitoring respectively for site-specific and uniform treatment. To collect imaging data and mapping the study area, the UAV-based monitoring approach used a DJI Matrice 210 quadcopter (Da-Jiang Innovations Science and Technology Co., Ltd., China) as an UAV platform which carried a multispectral imaging sensor Altum (MicaSense, Inc., USA). The camera on the UAV captured imagery in three visible spectral bands (BLUE: 475 nm ± 20 nm, GREEN: 560 nm ± 20 nm, red: 668 nm ± 10 nm), two near-infrared spectral bands (NIR : 840 nm ± 40 nm, REDEDGE: 717 nm ± 10 nm) and one thermal infrared band (LWIR, 11± 3 µm) according to Barreto *et al.* (2022), although the thermal band was not considered for data analysis (Figure 7-1, top). In order to facilitate accurate georeferencing and time-series overlaying, ground control points were strategically placed on the field and marked as reference points on the images for coordinate correction. These settings sought an average ground sample distance (GSD) of 3 mm for the multispectral orthomosaic images. The aerial images were acquired during flight missions conducted within three hours of local solar noon. In total three missions (each of 19 minutes) were required to map the complete experimental field. The flight parameters included a forward overlap of 70%, a lateral overlap of 70%, a flight speed of 0.6 m/s, and a flight altitude of 7 m above ground level. The expert-based monitoring consisted of visual assessment of DI following specifications of Wolf and Verreet (2002), and considering middle leaves as scoring unit. In view of an anticipated harvesting campaign concluding in late September 2022. The monitoring period for triggering fungicide spraying in both approaches was determined based on the growing stage and specific criteria outlined by fungicide producer and approved by the German Federal Office of Consumer Protection and Food Safety (BVL) in line to the Europe Union legal framework regulation N° 1107/2009 (EC, 2009). The monitoring period for application began when sugar beet row closure was achieved, indicating that the sugar beets had sufficiently grown and closed together within the row. This marked the initiation of monitoring activities for both the UAV system and the expert. On the other hand, the monitoring period ended on the last permissible date for fungicide application before sugar beet harvesting. This boundary was established to comply with

the guidelines and regulations set by the BVL, ensuring proper monitoring and treatment of sugar beet crops. During this period, data was collected at four monitoring timepoints (Figure 7-2): on June 30th, July 21st, August 8th, and August 19th; and June 30th, July 14th, August 8th, and August 26th for both the UAV-based and expert monitoring respectively. Additionally, for time-series analysis of UAV-based parameters, six further monitoring dates were conducted on May 31st, June 7th, June 16th, June 21st, September 1st, and November 6th.
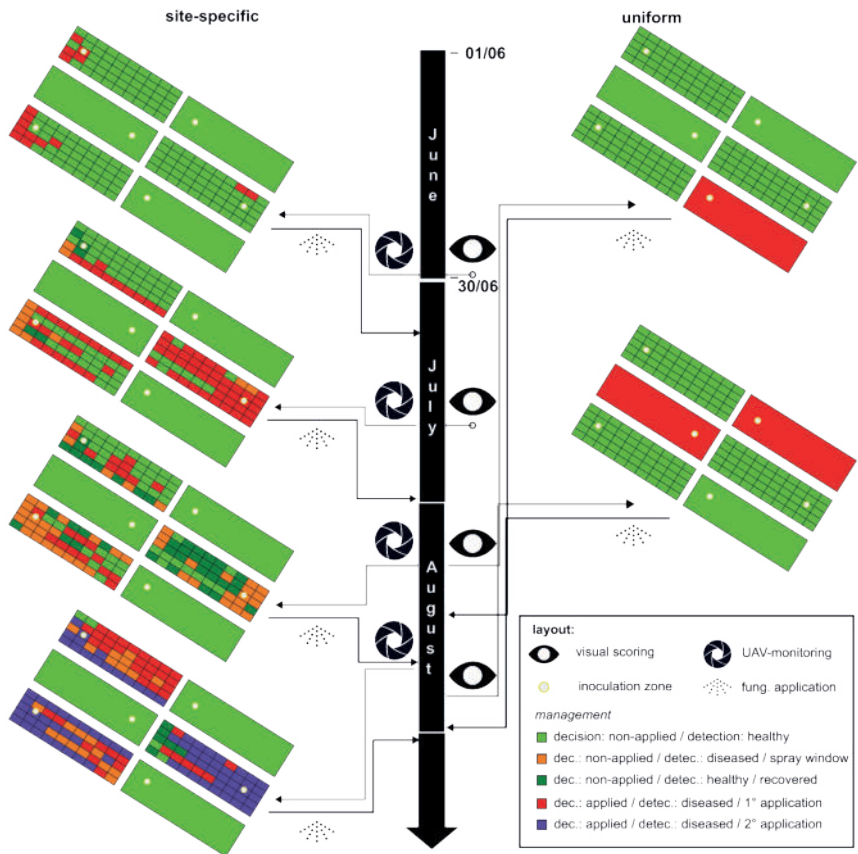
Figure 7-2. Application schedule for site-specific (left) and uniform (right) fungicide management. Gray and black arrows on the timeline visualize the monitoring and application date respectively. Decision-making for miniplots were ruled by healthy or diseased detection and the spray windows between applications according to fungicide manufacturer.

Data processing, automatic scoring, and UAV-based parameters

Multispectral raw images were truncated and calibrated from digital numbers to reflectance according to the camera manufacturer repository (MicaSense, 2018). For the

photogrammetry, we use the software Agisoft Metashape Professional (Version: 1.6.3 build 10732, 64 bit, Agisoft LLC, Russia) for stitching of truncated multichannel images, and export the output as orthomosaic as well as the Digital Surface Model (DSM). RGB composite image was generated from multispectral orthomosaic and used for leaf segmentation according to previous contribution (Barreto *et al.*, 2022), obtaining as result a GeoPackage file containing leaves as polygons (instance leaf segmentation array, I_{leaf}). For each miniplot, seventeen parameters were extracted from the instances circle (I) and leaf (L) as soring units according to Barreto *et al.* (2022, 2023). The parameters calculated were: foliage cover (FC), cover of diseased foliage (FC_d), cover of healthy foliage (FC_h), area of diseased foliage (A_D), area of healthy foliage (A_H), area of foliage (A_F), leaf area (A_l), area- and circle-based disease severity (DS), cover- and circle-based disease severity (ds), area- and leaf-based disease severity (DS_{leaf}), cover- and leaf-based disease severity (ds_{leaf}), leaf slope (ζ_l), leaf-based average cluster area ($A_{\bar{c}}$), number of clusters within circle unit (c_I) number of clusters within leaf unit (c_L), leaf-based disease incidence (DI_{leaf}) circle-based disease incidence (DI).

Generation of application maps

The decision-making process for site-specific management relied on the evaluation of the UAV- and leaf-based parameter DI_{leaf} as an indicator. A diseased unit was considered present if at least one cluster or CLS spot was detected on a segmented leaf. A visual representation of determined georeferenced DI_{leaf} is shown in Figure 7-1 (bottom-left). Drawing upon the findings from our previous study (Barreto *et al.*, 2022) and the performance assessment of DI_{leaf}, we established a fixed UAV-based epidemic threshold of 25% DI_{leaf} (Figure 7-1, bottom-right). Due to limited knowledge of UAV-based epidemic thresholds and the high occurrence of False Positive (FP) classifications in DI_{leaf} calculations, only one threshold was proposed for fungicide application. The timing of repetitive fungicide applications was determined by considering the minimal spray windows specified by the BVL, as well as exceeding the UAV-based epidemic threshold. Application maps were generated based on the scoring of each miniplot and the criteria for repetitive fungicide applications.

Analysis of temporal disease development

In accordance to Madden *et al.* (2007b), Area Under Disease Progress Curve (AUDPC) was calculated for UAV-based parameters. Our first assessment was considered on 31 May (first monitoring date) and the last on 6 November. In total 10 time points were used for calculating the AUDPCs.

Statistic

Quality analysis parameters and UAV-based AUDPCs were evaluated through various statistical tests including the outlier test, dispersion test, and Kolmogorov-Smirnov (KS) test. These tests were conducted to ensure the absence of outliers, normal distribution of variables, linearity, and homoscedasticity. In cases where no significant deviations were observed, linear modeling was employed. Additionally, ANOVA was applied with the randomized two-factorial design to determine the significance of fungicide management and the distance miniplot-hotspot factor.

For cases where significant observations were specifically reported for the dispersion and KS tests, Generalized Linear Model (GLM) frameworks were applied using various link functions such as gamma, gamma inverse, Gaussian, negative binomial, logarithmic transformation, Poisson, and Quasi-Poisson regression. The choice of a specific GLM framework was based on the outcomes of the dispersion and KS tests, respectively.

To evaluate the degree of linear correlation and identify significant differences between UAV-based parameters and WSY, Pearson's correlation coefficient (r) or Spearman's correlation coefficient (r_s) were calculated.

7.4. Results

Evaluated application dates, dynamic of site-specific decision-making, and fungicide consume

Four application dates were scheduled for the site-specific fungicide management treatment, while the uniform variant was treated twice with fungicide (Figure 7-2). On average, there was a 6-day delay between monitoring and application for the uniform fungicide treatment, while the site-specific treatment experienced an average delay of 10 days. The site-specific fungicide application began 38 days earlier than the uniform

treatment and targeted 16 miniplots near hotspots (Figure 7-2 and Table 7-1). The site-specific treatment followed a unique approach for deciding the fungicide spray on miniplots. In the first application, miniplots within plot samples were classified as "diseased" and sprayed if they met or exceeded the UAV-based epidemic threshold (25% DI_{leaf}). For the second site-specific application, an additional condition was taken into consideration, based on the specifications provided by the fungicide producer. Diseased miniplots were not sprayed if the minimum spray window between fungicide applications had not elapsed (Figure 7-2). Furthermore, it was possible to track the recovery of miniplots. Those miniplots that were sprayed in the previous date but detected as healthy in the subsequent assessment were identified. By the second application, 31% of miniplots had recovered, while the remaining miniplots were not sprayed due to the minimum spray window requirement. Sixty-nine miniplots were treated with the site-specific management on the second application date (Table 7-1). At the third monitoring date, both approaches required fungicide application. The uniform treatment reached the first epidemic threshold according to Gummert and Ladewig (2012) and 50 miniplots were sprayed (Table 7-1). On the other hand, the site-specific approach showed a 51% recovery rate among the miniplots treated in the previous date. Of all the miniplots detected as diseased, 68% were not sprayed due to the minimum spray window requirement. Only 21 miniplots were treated on this application date using the site-specific approach. In the final monitoring date, both approaches once again required fungicide applications. In the uniform approach, 100 miniplots met the second epidemic threshold and were treated (Figure 7-2 and Table 7-1). The site-specific approach detected 140 miniplots as diseased, out of which 85% were sprayed. Seventy-nine miniplots were treated for the second time, while 29% of the detected miniplots were treated for the first time (Table 7-1). Overall, the site-specific treatment involved 225 miniplot sprays, while the uniform treatment had 150 sprays, representing a 50% increase in miniplot applications compared to the fungicide management approach proposed by Gummert and Ladewig (2012).

Table 7-1. fungicide management for uniform (tractor-based) and site-specific application

	Application

| | application date | monitoring date | threshold | (N miniplot) | | |
				1°	2°	subtotal
uniform	16/08/2022	08/08/2022	DI (visual) = 5%	50	0	
	29/08/2022	25/08/2022	DI (visual) = 45%	100	0	150
site-specific	08/07/2022	30/06/2022	DI_{leaf}(UAV) = 25%	16	0	
	28/07/2022	21/07/2022	DI_{leaf}(UAV) = 25%	69	0	
	19/08/2022	08/08/2022	DI_{leaf}(UAV) = 25%	21	0	
	01/09/2022	19/08/2022	DI_{leaf}(UAV) = 25%	40	79[a]	225

DI(visual): disease incidence based on visual assessment with leaves as scoring units; DI_{leaf}(UAV): disease incidence based on automatic scoring using image-based leaves instances. [a]Previous application at 08/07/2022 and 28/07/2022.

Impact of fungicide strategy and inoculation distance on quality and canopy parameters

The results of the quality analysis indicated that neither the fungicide management nor the distance hotspot-miniplot factor had a significant effect on any of the sugar beet quality parameters, as shown in Table 7-2. However, when considering the combined effect of distance and management, there was an impact on the sugar content. Canopy parameters assessed by UAV such as A_H, A_F and FC_d were significantly influenced by the fungicide management when using circles as the scoring unit. The most notable differences were observed in the AUDPC values of A_H and A_F. On average, the site-specific fungicide management resulted in higher accumulative values of A_H compared to the uniform treatment, with AUDPCA_H values of 8754 and 8055 cm^2.days, respectively. Similar differences were observed with the parameter A_F, with AUDPCA_F values of 9523 and 8783 cm2.days, respectively. None of the circle-based parameters (FC, DI, ds, DS, and FC_h) met the requirements for linear or GLM modeling.

When using segmented leaves as the scoring unit, both the distance and fungicide management factors significantly influenced the disease control parameter DI_{leaf}

according to GLM (Gamma inverse) modeling (Table 7-2). On average, the uniform management exhibited a lower AUDPCDI_{leaf} compared to the site-specific management. In both treatments, the amount of AUDPCDI_{leaf} decreased as the miniplot deviated from the inoculation point. The parameter c_L was strongly influenced only by the distance to the hotspot (Table 7-2), with no significant influence observed for AUDPCc_L by the fungicide management factor. Similar behaviors were observed for AUDPCs of ds_{leaf} and DS_{leaf}, but with a lower level of significance for the distance factor. All the mentioned parameters with leaves as instances were suitable for modeling with GLMs using Gamma inverse and logarithmic transformations as link functions (Table 7-2). Linear modeling was feasible for the parameters A_l and ζ_l. The AUDPCA_l did not show any significant influence from the fungicide management or distance hotspot-miniplot factors. AUDPCζ_l showed a combined effect of management and distance, while the leaf-based parameter $A_{\bar{c}}$ did not meet the requirements for linear or GLM modeling.

Relationship between UAV-based AUDPC's, yield and quality parameters

After evaluating the normal distribution of the data, both parametric and non-parametric correlation tests were conducted to assess the relationship between UAV-based AUDPCs and WSY, as shown in Table 7-3. Out of the fourteen parameters analyzed, significant correlations were found between WSY and FC, FC_h, A_H, A_F, A_l DS, ds, DS_{leaf} and ds_{leaf} (Table 7-3). The circle-based parameters, including FC, FC_h, A_H, A_F, exhibited the highest correlation coefficients. Among them, the area-based parameters allowed for parametric correlation testing. Notably, AUDPCA_l showed the highest correlation with WSY among all leaf- and UAV-based parameters (Table 7-3). A significant negative correlation was observed between all UAV-based DS parameters and WSY, indicating an inverse relationship. The strongest correlations within the DS parameters were observed when using circles as the scoring units compared to using leaves.

Table 7-2. Analysis of variance results for quality, circle-based and leaf-based unmanned aerial vehicle (UAV) parameters

	Parameter	model			distance	management	D-M
		normality	type	link function			
quality	beet yield	significant	linear	-	n.s.	n.s.	n.s.
	sugar content	significant	linear	-	n.s.	n.s.	**
	WSY	significant	linear	-	n.s.	n.s.	n.s.
UAV (circle)	area of healthy foliage (A_H)	significant	linear	-	n.s.	***	n.s.
	area of foliage (A_F)	significant	linear	-	n.s.	***	n.s.
	cover of diseased foliage (FC_d)	significant	linear	-	n.s.	*	*
	number of clusters (c_l)	significant	linear	-	n.s.	n.s.	***
	area of diseased foliage (A_D)	n.s.	GLM	gamma inverse	n.s.	n.s.	**
	foliage cover (FC)[a]	n.s.	-	-	-	-	-
	disease incidence (DI)[a]	n.s.	-	-	-	-	-
	disease severity (dS-cover based)[a]	n.s.	-	-	-	-	-
	disease severity (DS-area based)[a]	n.s.	-	-	-	-	-
	cover of healthy foliage (FC_h)[a]	n.s.	-	-	-	-	-
UAV (leaf)	disease incidence (DI_{leaf})	n.s.	GLM	gamma inverse	***	**	n.s.
	number of clusters (c_l)	n.s.	GLM	gamma inverse	***	n.s.	n.s.
	disease severity (dS_{leaf}- cover based)	n.s.	GLM	log. transformation	*	n.s.	n.s.
	disease severity (DS_{leaf} -area based)	n.s.	GLM	log. transformation	*	n.s.	n.s.
	leaf area (A_l)	significant	linear	-	n.s.	n.s.	n.s.
	leaf slope (z_l)	significant	linear	-	n.s.	n.s.	***
	average cluster area ($A_{\bar{c}}$)	n.s.	-	-	-	-	-

a=no model found, n.s. = no significance identified, GLM= generalized linear model. For GLMs evaluated link functions were: gamma, gamma inverse, gaussian, negative binomial, as well as logarithmic transformation, Poisson, and Quasi-Poisson regression. Asterisks *, **, and *** indicate significant at the P ≤ 0.05, 0.01, and 0.001 levels, respectively.

Table 7-3. summary of correlation test between AUDPC of UAV-based parameters and white sugar yield (WSY) considering Pearson (parametric) or Spearman's rank (non-parametric) method

Parameter	instance	coefficient	test
foliage cover (FC)	circle	0.76	non-parametric
cover of healthy foliage (FC_h)	circle	0.76	non-parametric
area of healthy foliage (A_H)	circle	0.76	parametric
area of foliage (A_F)	circle	0.75	parametric
leaf area (A_l)	leaf	0.70	non-parametric
disease severity (DS-area based)	circle	-0.54	non-parametric
disease severity (ds-cover based)	circle	-0.54	non-parametric
disease severity (DS_{leaf} -area based)	leaf	-0.27	non-parametric
disease severity (ds_{leaf} -cover based)	leaf	-0.26	non-parametric
area of diseased foliage (A_D)	circle	-0.23 [n.s.]	non-parametric
leaf slope (ζ_l)	leaf	0.20 [n.s.]	parametric
average cluster area ($A_{\bar{c}}$)	leaf	-0.19 [n.s.]	non-parametric
cover of diseased foliage (FC_d)	circle	-0.17 [n.s.]	non-parametric
number of clusters (c_L)	leaf	-0.17 [n.s.]	non-parametric
number of clusters (c_I)	circle	-0.16 [n.s.]	parametric
disease incidence (DI_{leaf})	leaf	-0.12 [n.s.]	non-parametric
disease incidence (DI)	circle	-0.03 [n.s.]	non-parametric

n.s. = no significance identified; parametric and non-parametric data used respectively a Pearson and Spearman's rank coefficient
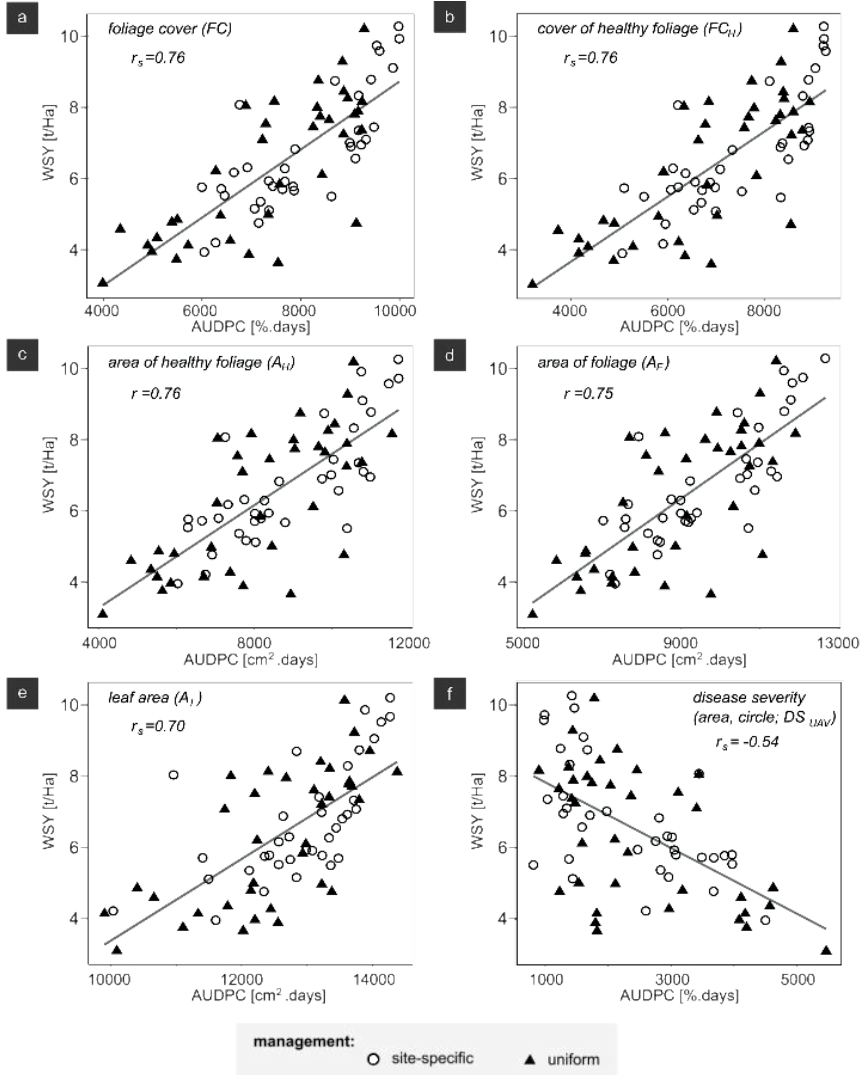
Figure 7-3. Relationship of AUDPC for six UAV-based parameters and white sugar yield (WSY). The shape of the data points in the graphic enables the identification of both uniform and site-specific fungicide management practices. The strength of the correlation is represented by the Pearson coefficient (r) and the Spearman's rank coefficient (r_s).

7.5. Discussion

In this study we developed a multispectral UAV-imaging data analysis approach for disease quantification to deliver geo-referenced fungicide application maps to control CLS in sugar beet. By employing a UAV-based CLS epidemic threshold of 25% DI_{leaf}, it was possible to generate application maps that strongly supported site-specific CLS control. A difference of over a month was observed between the first fungicide application in the site-specific and uniform management approaches. Despite the year 2022 being characterized by low precipitation and high temperatures, which typically indicate slow CLS development (Lang, 2005), this study demonstrated that conducting multiple geo-referenced disease assessments can enable earlier disease control measures within a field compared to relying on unique visual assessments as suggested by Wolf and Verreet (2002). This highlights the importance of utilizing multispectral UAV systems for monitoring sugar beet fields and CLS management.

No significant effects on yield and quality parameters were observed due to either fungicide management or distance to hotspot. When considering the behavior of the white sugar yield parameter, it was found that economic losses caused by the pathogen were controlled to the same degree by both, the uniform and the site-specific management. The main reason for this analogy in performance is that none of the fungicide management strategies exceeded the economic damage threshold of 5% DS, indicating control of the pathogen (Wolf *et al.*, 1998a). Foliage and healthy foliage area were strongly associated with the fungicide management strategy. The miniplots with site-specific fungicide management kept over the complete monitoring season the highest amount of healthy foliage and total foliage tissue. This strong association is probably related to the higher fungicide consume and the systemic effect of used fungicides. Site-specific fungicide management used 50% more fungicide compared to the uniform variant.

The distance to the hotspot has a significant impact on AUDPCDI_{leaf}, but it particularly affects AUDPCc_L. Using Gamma Inverse models, both AUDPCDI_{leaf} and AUDPCc_L exhibited an exponential decay as the miniplot moved further away from the hotspot. This characteristic emphasizes the importance of these parameters for implementing effective

disease control measures. The parameter c_L has the potential to describe the stages of CLS disease development in a similar manner to DI_{leaf}.

Foliage, specifically healthy foliage tissue, plays a crucial role in the absorption of energy and dry matter through the surface of photosynthetically active tissues (Draycott, 2006). Consequently, the parameters FC, FC_h, A_H and A_F exhibit the strongest correlation in this regard. Additionally, the average area of sampled leaves (A_l) could potentially serve as an immediate means of quantifying photosynthetically active tissue. The loss of healthy tissue, quantified by DS, directly impacts yield reduction (Draycott, 2006). As a result, significant correlations between UAV-based DS and WSY are observed in the context of this experiment.

In this study, unexpected amount of fungicide applications were observed for site-specific fungicide management, with a 50% higher application rate compared to uniform management. Mahlein *et al.* (2012) have highlighted that the utilization of sensor-based support systems for site-specific application necessitates an understanding of disease spread to effectively prevent disease intensity from surpassing the economic damage threshold. The IPM model proposed by Gummert and Ladewig (2012) is the culmination of nearly 20 years of extensive research aimed at optimizing fungicide application through the incorporation of knowledge on CLS epidemics. This model utilizes indicators obtained through visual assessments (Gummert and Ladewig, 2012; Wolf *et al.*, 1995). However, in order to establish new UAV-based thresholds for CLS control, it is imperative to acquire a deeper comprehension of the parameters developed using UAV technology for monitoring CLS spread, along with their equivalence to the parameters obtained through visual assessments. By implementing site-specific management for disease control, precisely targeting the right location and timing to minimize fungicide application, the principles of precision crop protection are upheld (Oerke *et al.*, 2010). These advancements have the potential to make a tremendous contribution to modern and sustainable sugar beet production.

In summary, this study successfully applied a multispectral UAV-imaging data analysis approach as a decision-making support system for quantifying CLS disease. This approach enabled the implementation of site-specific control measures. The findings

highlighted the importance of conducting geo-referenced disease assessments using UAV technology to potentially achieve early disease control in sugar beet fields. Furthermore, the study highlighted the significant role of fungicide management strategies in influencing the health of foliage. It also revealed a strong relationship between yield and circle-based foliage parameters. Additionally, the study demonstrated the sensitivity of DI_{leaf} and c_L parameters related to disease intensity and development stages, to hotspot distance, which is vital for effective CLS management practices. Overall, these advancements hold great potential for enhancing modern and sustainable sugar beet production.

CHAPTER 8:   General Discussion

This thesis demonstrated the feasibility of multispectral unmanned aerial vehicle (UAV) systems to support an integrated Cercospora leaf spot (CLS) management by assessing disease intensity accurately. Screening sugar beet genotypes for CLS resistance in breeding programs and decision supporting systems for precise crop protection measures are the two main applications scenarios of such a monitoring system. As shown in this thesis, multispectral UAV-systems allow determination of CLS susceptibility of sugar beet genotypes precisely. However, the application for disease control measures requires further optimization in future studies. This chapter bridges the findings of Chapter 3 and Chapter 7 with the specific objectives outlined in Chapter 2. These objectives encompass: (I) identifying plants as scoring units for quantifying plant-based disease severity (DS_{plant}); (II) establishing a continuous ratio-scale parameter for disease severity (DS); (III) integrating an instance-based leaf segmentation approach to determine leaf-specific disease intensity parameters; and (IV) generating application maps based on UAV-derived disease incidence (DI) parameter. The ultimate goal is to enable precise, and site-specific CLS control.

Image detection and georeferencing of plants for disease severity prediction

The identification of plants as scoring unit is a primary task for disease quantification. Chapter 3 focused on optimal conditions of flight timing and the detection of plant position based on UAV images. Two factors were evaluated for performance of detection and counting of sugar beet plants: the intra-row distance and the growing stage (BBCH). The study used a previously trained fully convolutional network (FCN) pipeline for detection and classification of crop and weed plants (Lottes *et al.*, 2018a). The best detection and count of sugar beet plants were obtained by BBCH 16-18 with an intra-row distance of 20-21 cm (Barreto *et al.*, 2021). The principals for robustness of the FCN pipeline are connected to the regular field arrangement and intra-row distance of crops (Lottes *et al.*, 2018b; Sa *et al.*, 2018). Loss of counting performance is observed by reducing the intra-row distance. Here misdetection and under-count is related to narrow distance by counting two plants as one, especially if the midrib and tip leaf is aligned and substantially close to the neighbor plant (Barreto *et al.*, 2021). No indications of performance decline were observed when comparing the feasible multispectral image resolution (approximately 3

mm ground sample distance, GSD) and RGB images (approximately 1 mm GSD) in terms of crop detection and counting (Barreto *et al.*, 2021). Unfortunately, the influence of light condition, especially on cloudy and sunny days, for detection and counting performance was not determined.

The detection of plant position before canopy closure is a crucial element that allows time-series image-based monitoring of individual plants, including their health condition. Chapter 4 is as well linked to specific objective I, which centers on the quantification of DS_{plant}. When plant position or plant centroid are identified before canopy closure and after image analysis, the geographic information of plants keep stored and can be used later for time-series segmentation of plant regions within orthomosaics, here the estimation of disease intensity parameters such as DS is possible. In Chapter 4, an ordinal and categorical pipeline was proposed for estimating plant-based DS. The image analysis pipeline used the plant centroid coordinates as image center to crop and generate squared RGB composite images with 224 x 224 pixels standard by 0.2 cm/px GSD. A trained LeNet CNN model classified each plant image into ten categories (0 to 9 scale), where category 1-9 emulates the KWS-scale explained in Chapter 1, moreover, the category 0 was ordered to healthy plants before canopy closure. All plants classified as 0 were reordered to category 1 in a post-processing step. In this thesis, we found two limitations of the plant- and image-based automatic scoring especially if CLS resistance screening is desired. The first is related to the ground truth. As mentioned in Chapter 1, the KWS-scale is a categorical and ordinal scale that deliver limited epidemiological information in comparison of a ratio scale. This information loss can be essential for ranking disease susceptibility, especially in the case of narrow quantitative resistance range. Three-dimensional scoring objects such as plants are difficult to estimate, being recommended the smallest possible scoring units such as a leaf (Kranz, 1988). Lastly, Vereijssen *et al.* (2003) mentioned that a categorical CLS scale delivers assessment errors when monitoring in sunny days, on wet plants or on darker colored varieties. However, categorical DS assessment is faster, less costly and less destructive in comparison to ratio or percentage scales, making these facts attractive for breeders (Bock *et al.*, 2020). The second limitation is influenced by the accuracy of categorical automatic prediction, but also connected to the performance of the classification task during machine learning

modeling. Here aspects such as imbalanced datasets, class separability (Sokolova and Lapalme, 2009) and beet field distribution impact the UAV-based assessment of DS parameter. In this thesis we found that the degree of KWS-scale is drastically variable on the collected data of a field. Both, healthy and diseased plants with total foliage death (KWS-scale 1 and 9) are the most frequent samples, collected during the monitoring season (Table 4-1). Considering multiclass performance metrics, high F1-score indicates a good balance between Precision and Recall, which is especially useful when dealing with imbalanced datasets and can indicate that the model is effectively separating different disease categories. The best results in terms of F1-score are related to the most frequently labeled classes (KWS-scale 1 and 9; healthy and diseased with total foliage death). KWS-scale 8 is the worthiest trained class with less frequency on the training set with high Precision values. The classification of remaining KWS-scales (2, 3, 4, 5, 6, and 7) is inaccurate with F1-scores lower than 40%, which suggest limited properties of trained classifier for class separability, and this can suggest the reduction of KWS-categories (Sokolova and Lapalme, 2009). Besides accuracy of expert estimation, the factors for this inaccurate prediction within KWS-categories should be related to similar intra-class features for class discrimination (Sokolova and Lapalme, 2009), and sugar beet plants distribution on the field, where neighbor plants with low or higher severity affected the performance of the prediction (Ispizua Yamati *et al.*, 2022). Reducing the number of classes may indeed enhance the robustness of automatic predictions using UAV-based data. However, it is important to note that decreasing the granularity of disease severity classes/categories may diminish the UAV-pipeline's ability to discern varying resistance levels. This, in turn, compromises the primary objective of aiding plant breeding efforts.

The categorical plant and UAV-based scoring present also a limitation for crop protection. By analyzing Table 4-1, diseased plant units during first symptoms (KWS scale 2) present the lowest Precision performance (15%). This metric reflects a high ratio of False Positive classification of diseased plants (Sokolova and Lapalme, 2009). High accurate classification of diseased plants during first symptoms is relevant for the determination of DI and decision-making in crop protection measures. The limitations of a plant- and categorical-automatic scoring, especially for plant breeding in assessing variety trials but also for crop protection measures, promotes the establishment of a new scoring pipeline

cover aiming a pixel-wise scoring to avoid DS information leakage and evaluate the determination of DI (see Chapter 5).

Ratio scale disease severity estimation for ranking resistance

Chapter 5 is connected to the second objective of this thesis for establishing a continuous ratio-scale parameter for DS. For this task, it was proposed a pixel-wise classification of diseased and healthy tissue from multispectral UAV-images. The image analysis approach in Chapter 5 ignores the 2D morphological structure and focuses on exploring multispectral bands and features of a digital surface model to feed 1D machine learning methods such as partial least squares discriminant analysis (PLS-DA) and support vector machine radial (SVMR) in a multiclass classification approach. During machine learning modeling, pixels were classified in four classes: "healthy", "diseased", "soil", and "other". In Chapter 5 is observed the same phenomenon as in Chapter 4, imbalance class distribution. Only 3% of labeled pixels belonged to diseased canopy tissue, while 77% of labeled samples belonged to healthy tissue. The proposed approach in Chapter 5 is a two-classifier (PLS-DA and SVMR) pipeline. High perform in terms of Precision and Recall was reported for the healthy class (Precision = 95% and Recall= 92%) (Barreto *et al.*, 2023). However, only 33% of Precision and 62% of Recall was achieved for classifying diseased regions. By considering the importance of each input variable to classifiers, it was found that the NIR channel or a vegetation index such as MCARI$_2$ highly presents impact for classifying healthy tissue and soil regions within an image.

Implementing the use of the digital surface model (DSM), this thesis proposes the calculation of a list of cover-based and area-based phenotyping parameters considering circular areas as scoring units. For variety trials, accurate determination of ratio scale DS (area based DS_{UAV}) was observed with a high degree of relationship between DS_{UAV} and Expert-based DS (R^2=0.87%). A slightly underestimation of DS_{UAV} was observed in comparison to expert-based scoring. This underestimation is likely related to the nadir perspective. Multispectral camera arranged in a nadir perspective record middle leaves but also unfolded new leaves, and petioles, which are mostly healthy, influencing the score of DS_{UAV} within circular areas. Leaf inclination and pixel-resolution should also contribute to an underestimation, due to the mixed-pixel effect of healthy and diseased inclined tissue. Further phenotyping parameters were also defined in this thesis, including foliage

cover (FC), cover of healthy foliage (FC_h), cover of diseased foliage (FC_d), area of foliage (A_F), area of healthy foliage (A_H), area of diseased foliage (A_D), disease severity (cover based, ds_I), number of clusters (c), number of clusters per unit of foliage area (c_F), mean cluster area ($A_{\bar{c}}$), mean cover cluster per unit of foliage cover ($C_{\bar{c}/F}$), mean area of cluster by unit of foliage area ($A_{\bar{c}/F}$), and disease incidence within circular regions (DI_{UAV}).

This thesis significantly advances our comprehension of epidemiological CLS development in distinct varieties. In Chapter 5, the temporal dynamics of both the number and area of singular necrotic regions, characterized by parameters c and $A_{\bar{c}/F}$, illustrate the contrast between susceptible and resistant varieties (see Figure *5-4*). The susceptible variety exhibits an early, sharp increase in c, followed by a rise in the parameter $A_{\bar{c}/F}$; whereas the resistant variety demonstrates a gradual increase in c, followed by a more subdued rise in $A_{\bar{c}/F}$ compared to its susceptible counterpart. This observation aligns with the disease progression described by Rangel *et al.*, (2020), and Weiland and Koch (2004), wherein an increase in the number of CLS spots is succeeded by the formation of larger necrotic areas after coalescence of individual spots. This thesis introduces a non-destructive, image-based assessment method to quantify these progression steps using the parameters c and $A_{\bar{c}/F}$.

Time-series UAV monitoring and image analysis allows determination of the area under disease progress curve (AUDPC) individually for UAV-based parameters including DS. This thesis highlights the applicability of UAV-based AUDPC_{DS} for ranking CLS resistance. Area-based DS allows better differentiations of variety performance in comparison to cover-based parameters. In Chapter 5, it was also found that parameters such as A_F, A_H, and $A_{\bar{c}}$ are relevant parameters for ranking CLS resistance and might be considered if multispectral UAV-systems are used as monitoring tools in variety trials.

Although the mentioned advantages for the application of multispectral UAV-based pipeline for ranking CLS resistance in variety trials, crucial limitations for robust application in crop protection were observed. The determination of UAV-based DI within circular regions showed in time-series a high detection of diseased circular units (circular regions with at least one cluster, $c \geq 1$), when plants were healthy. This discrepancy is primarily attributed to a low Precision and an elevated rate of False Positives (FP) in classifying

diseased pixels. As illustrated in Figure *5-2*, a substantial decline in Precision is primarily caused by the misclassification of soil regions as diseased plant regions. Notably, the presence of plant debris on the ground emerges as a predominant factor contributing to the misclassification of the 'diseased' class. Organ segmentation such as leaf segmentation should reduce the change of any misclassification of regions belonging to classes "soil" and "other" by reducing FP rate of "diseased" class and enhancing the accuracy of UAV-based DI. This advancement holds promise for expanding the potential of multispectral UAV imagery in crop protection measures. Therefore, Chapter 6 focuses on the segmentation of singular leaves.

Controlling false positive rate by leaf segmentation

In connection to objective III of this thesis, Chapter 6 focuses on the development of an image-based leaf segmentation approach including the use of the instance segmentation technique called Mask-RCNN (He *et al.*, 2017). The focus of this Chapter is to reduce the FP rate of diseased regions. However, a possible improvement in the determination of UAV-based DS is also reached by leaf segmentation. The chosen approach includes the modeling of a Mask-RCNN approach, having as first disadvantage the requirement of high number of labeled images. The demand of labels for training data is compensated by implementing augmentation data, where two methodologies were evaluated (standard- and copy-paste augmentation). Simple augmentation techniques showed the best performance for instance leaf segmentation, while under sunny light condition segmentation performance tends to decrease in Precision. The integration of leaf instance segmentation allows the determination of new phenotyping parameters including DI_{leaf} and DS_{leaf} (UAV- and leaf-based assessment), but also leaf area (A_L), leaf slope (ζ_l), disease leaf area (A_D), healthy leaf area (A_H), and number of clusters (c_L) and mean cluster area ($A_{\tilde{c}}$). Considering the application scenario in variety trials, it was found that DS_{leaf} is not relevant for determining CLS resistance in sugar beet varieties. Low correlation between UAV-based and expert-based scoring was observed especially under heavy CLS damage. When expert-based DS exceed 40%, leaf- and UAV-based DS_{leaf} drops. This behavior can be attributed to the regrowth of new leaves as a response of sugar beet plants to complete canopy damage (Weiland and Koch, 2004). This regrowth, likely captured by the UAV-system, exhibits a healthy leaf appearance. This

epidemiological progression of DS_{leaf} differs from the DS_{UAV} (circle-based DS), underscoring the importance of image-based segmentation in defining the scoring unit. A similar phenomenon is also observed with parameters c and c_L, both circle- and leaf-based. In the variance analysis results presented in Chapter 5, the circle-based parameter c shows no significant influence in terms of variety factor. However, in Chapter 6, clear distinctions in the disease progress of c_L are visually apparent, providing a means to differentiate between sugar beet genotypes.

The application scenario for controlling CLS necessitates precise UAV-based indicators for effective decision-making (Wolf and Verreet, 2002). To enhance the accuracy of UAV-based DI through leaf segmentation, it is imperative to define 'diseased' units at the image-based and leaf-level. In Chapter 6, c_L emerged as the parameter with the highest potential for implementing crop protection measures. By employing the criterion "$c_L \geq 1$" for disease detection and calculating DI_{leaf}, a noticeable reduction in the FP rate was achieved when compared to the circle-based DI_{UAV}. However, complete eradication of FP classifications proved elusive and may necessitate improvements in the Precision of the pixel-wise classification pipeline for robust deployment in crop protection. A potential strategy for reducing the FP rate was demonstrated by increasing the threshold for the number of clusters within a leaf ($c_L \geq 5$). Nonetheless, this adjustment shifted the exponential phase of DI_{leaf} to a later time point, rendering it suboptimal for practical implementation.

The question remains whether the delayed development of DI_{leaf} with a less stringent disease detection criteria continues to exhibit advantages, especially when combined with georeferencing of scoring. The georeferenced analysis of subsampled areas within the field offers the potential to provide georeferenced threshold values, enabling individualized decision-making and a potential reduction in fungicide application. This issue of site-specific CLS control is addressed in Chapter 7.

Site-specific disease control based on multispectral UAV-data
One highlight of this thesis, the first study for site-specific and curative fungicide management was reported in Chapter 7. Achievements from Chapter 5 and 6 are integrated on the georeferenced and UAV-based assessment to generate application maps, considering disease development for calculating DI_{leaf}. Two management

strategies, a uniform and a site-specific application were evaluated regarding fungicide consumption and within a well-known CLS inoculated regions. White sugar yield (WSY) and AUDPCs for UAV-based parameters were evaluated in this Chapter. To better understand disease spread after site-specific application, an analysis of distance between inoculated zone and subsamples fields was performed.

It was observed that, AUDPCs of UAV- and leaf-based DI_{leaf} and number of clusters (c_L) are strongly influenced by the distance to inoculation zone, becoming potential parameters for site-specific crop protection measures. AUDPCs of parameters foliage cover (FC), cover of healthy foliage (FC_h), area of healthy foliage (A_H), area of foliage (A_F), and leaf area (A_l) are strongly correlated to yield, however, WSY itself is not influenced by distance to inoculation zone and fungicide management.

For decision-making purposes and generating application maps, UAV-based CLS epidemic threshold of 25% DI_{leaf} was decided to mitigate the FP rate. Although, no significant effect on yield and quality parameters was observed due to fungicide management; and regarding fungicide use, 50% higher application rate in the site-specific management compared to uniform management was reported on this research. Chapter 7 highlights the importance for establishing accurate UAV-based CLS epidemic thresholds for a second or third fungicide application to effectively reduce fungicide consumption. CLS economic damage threshold based on UAV-based parameters might take place in the future for effective site-specific disease control based on multispectral UAV-imagery information.

Use of imaging UAV-based pipeline in practical scenarios

The use of imaging UAV-systems for evaluating CLS resistance is highly recommended by assessing DS in a ratio scale or by quantifying healthy foliage (Barreto *et al.*, 2023). For this purpose, pixel-wise classification pipelines are superior to categorical pipelines. The pixel-wise approaches applied to variety trials should result in high Recall and Precision for classification of healthy tissue and soil regions. These two classes are the most frequent areas observed in images captured from a nadir perspective using UAVs in sugar beet fields. Their quantification delivers information of healthy and photosynthetic active areas in the canopy positively influencing yield development. Within this context,

REDEDGE and NIR channels of multispectral cameras are crucial for discriminating soil regions and healthy vegetation, while resolution lower than 5 mm should not be on limiting factor.

The requirements of a machine/deep learning pipeline for the control of CLS are different than for plant breeding. Here the identification and standardization of image-based scoring units is highly relevant. In the case of leaf diseases, the affected organ is the principal aim for individual segmentation and analysis. For identification of the scoring unit, two scenarios are identified in this thesis. In the first case, high Precision and principally a low rate of FP classification of diseased image-based specimens (pixel, bounding box, instance, patch image) are desired, and the consequences of low Precision are related to incorrect warning signals and inaccurate application maps in early time points of disease development when application is even not required. Decision-making with low Precision leads to economical disadvantages due to misspend of fungicide with further consequences in development of pathogen resistance. The second case is related to low Recall or a low rate of TP which can bring to a low sensitivity of diseased image-based specimens and a later detection and decision for fungicide application during the growing season with consequences in disease spread and yield loss. High Precision and high Recall of diseased image-based specimens are required for efficient site-specific disease management. Moreover, the current multispectral UAV-systems present the principal limitation in terms of spatial resolution that should contribute to low Recall by comparing with ground truth data. Nadir UAV-perspective and development of CLS are also limiting, if first symptoms of primary inoculum are affecting middle to old leaves in the canopy, because these leaves are hardly recorded by UAV-systems with nadir perspective. In the next paragraphs possible development and future perspective are mentioned to contribute with the breeding process and deal with an accurate detection of diseased specimens.

Challenges and Future perspectives

Future perspective in breeding for resistance: Breeding procedures includes an assessment of disease intensity in variety trials conducted across different environments and multiple years. Therefore, robustness of the pipeline is compulsory to deliver accurate DS parameters. Pipelines based on machine learning and deep learning require continuous maintenance to keep their prediction fit for any field situation. Weather

conditions, soil tillage, additional pest and diseases occurrence, but also sensor status can influence the assessment of disease intensity leading to wrong prediction (Barreto *et al.*, 2023). Continuous maintenance by modeling and testing of new datasets according to new field conditions, sensors and platform development are necessary to improve generalization properties of plant breeding for resistance pipelines. A pipeline for breeding should not only be fit for multi-year and multi-site trials, but also cover all stages of breeding process from mass selection, throughout family selection, recurrent selection and hybrid production (Biancardi *et al.*, 2010). The pipeline for breeding might show independence in terms of assessment by dealing with individuals phenotypically diversity in leaf form and color by analyzing the canopy. A relevant contribution for automatic analysis of multispectral imaging is to consider the parallel quantification of combined phenotypic abilities. Breeding for resistance in sugar beet plants includes the discard undesired traits, such as lack of bolting resistance, low sugar content and beet yield, low germination rate, slow canopy development, etc. (Biancardi *et al.*, 2010). Therefore, generalization properties and detection of combined abilities might improve the precision in breeding selection for resistance.

Future perspective for disease control: The use of multispectral UAV-systems for disease control scenarios must be a focus of research in the following years due to the challenging application in the field. Sensor and platform development are principal promising aspects of dealing with low Precision of diseased specimens. In this thesis, the utilized multispectral bands do not show advantages for discrimination of diseased tissue, bare soil and vegetation rest under sunny light conditions. Novel multispectral sensor are available on the market, with additional multispectral bands and their properties for detection CLS infected pixels are unknown. Moreover, panchromatic bands and pansharpening techniques (AgEagle, 2023a, 2023b) will contribute to deliver high resolution information within multispectral bands and reducing the intensity of field mapping activities. New spectral or morphological features will be the principal pillars for coming machine or deep learning approaches (Chai *et al.*, 2021; Chandra *et al.*, 2020) to support high Precision and Recall disease detection. Improvement of performance of diseased specimens includes having a new level of ground truth. In this thesis, it was mainly acquired ground truth at the plot level. However, the imbalanced distribution,

especially low frequency of diseased specimens, and environmental light conditions lead to corroborate the disease status of leaf scoring units when first symptoms appear (Barreto *et al.*, 2023; Ispizua Yamati *et al.*, 2022). An acquisition of unit-to-unit ground truth data will be necessary in future studies for sensitivity determination in future approaches. Here, devices such as RTKs and georeferenced sampling of leaves can improve proximity of test sets to gold standard. Although unit-to-unit ground truth data will support pipeline performance, a decision for disease control can only be taken with UAV-based thresholds as indicators. In the past human-based DI_{plant} and DI_{leaf} were establish as thresholds for fungicide applications and economic damage (Wolf *et al.*, 1998b). Equivalents of UAV-based DI to human-based DI_{plant} and DI_{leaf} might be well-known in the future, especially for a second or third application when disease pressure is high. As last aspect to cover in future studies related to UAV-based disease control, is the dynamic curative site-specific fungicide application and the generation of application maps. The potential of curative site-specific disease control must be evaluated first by application maps based on visual scoring DI_{leaf}, because human-based indicator has been intensively studied in the past (Wolf, 2002; Wolf *et al.*, 2001; Wolf and Verreet, 2002) and can deliver the maximal possible fungicide reduction. Optimization of the site-specific management should be first established in terms of proofing the valuability of indicators created for uniform application, determine periods for following site-specific applications, determine size of minimal application region, buffer regions, and determine minimal fungicide site-specific application for economic advantages in term of logistic. When the dynamic of site-specific application is understandable, it would be possible to integrate the use of UAV-based application maps. For short term, current UAV-based application maps can fill the gap of Precision by complementing input information with buffer zones and IoT sensors, adjusted UAV-based thresholds by different light conditions; and can speed processing time by changing from off-line to on-line systems and implementing parallel processing on computer time demanding procedures.

Transfer knowledge from CLS to multiple diseases: In this thesis we focused on a plant-pathogen interaction of *Cercospora beticola* Sacc. and sugar beet; however, this work also gives the principles for establishing UAV-based assessment pipelines for quantification of disease intensity of other relevant sugar beet diseases and for foliar

diseases in other crops. The pipeline presented in this thesis is highly compatible with further leaf diseases such as Powdery mildew, Rust, and virus yellows due to the available leaf segmentation Mask-RCNN model. A multiclass object detection for all these three additional diseases must be evaluated in future research as well as the capacity of current multispectral and morphological features for classification performance. The potential to build multi-disease heat maps will deliver new alternatives for disease management in the future. Georeferenced assessment of soil-borne diseases may necessitate a plant-center approach, with accurate determination of the plant center being a crucial aspect for quantifying disease intensity. Disease severity of soil-borne diseases, such as Beet Cyst Nematode and Rhizoctonia Root Rot, is assessed using disease diagrams based on plants as scoring units. The availability of ground truth data pertaining to plant-based metrics and precise plant center detection prior to canopy closure could potentially facilitate the application of deep learning models for soil-borne diseases, as corroborated by Ispizua Yamati *et al.* (2023) in their study.

Employing imaging UAV-systems for evaluating CLS resistance is strongly recommended, particularly through the assessment of DS using a ratio scale or quantification of healthy foliage. For ranking CLS resistance in variety trials, pixel-wise methods should exhibit high Recall and Precision in classifying healthy tissue and soil regions. These prevalent regions, commonly observed in imbalanced UAV-based nadir perspectives within sugar beet fields, provide essential data on healthy and photosynthetically active canopy areas, ultimately contributing to improved yield outcomes. The use of multispectral UAV-systems for disease control presents a compelling avenue for future research. Overcoming challenges related to low Precision in diseased specimen detection and accurate determination of UAV-based DI requires advancements in sensor and platform development. Novel multispectral sensors with additional bands hold promise for enhancing the discrimination of CLS-infected pixels. Panchromatic bands and pansharpening techniques can contribute to higher resolution imaging, reducing the need for intensive field mapping activities.

This study convincingly demonstrates that multispectral UAV-based methodologies can advance disease resistance breeding and precise disease control. Optical sensor and UAV technologies exposed in this thesis have the potential to be applied in practical

agriculture for decision-making in Integrated control of Cercospora leaf spot, laying the foundation for more effective and efficient sugar beet production.

CHAPTER 9: References

Aasen, H., Honkavaara, E., Lucieer, A., Zarco-Tejada, P., 2018. Quantitative remote sensing at ultra-high resolution with UAV spectroscopy: A review of sensor technology, measurement procedures, and data correction workflows. Remote Sensing, 10, 1-42. https://doi.org/10.3390/rs10071091

AgEagle, 2023a. Optimized 3-in-1 solution for advanced remote sensing and agricultural research. Altum-PT. URL https://ageagle.com/drone-sensors/altum-pt-camera/ (accessed 9.28.23).

AgEagle, 2023b. RedEdge-P dual: 10 spectral bands for enhanced data comparison with satellites. RedEdge-P dual. URL https://ageagle.com/drone-sensors/rededge-p-dual-camera (accessed 9.22.23).

Anonymous, 1970. Cercospora Tafel.

Barreto, A., Ispizua Yamati, F., Varrelmann, M., Paulus, S., Mahlein, A.-K., 2023. Disease incidence and severity of Cercospora leaf spot in sugar beet assessed by multispectral unmanned aerial images and machine learning. Plant Disease, 107, 188–200. https://doi.org/10.1094/pdis-12-21-2734-re

Barreto, A., Lottes, P., Ispizua Yamati, F., Baumgarten, S., Wolf, N., Stachniss, C., Mahlein, A.-K., Paulus, S., 2021. Automatic UAV-based counting of seedlings in sugar-beet field and extension to maize and strawberry. Computers and Electronics in Agriculture, 191, 1-10. https://doi.org/10.1016/j.compag.2021.106493

Barreto, A., Paulus, S., Varrelmann, M., Mahlein, A.-K., 2020. Hyperspectral imaging of symptoms induced by *Rhizoctonia solani* in sugar beet: comparison of input data and different machine learning algorithms. Journal of Plant Diseases and Protection, 127, 441–451. https://doi.org/10.1007/s41348-020-00344-8

Barreto, A., Reifenrath, L., Vogg, R., Sinz, F., 2022. Using UAV-imagery for leaf segmentation in diseased plants via mask-based data augmentation and extension of leaf-based phenotyping parameters. https://doi.org/10.1101/2022.12.19.520984

Biancardi, E., McGrath, J., Panella, L., Lewellen, R., Stevanato, P., 2010. Sugar Beet, in: Bradshaw, J.E. (Ed.), Root and Tuber Crops. Springer New York, New York, NY, 173–219. https://doi.org/10.1007/978-0-387-92765-7_6

Birla, K., Rivera-Varas, V., Secor, G., Khan, M., Bolton, M., 2012. Characterization of cytochrome b from European field isolates of *Cercospora beticola* with quinone outside inhibitor resistance. European Journal of Plant Pathology, 134, 475–488. https://doi.org/10.1007/s10658-012-0029-y

Bishop, C., Nasrabadi, N., 2006. Pattern recognition and machine learning. Springer.

Bock, C., Barbedo, J., Del Ponte, E., Bohnenkamp, D., Mahlein, A.-K., 2020. From visual estimates to fully automated sensor-based measurements of plant disease severity: status and challenges for improving accuracy. Phytopathology Research, 2, 9, 1-30. https://doi.org/10.1186/s42483-020-00049-8

Bock, C., Pethybridge, S., Barbedo, J., Esker, P., Mahlein, A.-K., Del Ponte, E., 2022. A phytopathometry glossary for the twenty-first century: towards consistency and precision in intra- and inter-disciplinary dialogues. Tropical Plant Pathology, 47, 14-24, https://doi.org/10.1007/s40858-021-00454-0

Bock, C., Poole, G., Parker, P., Gottwald, T., 2010. Plant disease severity estimated visually, by digital photography and image analysis, and by hyperspectral imaging. Critical Reviews in Plant Sciences, 29, 59–107. https://doi.org/10.1080/07352681003617285

Bohnenkamp, D., Behmann, J., Paulus, S., Steiner, U., Mahlein, A.-K., 2021. A hyperspectral library of foliar diseases of wheat. Phytopathology 1–41. https://doi.org/10.1094/phyto-09-19-0335-r

Bundessortenamt, 2022. Beschreibende Sortenliste Getreide , Mais Öl- und Faserpflanzen Leguminosen Rüben Zwischenfrüchte.

Chai, J., Zeng, H., Li, A., Ngai, E.W.T., 2021. Deep learning in computer vision: A critical review of emerging techniques and application scenarios. Machine Learning with Applications, 6, 1-13. https://doi.org/https://doi.org/10.1016/j.mlwa.2021.100134

Chandra, A., Desai, S., Balasubramanian, V., Guo, W., 2020. Computer vision with deep learning for plant phenotyping in agriculture: A survey. ArXiv, 1-26. https://doi.org/10.34048/acc.2020.1.f1

Chen, L.-C., Papandreou, G., Kokkinos, I., Murphy, K., Yuille, A., 2018. DeepLab: Semantic image segmentation with deep convolutional nets, Atrous convolution, and fully connected CRFs. IEEE Transactions on Pattern Analysis and Machine Intelligence, 40, 834–848. https://doi.org/10.1109/tpami.2017.2699184

Cioni, F., Collina, M., Maines, G., Khan, M., Secor, G., Rivera, V., 2014. A new integrated pest management (IPM) model for Cercospora leaf spot of sugar beets in the Po Valley, Italy. Sugar Tech, 16, 92–99. https://doi.org/10.1007/s12355-013-0260-7

Dammer, K.-H., Wollny, J., Giebel, A., 2008. Estimation of the leaf area index in cereal crops for variable rate fungicide spraying. European Journal of Agronomy, 28, 351–360. https://doi.org/10.1016/j.eja.2007.11.001

Deng, L., Mao, Z., Li, X., Hu, Z., Duan, F., Yan, Y., 2018. UAV-based multispectral remote sensing for precision agriculture: A comparison between different cameras. ISPRS Journal of Photogrammetry and Remote Sensing, 146, 124–136. https://doi.org/10.1016/j.isprsjprs.2018.09.008

Draycott, A., 2006. Sugar beet. Blackwell Publishing Ltd.

EC, 2009. No 1107/2009 of the European Parliament and of the Council of 21 October 2009 concerning the placing of plant protection products on the market and repealing Council Directives 79/117/EEC and 91/414/EEC. EU, Brussels.

Ehlert, D., Dammer, K.-H., 2006. Widescale testing of the crop-meter for site-specific farming. Precision Agriculture, 7, 101–115. https://doi.org/10.1007/s11119-006-9003-z

Görlich, F., Marks, E., Mahlein, A.-K., König, K., Lottes, P., Stachniss, C., 2021. UAV-based classification of Cercospora leaf spot using RGB images. Drones 5, 1–15. https://doi.org/10.3390/drones5020034

Gummert, A., Ladewig, E., 2012. Leitlinien des integrierten Pflanzenschutzes im Zuckerrübenanbau Ermittlung von Pflanzenschutzstrategien im Zuckerrübenanbau. 58. Deutsche Pflanzenschutztagung.

Gummert, A., Ladewig, E., Bürcky, K., Märländer, B., 2015. Variety resistance to Cercospora leaf spot and fungicide application as tools of integrated pest management in sugar beet cultivation - German case study. Crop Protection, 182–194. https://doi.org/10.1016/j.cropro.2015.02.024

He, K., Gkioxari, G., Dollár, P., Girshick, R., 2017. Mask R-CNN. 2017 IEEE International Conference on Computer Vision (ICCV). 2980–2988. https://doi.org/10.1109/iccv.2017.322

Hillnhütter, C., Mahlein, A.-K., Sikora, R., Oerke, E., 2012. Use of imaging spectroscopy to discriminate symptoms caused by *Heterodera schachtii* and *Rhizoctonia solani* on sugar beet. Precision Agriculture, 13, 17–32. https://doi.org/10.1007/s11119-011-9237-2

Hillnhütter, C., Mahlein, A.-K., Sikora, R., Oerke, E., 2011. Remote sensing to detect plant stress induced by *Heterodera schachtii* and *Rhizoctonia solani* in sugar beet fields. Field Crops Research, 122, 70–77. https://doi.org/10.1016/j.fcr.2011.02.007

Hoffmann, C., 2010. Root quality of sugarbeet. Sugar Tech 12, 276–287. https://doi.org/10.1007/s12355-010-0040-6

Hoffmann, C., Koch, H.-J., Märländer, B., 2021. Chapter 20 - Sugar beet, in: Sadras, V.O., Calderini, D.F. (Eds.), Crop Physiology: Case Histories for Major Crops. Academic Press, 634–672. https://doi.org/10.1016/b978-0-12-819194-1.00020-7

Hossain, R., Menzel, W., Lachmann, C., Varrelmann, M., 2021. New insights into virus yellows distribution in Europe and effects of beet yellows virus, beet mild yellowing virus, and beet chlorosis virus on sugar beet yield following field inoculation. Plant Pathology, 70, 584–593. https://doi.org/10.1111/ppa.13306

Imbusch, F., Liebe, S., Erven, T., Varrelmann, M., 2021. Dynamics of Cercospora leaf spot disease determined by aerial spore dispersal in artificially inoculated sugar beet fields. Plant Pathology, 70, 853–861. https://doi.org/10.1111/ppa.13337

References

Ispizua Yamati, F., Barreto, A., Günder, M., Bauckhage, C., Mahlein, A.-K., 2022. Sensing the occurrence and dynamics of Cercospora leaf spot disease using UAV-supported image data and deep learning. Zuckerindustrie, 79–86.

Ispizua Yamati, F., Günder, M., Barreto, A., Bömer, J., Laufer, D., Bauckhage, C., Mahlein, A.-K., 2023. Automatic scoring of Rhizoctonia crown and root rot affected sugar beet fields from orthorectified UAV images using machine learning. Plant Dissease. https://doi.org/10.1094/PDIS-04-23-0779-RE

Jarroudi, M. El, Chairi, F., Kouadio, L., Antoons, K., Sallah, A.-H.M., Fettweis, X., 2021. Weather-based predictive modeling of *Cercospora beticola* infection events in sugar beet in Belgium. Journal of Fungi 7, 1–20. https://doi.org/10.3390/jof7090777

Jay, S., Comar, A., Benicio, R., Beauvois, J., Dutartre, D., Daubige, G., Li, W., Labrosse, J., Thomas, S., Henry, N., Weiss, M., Baret, F., 2020. Scoring Cercospora leaf spot on sugar beet: Comparison of UGV and UAV phenotyping systems. Plant Phenomics, 2020, 1–18. https://doi.org/10.34133/2020/9452123

Jones, R., Windels, C., 1991. A management model for Cercospora leaf spot of sugarbeets. University of Minnesota Extension Service 1–8.

Khan, J., Qi, A., Khan, M., 2009. Fluctuations in number of *Cercospora beticola* conidia in relationship to environment and disease severity in sugar Beet. Phytopathology, 99, 796–801. https://doi.org/10.1094/phyto-99-7-0796

Koch, H.-J., Trimpler, K., Jacobs, A., Stockfisch, N., 2018. Crop rotational effects on yield formation in current sugar beet production – results from a farm survey and field trials. Frontiers in Plant Science, 8, 1–11. https://doi.org/10.3389/fpls.2018.00231

Kozłowska-Makulska, A., Beuve, M., Syller, J., Szyndel, M., Lemaire, O., Bouzoubaa, S., Herrbach, E., 2009. Aphid transmissibility of different European beet polerovirus isolates. European Journal of Plant Pathology, 125, 337–341. https://doi.org/10.1007/s10658-009-9474-7

Kranz, J, 1988. Measuring plant disease, in: Kranz, Jürgen, Rotem, J. (Eds.), Experimental Techniques in Plant Disease Epidemiology. Springer Berlin

Heidelberg, Berlin, Heidelberg, 35–50. https://doi.org/10.1007/978-3-642-95534-1_4

Lang, C., 2005. Control of leaf diseases: Monitoring, control thresholds and practical application. Zuckerindustrie, 130, 388–396.

Lawrence, J., Meredith, D., 1970. Wind dispersal of conidia of Cercospora beticola. Phytopathology 60, 1076–1078.

Leucker, M., Mahlein, A.-K., Steiner, U., Oerke, E.-C., 2016. Improvement of lesion phenotyping in *Cercospora beticola* –sugar beet interaction by hyperspectral imaging. Phytopathology, 106, 177–184. https://doi.org/10.1094/phyto-04-15-0100-r

Loel, J., Kenter, C., Märländer, B., Hoffmann, C., 2014. Assessment of breeding progress in sugar beet by testing old and new varieties under greenhouse and field conditions. European Journal of Agronomy, 52, 146–156. https://doi.org/10.1016/j.eja.2013.09.016

Long, J., Shelhamer, E., Darrell, T., 2015. Fully convolutional networks for semantic segmentation. Computer Vision and Pattern Recognition. https://doi.org/10.48550/arxiv.1411.4038

Lottes, P., Behley, J., Chebrolu, N., Milioto, A., Stachniss, C., 2018a. Joint stem detection and crop-weed classification for plant-specific treatment in precision farming. IEEE International Conference on Intelligent Robots and Systems 8233–8238. https://doi.org/10.1109/IROS.2018.8593678

Lottes, P., Behley, J., Milioto, A., Stachniss, C., 2018b. Fully convolutional networks with sequential information for robust crop and weed detection in precision farming. IEEE Robot Autom Lett. https://doi.org/10.48550/arXiv.1806.03412

Madden, L., Hughes, G., van den Bosch, F., 2007a. Measuring plant diseases, in: Hughes, G., Bosch, F. van den, Madden, L. V (Eds.), The Study of Plant Disease Epidemics, Epidemiology. The American Phytopathological Society, 11–31. https://doi.org/10.1094/9780890545058.002

Madden, L., Hughes, G., van den Bosch, F., 2007b. Temporal analysis I: Quantifying and comparing epidemics, in: Bosch, F. van den, Madden, L. V, Hughes, G. (Eds.), The Study of Plant Disease Epidemics, Epidemiology. The American Phytopathological Society, 63–116. https://doi.org/10.1094/9780890545058.004

Maes, W., Steppe, K., 2019. Perspectives for remote sensing with unmanned aerial vehicles in precision agriculture. Trends in Plant Science, 24, 152–164. https://doi.org/10.1016/j.tplants.2018.11.007

Mahlein, A.-K., 2015. Plant disease detection by imaging sensors – parallels and specific demands for precision agriculture and plant phenotyping. Plant Disease, 100, 241–251. https://doi.org/10.1094/pdis-03-15-0340-fe

Mahlein, A.-K., Kuska, M., Behmann, J., Polder, G., Walter, A., 2018. Hyperspectral sensors and imaging technologies in phytopathology: State of the art. Annual Review of Phytopathology, 56, 535–558. https://doi.org/10.1146/annurev-phyto-080417-050100

Mahlein, A.-K., Oerke, E.-C., Steiner, U., Dehne, H.-W., 2012. Recent advances in sensing plant diseases for precision crop protection. European Journal of Plant Pathology, 133, 197–209. https://doi.org/10.1007/s10658-011-9878-z

Mahlein, A.-K., Rumpf, T., Welke, P., Dehne, H.W., Plümer, L., Steiner, U., Oerke, E.C., 2013. Development of spectral indices for detecting and identifying plant diseases. Remote Sensing of Environment, 128, 21–30. https://doi.org/10.1016/j.rse.2012.09.019

Märländer, B., Hoffmann, C., Koch, H.J., Ladewig, E., Merkes, R., Petersen, J., Stockfisch, N., 2003. Environmental situation and yield performance of the sugar beet crop in Germany: Heading for sustainable development. Journal of Agronomy and Crop Science, 189, 201–226. https://doi.org/10.1046/j.1439-037X.2003.00035.x

Martín Gil, A., Cepeda Castro, S., Ayala García, J., 2018. Guía de gestión integrada de plagas: Remolacha. Ministerio de Agricultura, Pesca y Alimentación 1–176.

References

Meghana, M., Shastri, Y., 2020. Sustainable valorization of sugar industry waste: Status, opportunities, and challenges. Bioresource Technology, 303, 122929. https://doi.org/https://doi.org/10.1016/j.biortech.2020.122929

MicaSense, 2018. Batch processing example. Micasense Rededge and Altum image processing tutorials. URL https://github.com/micasense/imageprocessing/blob/master/Batch Processing.ipynb (accessed 9.22.23).

Neven, D., Brabandere, B. De, Proesmans, M., Gool, L. Van, 2019. Instance segmentation by jointly optimizing spatial embeddings and clustering bandwidth. 2019 IEEE/CVF Conference on Computer Vision and Pattern Recognition 8829–8837. https://doi.org/10.48550/arXiv.1906.11109

Nutter, F., Teng, P., Shokes, F., 1991. Disease assessment terms and concepts. Plant Disease, 75, 1187–1188.

Oerke, E.-C., Dehne, H.-W., 2004. Safeguarding production-losses in major crops and the role of crop protection. Crop Protection 23, 275–285. https://doi.org/10.1016/j.cropro.2003.10.001

Oerke, E.-C., Gerhards, R., Menz, G., Sikora, R.A., 2010. Precision crop protection - the challenge and use of heterogeneity, 2010th ed. Springer, Dordrecht, Netherlands.

Ossenkop, A., Ladewig, E., Manthey, R., 2005. Variety performance of sugarbeet under the attack of foliar diseases - opportunities and limitations of the variety trial system. Zuckerindustrie, 130, 25–31.

Ossenkop, A., Ladewig, E., Manthey, R., 2002. Performance of Cercospora resistant varieties - consequences for variety testing and advisory service. Zuckerindustrie, 127, 867–871.

Pfitzer, R., Varrelmann, M., Schrameyer, K., Rostás, M., 2022. Life history traits and a method for continuous mass rearing of the planthopper *Pentastiridius leporinus*, a vector of the causal agent of syndrome "basses richesses" in sugar beet. 78, 4700-4708. https://doi.org/10.1002/ps.7090

126

References

Rangel, L., Spanner, R., Ebert, M., Pethybridge, S., Stukenbrock, E., de Jonge, R., Secor, G., Bolton, M., 2020. *Cercospora beticola*: The intoxicating lifestyle of the leaf spot pathogen of sugar beet. Molecular Plant Pathology, 21, 1020–1041. https://doi.org/10.1111/mpp.12962

Rathaiah, Y., 1977. Stomatal tropism of *Cercospora beticola* in sugarbeet. Phytopathology 67, 358–362.

Reynolds, G., Windels, C., MacRae, I., Laguette, S., 2011. Remote sensing for assessing Rhizoctonia crown and root rot severity in sugar beet. Plant Disease, 96, 497–505. https://doi.org/10.1094/pdis-11-10-0831

Rossi, V., 1995. Effect of host resistance in decreasing infection rate of Cercospora leaf spot epidemics on sugarbeet. Phytopathologia Mediterranea, 34, 149–156.

Sa, I., Chen, Z., Popovic, M., Khanna, R., Liebisch, F., Nieto, J., Siegwart, R., 2018. weedNet: Dense semantic weed classification using multispectral Images and MAV for smart farming. IEEE Robot Autom Lett 3, 588–595. https://doi.org/10.1109/lra.2017.2774979

Schmidhuber, J., 2015. Deep learning in neural networks: An overview. Neural Networks 61, 85–117. https://doi.org/10.1016/j.neunet.2014.09.003

Schmidt, K., Pflugmacher, M., Klages, S., Mäser, A., Mock, A., Stahl, D.J., 2008. Accumulation of the hormone abscisic acid (ABA) at the infection site of the fungus *Cercospora beticola* supports the role of ABA as a repressor of plant defence in sugar beet. Molecular Plant Pathology, 9, 661–673. https://doi.org/10.1111/j.1364-3703.2008.00491.x

Setiawan, A., Koch, G., Barnes, S., Jung, C., 2000. Mapping quantitative trait loci (QTLs) for resistance to Cercospora leaf spot disease (*Cercospora beticola* Sacc.) in sugar beet (Beta vulgaris L.). Theoretical and Applied Genetics, 100, 1176–1182. https://doi.org/10.1007/s001220051421

Shane, W., Teng, P., 1992. Impact of Cercospora leaf spot on root weight, sugar yield, and purity of *Beta vulgari*. Plant Disease, 76, 812–820.

References

Skaracis, G., Pavli, O., Biancardi, E., 2010. Cercospora Leaf Spot Disease of Sugar Beet. Sugar Tech 12, 220–228. https://doi.org/10.1007/s12355-010-0055-z

Sokolova, M., Lapalme, G., 2009. A systematic analysis of performance measures for classification tasks. Information Processing & Management, 45, 427–437. https://doi.org/10.1016/j.ipm.2009.03.002

Steddom, K., 2005. Comparison of visual and multispectral radiometric disease evaluations of Cercospora leaf spot of sugar beet. Plant Disease, 89, 153-158. https://doi.org/10.1094/pd-89-0153

Steinkamp, M., Martin, S., Hoefert, L., Ruppel, E., 1979. Ultrastructure of lesions produced by *Cercospora beticola* in leaves of Beta vulgaris. Physiological Plant Pathology, 15, 13–26. https://doi.org/10.1016/0048-4059(79)90035-3

Stevanato, P., Chiodi, C., Broccanello, C., Concheri, G., Biancardi, E., Pavli, O., Skaracis, G., 2019. Sustainability of the sugar beet crop. Sugar Tech, 21, 703–716. https://doi.org/10.1007/s12355-019-00734-9

Tackenberg, M., Volkmar, C., Dammer, K.-H., 2016. Sensor-based variable-rate fungicide application in winter wheat. Pest Management Science, 72, 1888–1896. https://doi.org/10.1002/ps.4225

Thiessen, E., Heege, H., 2013. Site-specific sensing for fungicide spraying, in: Heege, H.J. (Ed.), Precision in Crop Farming: Site Specific Concepts and Sensing Methods: Applications and Results. Springer Netherlands, Dordrecht, 295–311. https://doi.org/10.1007/978-94-007-6760-7_11

Thomas, S., Kuska, M., Bohnenkamp, D., Brugger, A., Alisaac, E., Wahabzada, M., Behmann, J., Mahlein, A.-K., 2018. Benefits of hyperspectral imaging for plant disease detection and plant protection: A technical perspective. Journal of Plant Diseases and Protection, 125, 5–20. https://doi.org/10.1007/s41348-017-0124-6

Varrelmann, M., Märländer, B., 2018. Risk assessment for pesticide resistance in sugar beet pathogens, pests and weeds. Sugar Industry, 143, 414–423.

Vereijssen, J., Schneider, J., Termorshuizen, A., Jeger, M., 2003. Comparison of two disease assessment methods for assessing Cercospora leaf spot in sugar beet. Crop Protection, 22, 201–209. https://doi.org/10.1016/s0261-2194(02)00146-1

Vogel, J., Kenter, C., Holst, C., Märländer, B., 2018. New generation of resistant sugar beet varieties for advanced integrated management of Cercospora leaf spot in central Europe. Frontiers in Plant Science, 9, 1-12. https://doi.org/10.3389/fpls.2018.00222

Weiland, J., Koch, G., 2004. Sugarbeet leaf spot disease (*Cercospora beticola* Sacc.). Molecular Plant Pathology, 5, 157–166. https://doi.org/10.1111/j.1364-3703.2004.00218.x

Weltmeier, F., Mäser, A., Menze, A., Hennig, S., Schad, M., Breuer, F., Schulz, B., Holtschulte, B., Nehls, R., Stahl, D.J., 2011. Transcript profiles in sugar beet genotypes uncover timing and strength of defense reactions to *Cercospora beticola* infection. Molecular Plant-Microbe Interactions MPMI, 24, 758–772. https://doi.org/10.1094/mpmi

Wierzbicki, D., 2018. Multi-camera imaging system for UAV photogrammetry. Sensors, 18, 1-21. https://doi.org/10.3390/s18082433

Wiessner, J., Stockfisch, N., Marlander, B., 2010. Approach for determining the eco-efficiency of sugar beet cultivation in Germany. Journal fur Kulturpflanzen, 62, 409–418.

Windels, C., Lamey, H., Hilde, D., Widner, J., Knudsen, T., 1998. A Cercospora leaf spot model for sugar beet: In practice by an industry. Plant Disease, 82, 716–726. https://doi.org/10.1094/pdis.1998.82.7.716

Wirtschaftliche Vereinigung Zucker (WVZ), Verein der Zuckerindustrie (VdZ), 2021. Jahresbericht. Berlin.

Wolf, P., 2002. Über die Integration von Bekämpfungsmaßnahmen gegen pilzliche Blattkrankheiten der Zuckerrübe-IPS-Modell Zuckerrübe. Habilitationsschrift. 89-103.

Wolf, P., Kraft, R., Verreet, J., 1998. Characteristics of damage caused by *Cercospora beticola* (Sacc.) in sugar beet as a base of yield loss forecast. Journal of Plant Diseases and Protection, 105, 462–474.

Wolf, P., Verreet, J., 2002. An integrated pest management system in Germany for the control of fungal leaf diseases in sugar beet: The IPM sugar beet model. Plant Disease, 86, 336–344. https://doi.org/10.1094/pdis.2002.86.4.336

Wolf, P., Verreet, J., 1997. Epidemiological development of *Cercospora beticola* (Sacch.) in sugar beet crops. Journal of Plant Diseases and Protection 545–556.

Wolf, P., Weis, F., Verreet, J., 2001. Threshold values as indicators of fungicide treatments for the control of leaf blotching caused by *Cercospora beticola* (Sacc.) in sugar beets. Journal of Plant Diseases and Protection, 108, 244–257.

Wolf, P., Weis, F., Verreet, J., 1995. Principles of an integrated pest management of *Cercospora beticola* in sugar beets. Journal of Plant Diseases and Protection, 102, 574–585.

Wolf, P., Weis, F., Verreet, J., Bürcky, K., Maier, J., Tischner, H., 1998. IPS (Integriertes Pflanzenschutzsystem)-Modell Zuckerrube - Entwicklungsschritte und einfuhrung in die praxis. Gesunde Pflanzen 50, 264–272.

Yang, C., 2020. Remote sensing and precision agriculture technologies for crop disease detection and management with a practical application example. Engineering, 6, 528–532. https://doi.org/10.1016/j.eng.2019.10.015

Ziya, A., Mehmet, M., Yusuf, Y., 2018. Determination of sugar beet leaf spot disease level (*Cercospora beticola* Sacc.) with image Processing technique by using drone. Current Investigations in Agriculture and Current Research 5, 621–631. https://doi.org/10.32474/ciacr.2018.05.000214

Acknowledgment

Agradecimiento

Quisiera extender mi gratitud a mi mentora y supervisora, la Prof. Dr. Anne-Katrin Mahlein. Gracias a las oportunidades que me brindó, pude adentrarme en el mundo de los sensores de imágenes, así como aprender y utilizar la tecnología de drones como plataformas para el mapeo en campo. La experiencia adquirida en estos últimos años ha contribuido significativamente a mi desarrollo, tanto a nivel profesional como personal.

Asimismo, quiero agradecer a mis colegas del Instituto de Investigación de Remolacha Azucarera (IfZ), especialmente a nuestro grupo de trabajo de "sensores". Facundo Ispizua, Jonas Bömer y Justus Detring, quienes no solo son colegas, sino también amigos incondicionales. También a Dirk Koops y Jonathan Eggers, cuya experiencia técnica y en campo fue esencial para obtener resultados de calidad en esta investigación. Por último, agradezco a los Drs. Stefan Paulus y Rene Heim, cuyas contribuciones innovadoras y científicas guiaron la planificación experimental.

Aunque mi familia sanguínea no pudo estar cerca, mis amigos llenaron ese vacío con creces. Una vez más, Facundo y Antonio estuvieron ahí en cada momento, brindando apoyo en lo personal y emocional, convirtiéndose en pilares fundamentales para mi equilibrio emocional. También quiero mencionar a Matías, Samuel, Alberto y Adán, por esos momentos de armonía que compartimos.

Finalmente, deseo expresar mi profundo agradecimiento a mi familia. En primer lugar, a mi hijo Mateo, quien me acompañó prácticamente durante todo mi proceso de doctorado, siendo un motor y una fuente de motivación en los altibajos emocionales que son característicos de esta etapa. A mi padre, quien libró una batalla titánica contra el cáncer en los últimos años, emergiendo como un vencedor a pesar de su edad, y demostrándome una vez más con su ejemplo cómo mantenerse fuerte en tiempos difíciles. A mi madre, quien a pesar de sus propias dolencias y el paso de los años, siempre estuvo presente con palabras amorosas y alentadoras. También quiero agradecer a mis hermanos, Cintya, Lino y Miguel, quienes también fueron parte fundamental de mi crecimiento emocional. ¡Gracias por los consejos y el apoyo, hermanos!

Espero que disfruten esta tesis tanto como yo disfruté investigando y escribiéndola.

Curriculum Vitae

Abel Andree Barreto Alcántara

Agricultural Sciences, M. Sc.

Personal details

Gender: Male

Date of birth: 06.03.1991

Place of birth: Chimbote, Ancash, Peru

Nationality: Peruvian

Education

Since 2019	PhD Studies in Agricultural Sciences
	Georg-August-Universität
	Supervisor: Prof. Dr. Anne-Katrin Mahlein
	Topic: Sensing of Plant Diseases by Spectral Imaging and UAVs
10/2016 – 02/2019	Agricultural Sciences (Master)
	Georg-August-Universität
04/2009 – 12/2013	Agroindustrial Engineering (Bachelor)
	Universidad Nacional de Trujillo

Projects

- Since 2023 – PhD Student: Digital experimental field Farmerspace, supported by the Federal Office for Agriculture and Food (BLE) that provides coordinating support for artificial intelligence (AI) in agriculture as funding organisation, grant number FKZ 28DE104A18.
- Phenorob, In-Field Detection of Plant Diseases and Site or Spot-specific control; Institute of Sugar Beet Research at the University of Göttingen

- 2022/2023 – PhD Student: Cluster of Excellence: Phenorob, In-Field Detection of Plant Diseases and Site or Spot-specific control; Institute of Sugar Beet Research at the University of Göttingen
- 2019/2021 - PhD Student: Sensing of Plant Diseases by Hyperspectral Imaging and UAVs; Coordination Beet Research International (COBRI); Institute of Sugar Beet Research at the University of Göttingen
- 2014/2015 - Junior Researcher: Quality Analysis of Agricultural Products by using Hyperspectral Imaging; Peruvian Program of Innovation – Ex-FINCyT (Contract 407-PNICP-PIAP-2014); Universidad Nacional Toribio Rodriguez de Mendoza de Amazonas, Peru